

A mathematical model for simulation of fetal heart rate decelerations in labor

Citation for published version (APA):

Hout - van der Jagt, van der, M. B. (2013). *A mathematical model for simulation of fetal heart rate decelerations in labor*. [Phd Thesis 2 (Research NOT TU/e / Graduation TU/e), Biomedical Engineering]. Technische Universiteit Eindhoven. <https://doi.org/10.6100/IR752334>

DOI:

[10.6100/IR752334](https://doi.org/10.6100/IR752334)

Document status and date:

Published: 01/01/2013

Document Version:

Publisher's PDF, also known as Version of Record (includes final page, issue and volume numbers)

Please check the document version of this publication:

- A submitted manuscript is the version of the article upon submission and before peer-review. There can be important differences between the submitted version and the official published version of record. People interested in the research are advised to contact the author for the final version of the publication, or visit the DOI to the publisher's website.
- The final author version and the galley proof are versions of the publication after peer review.
- The final published version features the final layout of the paper including the volume, issue and page numbers.

[Link to publication](#)

General rights

Copyright and moral rights for the publications made accessible in the public portal are retained by the authors and/or other copyright owners and it is a condition of accessing publications that users recognise and abide by the legal requirements associated with these rights.

- Users may download and print one copy of any publication from the public portal for the purpose of private study or research.
- You may not further distribute the material or use it for any profit-making activity or commercial gain
- You may freely distribute the URL identifying the publication in the public portal.

If the publication is distributed under the terms of Article 25fa of the Dutch Copyright Act, indicated by the "Taverne" license above, please follow below link for the End User Agreement:

www.tue.nl/taverne

Take down policy

If you believe that this document breaches copyright please contact us at:

openaccess@tue.nl

providing details and we will investigate your claim.

A mathematical model for simulation of fetal heart rate decelerations in labor

PROEFSCHRIFT

ter verkrijging van de graad van doctor aan de Technische Universiteit Eindhoven,
op gezag van de rector magnificus, prof.dr.ir. C.J. van Duijn,
voor een commissie aangewezen door het College voor Promoties
in het openbaar te verdedigen op woensdag 3 april 2013 om 16.00 uur

door

Marieke Beatrijs van der Hout-van der Jagt

geboren te 's-Gravenhage

Dit proefschrift is goedgekeurd door de promotoren:

prof.dr. S.G. Oei

en

prof.dr.ir. F.N. van de Vosse

Copromotor:

dr.ir. P.H.M. Bovendeerd

ISBN: 978-94-6182-246-8

NUR 954

Printed by: Off Page, Amsterdam

Cover design: **gedesign** by Gerda Spee

© Copyright 2013, M.B. van der Hout-van der Jagt

All rights reserved. No part of this publication may be reproduced, stored in a retrieval system, or transmitted, in any form or by any means, electronic, mechanical, photocopying, recording or otherwise, without the prior written permission from the copyright owner.

The research described in this thesis is funded by the Dutch Technology Foundation STW, which is part of the Dutch Organisation for Scientific Research (NWO). Financial support for the printing of this thesis was kindly provided by Signal Processing Systems group at Eindhoven University of Technology, Stichting De Weijerhorst, Skills Meducation B.V., Chipsoft B.V., GrafiMedics B.V., Nemo Healthcare, BMA B.V. (Mosos) and Medical Dynamics.

Summary

A mathematical model for simulation of fetal heart rate decelerations in labor

Fetal wellbeing during labor and delivery is commonly monitored through the cardiotocogram (CTG), the combined registration of uterus contractions and fetal heart rate (FHR). From the CTG, the fetal oxygen state is estimated as the main indicator of the fetal condition. However, this estimate is difficult to make, due to the complex relation between CTG and oxygen state. Mathematical models can be used to assist in interpretation of the CTG, since they enable quantitative modeling of the flow of events through which uterine contractions affect fetal oxygenation and FHR. This thesis describes the development of a model that can be used to reproduce FHR response to uterine contractions during several clinical scenarios.

First, a model was developed that describes the relation between uterine contractions, maternal and fetal hemodynamics, oxygen distribution within the fetomaternal circulation and cardiovascular (reflex) regulation in the fetus in response to deviations in blood- and oxygen pressures. The model is partly based on previously presented models for cardiac function, chemoreceptor control in adults and oxygen distribution in the fetal circulation. These modules are coupled and scaled to meet requirements for the (pregnant) maternal and fetal condition. The model is completed with a module for uterine contractions and a module of the vascular system of both mother and fetus. A first clinical scenario was simulated with the model to test model response to changes in cerebral blood flow during the descent of the fetal head in the birth canal. A validation pilot was performed to investigate the quality of model outcome via expert opinion. Experts were unable to discriminate between real and simulated signals, suggesting that the model can be used for educational training.

Second, the model was extended with the baroreceptor reflex. This allowed simulation of a second clinical scenario, where both chemo- and baroreflex pathways lead to a FHR decelera-

tion in response to uterine flow reduction during contractions. Results for the uncompromised fetus show that partial oxygen pressures reduce in relation to the strength and duration of the contraction. Furthermore, decelerations during several scenarios of uteroplacental insufficiency were studied. Results for reduced uterine blood supply or reduced placental diffusion capacity, demonstrated lower baseline FHR and smaller decelerations during contraction. Reduced uteroplacental blood volume was found to lead to deeper decelerations only. The model response in several nerve blocking simulations is similar to experimental findings.

Third, the model was used to simulate a third type of decelerations, i.e. variable heart rate decelerations, originating from umbilical cord compression. Different degrees of compression were investigated. An increase in contraction amplitude and duration leads to increased umbilical cord compression grade and thus affects the extent of blood pressure increase, flow redistribution and FHR response. There is a clear relation between fetal oxygenation, blood pressure and the resulting FHR. The extent of umbilical compression and thus FHR deceleration is positively related to increased contraction duration and amplitude, and increased sensitivity of the umbilical resistance to uterine pressure.

Fourth, gynaecologists, midwives and residents were asked to rate a set of both model-generated CTGs and real CTGs for the three clinical scenarios. Although real tracings were more likely to be recognized correctly, the suitability for use in simulation training was found to be almost equal for real and computer-generated tracings. Due to limited numbers for early and variable deceleration evaluation, statistical analysis turned out to be valid only for the CTG's with late decelerations. Additional comments from the respondents revealed that variability and regularity of the simulated signals greatly influence the perception of a tracing. Clinicians agreed that a tracing is suitable for use in simulation training when it is clear and free of physiological incompatibilities, which is the case for all simulated tracings.

Fifth, the model was used to test the clinical hypothesis that administration of oxygen to the mother may increase FHR during variable fetal heart rate decelerations. The model was used to test the response of fetal oxygenation and heart rate to maternal oxygen increase following 100% oxygen administration. Model outcome suggests that FHR benefits from oxygen administration as the duration and depth of FHR decelerations and fetal oxygenation improves. However, the beneficial effect of maternal hyperoxygenation on FHR and oxygenation reduces during more severe variable decelerations.

In conclusion, a model was developed to simulate the physiologic cascade from uterine contraction to changes in fetal heart rate. Model outcome for various scenarios is in correspondence with findings from animal experiments. The model can be used in an educational setting for the simulation of short-term changes in fetal hemodynamics and oxygenation status in response to uterine contractions to increase insight into the complex physiology. In addition, it can be integrated in a full-body delivery simulator to enhance obstetric team training.

Contents

Summary	iii
1 Introduction	1
1.1 Introduction	2
1.2 Objective and outline	4
2 A mathematical model for simulation of early decelerations in the cardiotocogram during labor	7
2.1 Introduction	9
2.2 Materials & Methods	10
2.2.1 Physiology of early decelerations	10
2.2.2 Model of cardiovascular hemodynamics	10
2.2.3 Contraction generator	14
2.2.4 Model for oxygen distribution	15
2.2.5 Regulation model	17
2.2.6 Numerical implementation	17
2.2.7 Validation method	18
2.3 Results	18
2.3.1 Basic condition	18
2.3.2 Early decelerations	20
2.3.3 Validation	21
2.4 Discussion & conclusion	22
Appendix	25
3 Simulation of reflex late decelerations in labor with a mathematical model	29

3.1	Introduction	31
3.2	Materials & Methods	33
3.2.1	Mathematical model	33
3.2.2	Simulation protocol	37
3.3	Results	39
3.3.1	Intact nervous system	39
3.3.2	Neuronal blocking	42
3.4	Discussion & conclusion	43
	Appendix	46
4	Insight into variable fetal heart rate decelerations from a mathematical model	57
4.1	Introduction	59
4.2	Materials & Methods	60
4.2.1	Mathematical model	60
4.2.2	Simulation protocol	62
4.2.3	Clinical scenario	64
4.3	Results	64
4.3.1	Experimental scenarios	64
4.3.2	Clinical scenario	68
4.4	Discussion & conclusion	68
	Appendix	72
5	Validation of cardiocograms from a mathematical model for use in simulation training	75
5.1	Introduction	77
5.2	Methods	77
5.2.1	Simulation model	77
5.2.2	CTG tracings	77
5.2.3	CTG validation	79
5.2.4	Data analysis	80
5.3	Results	81
5.3.1	Qualitative data analysis	81
5.3.2	Statistical data analysis	83
5.4	Discussion	83
6	Intrauterine resuscitation by maternal hyperoxygenation evaluated in a simulation model	87
6.1	Introduction	89
6.2	Methods	90
6.2.1	Model design	90

6.2.2	Simulation	90
6.2.3	Outcome	91
6.3	Results	91
6.4	Discussion	92
7	General discussion	97
7.1	Introduction	98
7.2	Main contributions	98
7.3	Future perspectives	100
7.3.1	Simulation model	100
7.3.2	Application	101
7.4	Conclusion	102
	References	103
	Nederlandse samenvatting	115
	Dankwoord	119
	Curriculum Vitae	121
	Scientific output	123

List of Figures

1.1	Schematic view of the placenta.	3
1.2	Block diagram of the feto-maternal model.	5
2.1	Block diagram of the feto-maternal model.	10
2.2	Electric analog of the feto-maternal model.	12
2.3	Conceptual model of oxygen distribution.	15
2.4	Maternal and fetal cardiac performance during normal heart cycle.	20
2.5	Cascade leading to early decelerations.	21
2.6	CTG signal as calculated with the model.	22
3.1	Block diagram of the role of the nervous system in late decelerations.	32
3.2	Block diagram of the feto-maternal model.	33
3.3	Electric analog of the feto-maternal cardiovascular model to compute pressures p and flows q	34
3.4	Simulation results for normal labor and UPI.	40
3.5	Partial oxygen pressures and flow redistribution.	41

3.6	Simulation results for contraction variations.	53
3.7	Simulation results for normal labor and blocking simulations.	54
3.8	Block diagram of the regulatory model with details of modeled variables.	55
4.1	Electric analog of the feto-maternal cardiovascular model.	61
4.2	Variable response curve for umbilical resistances.	63
4.3	Umbilical cord occlusion.	65
4.4	Model response to changes in uterine contraction and umbilical resistance response curve.	67
4.5	Clinical scenario: CTG with variable decelerations and corresponding arterial oxygen and MAP signal.	68
5.1	Example of a computer-generated CTG.	78
5.2	Example of a real CTG.	79
5.3	Normalized response frequencies for origin and suitability of CTGs with late decelerations.	82
6.1	Maternal and fetal arterial pO_2 and fetal heart rate in relation to uterine contractions of 60, 70 and 80 mmHg.	95
6.2	Effect of hyperoxygenation on pO_2 in different compartments during contractions of 60, 70 and 80 mmHg.	96

List of Tables

2.1	Model target values and results.	19
2.2	Validation results.	23
2.3	Contraction parameters.	26
2.4	Maternal cardiovascular parameters.	26
2.5	Fetal cardiovascular parameters.	27
2.6	Oxygen distribution parameters.	28
2.7	Regulation parameters.	28
3.1	Settings for simulations with intact nervous system.	38
3.2	Fixed fire rates used in model simulations with blocked neuronal pathways. . .	39
3.3	Receptor parameters.	48
3.4	Uterine and cerebral resistance parameters.	51
3.5	Effector parameters.	52
3.6	CNS parameters.	52
4.1	Characteristics of the CTG in Figure 4.5.	69

4.2	Umbilical circulation parameters.	73
4.3	Baroreceptor parameters.	74
5.1	Input characteristics of the computer-generated CTGs.	78
5.2	Statistics of the rated CTGs.	84
6.1	Parameter settings for each simulation.	91
6.2	Differences in variable decelerations for normoxia and hyperoxia.	92
6.3	Fetal pO_2 during normoxia and hyperoxia.	92

Chapter 1

Introduction

1.1 Introduction

Most pregnancies and deliveries are uncomplicated, but when an emergency occurs, this has often lifelong consequences. In The Netherlands, antenatal and perinatal morbidity and mortality rates are relatively high in comparison with other countries in Europe [83, 97]. More recent data from a Dutch perinatal audit shows that perinatal mortality for term deliveries (between 37 to 41 weeks of pregnancy) is reduced by 39% from 2001-2010 [85], however, data for preterm deliveries and morbidity rates are not yet available, nor is a comparison with other European countries.

Perinatal morbidity and mortality rates are associated with fetal distress due to metabolic acidosis [69, 75]. A timely recognition of fetal distress via fetal monitoring contributes to a prompt and adequate intervention, and may thus positively affect fetal outcome. Fetal monitoring during labor and delivery is currently mainly achieved via observation of fetal heart rate (FHR) patterns, often in relation to uterine contractions. The simultaneous registration is known as the cardiotocogram (CTG), which is widely available at the hospital labor ward, whereas monitoring in the home delivery setting depends on non-continuous FHR detection without contraction pressure registration.

During pregnancy, anticipation of adverse outcome takes place via referral of women at risk to secondary or even tertiary pregnancy care, i.e. specialized labor care in a hospital. However, not all emergencies during labor and delivery can be anticipated. It is therefore of the utmost importance that obstetric personnel is capable of timely recognition of fetal stress and is well-trained to react adequately to these emergencies.

The maternal circulation adapts to pregnancy by an approximate 40% increase in cardiac output and blood volume [1, 33, 62], while the fetal circulation is optimized via regulatory mechanisms to endure short hypoxic episodes, for example introduced by labor contractions [34]. Since the fetus receives its oxygen via the placenta and umbilical cord, labor contractions that disturb these blood flows are possibly harmful.

Although oxygen is delivered from the mother to the fetus via the placenta, their circulations are separate, as they do not share blood or blood vessels (see Figure 1.1). The placenta provides an exchange platform between those two circulations, not only for oxygen, but also for nutrients and metabolic waste products. Oxygen exchange takes place via diffusion over the placental membrane, a thin cell layer that separates fetal and maternal blood. The fetus is thus fully dependent on its oxygen supply via the path of maternal respiration and circulation, uterine blood flow, placental diffusion capacity and fetal umbilical flow towards the fetal body.

During labor and delivery, uterine contractions may influence oxygen delivery to the fetus negatively: contractions can compress uterine blood vessels, contribute to umbilical cord compression, and induce fetal caput compression during descent in the birth canal [30, 39, 84]. This affects local blood flow and often induces changes in oxygen transport and fetal blood pres-

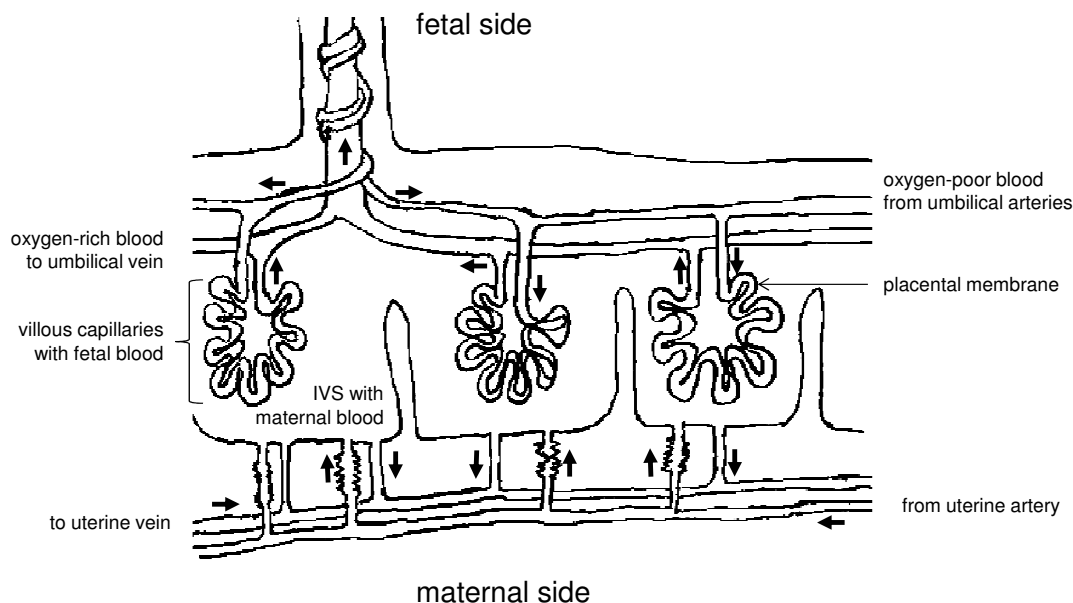


Figure 1.1: Schematic view of the placenta. Fetal oxygen-poor blood is transported via the umbilical arteries towards the placenta. In the placenta, fetal blood enters the villous capillaries, where it is oxygenated with oxygen from the maternal blood in the intervillous space (IVS) via diffusion over the placental membrane. The villous capillaries fuse in the umbilical vein that transports the oxygen-rich blood to the fetus. The IVS receives its blood via the maternal spiral arteries that sprout from the uterine arterial circulation. The uterine vein collects blood from the intervillous space, and thus has a lower oxygen pressure than the uterine artery.

sure [7, 78, 93]. The fetus responds to these changes by activation of a sparing mechanism to maintain fetal blood pressure and economize oxygen consumption [93]. Hence at the expense of peripheral perfusion, blood flow to the cerebral, myocard, adrenal and umbilical circulation is increased to secure oxygen delivery to these critical organs. The FHR drops temporarily to minimize cardiac work. This is recognized as a FHR deceleration.

Although often these short hypoxic episodes are well-supported by the fetus, long-lasting and/or fast-repeated episodes may lead to fetal deterioration. It is difficult to assess fetal wellbeing accurately, since no continuous information on fetal oxygenation is available. During labor, the main source of fetal wellbeing is the cardiotocogram (CTG), which is the simultaneous registration of fetal heart rate (FHR) and uterine contractions. However, the relationship between these two signals is far from straightforward as it is influenced by chemo- and baroreceptor feedback following changes in oxygenation and blood pressure. The trade-off between possible harmful effects of both intervention and awaiting for a safe vaginal delivery remains a daily challenge.

Due to the high complexity and low incidences of emergencies during labor and delivery, ob-

stetricians often cannot rely on previous experiences during a crisis. Simulation training can provide both experience and skills in a safe environment, such that complications due to emergencies can be reduced as much as possible. In the past decade, simulation of labor and delivery emergencies has proven its value in the prevention of severe outcome of obstetric emergencies [22, 23, 79]. Often labor scenarios are practiced with a simulation mannequin that can be accompanied with a patient monitor to emulate patient data. During a simulation scenario, both the trainees and the instructor may influence the flow of events in the scenario, and thus the physiologic state of the mother and fetus. E.g., providing oxygen to the mother will probably affect maternal and fetal oxygenation. Furthermore, the trainees may also influence the physiologic state through unanticipated actions, thus requiring flexibility of the instructor and the simulator engine [127]. As the CTG plays an important role in clinical decision making, ideally the CTG should also be available during simulation training. Some of the commercially available simulators provide a CTG, however, these are all instructor- and/or script-driven and do not include a physiological model.

Mathematical models provide an opportunity to study and simulate physiologic behaviour of a system in many conditions. A physiologic model that relates uterine contractions and FHR can thus not only be used to study the physiologic cascade between uterine contractions and FHR response, it can also be used in a simulated clinical environment for training purposes. Unfortunately, there is no mathematical model documented that describes the relation between uterine pressure, blood flow, blood pressure, oxygen pressure in the fetal and maternal circulation, baro- and chemoreceptor function, the sympathetic and vagal nerve system, and cardiovascular effectors as heart rate, cardiac contractility, venous unstressed vessel volume, peripheral resistance and cerebral autoregulation. These relationships are necessary to understand the physiologic cascade from uterus contraction to FHR deceleration via the regulatory mechanisms of the chemo- and baroreceptor and cerebral autoregulation.

1.2 Objective and outline

This thesis describes the design of a mathematical model that can be used to study and simulate FHR decelerations in labor evoked by uterine contractions. Figure 1.2 shows the relationship between the functional submodules of the model that are needed to simulate the cardiotocogram.

Although the previously-mentioned variables are not linked within one generalized fetomaternal model, there are well-documented models available that describe parts of the above-listed functions [5, 15, 40, 51, 52, 96, 108, 120, 122]. Although several of these models have been developed with other research or training purposes, some of these models can be coupled to cover most of the required functions. However, these models need to be adapted to account for the fetal cardiovascular working points (blood pressure, oxygen pressure, heart rate) [5, 122] and extended to include cerebral oxygenation [108]. Furthermore, a contraction generator is needed

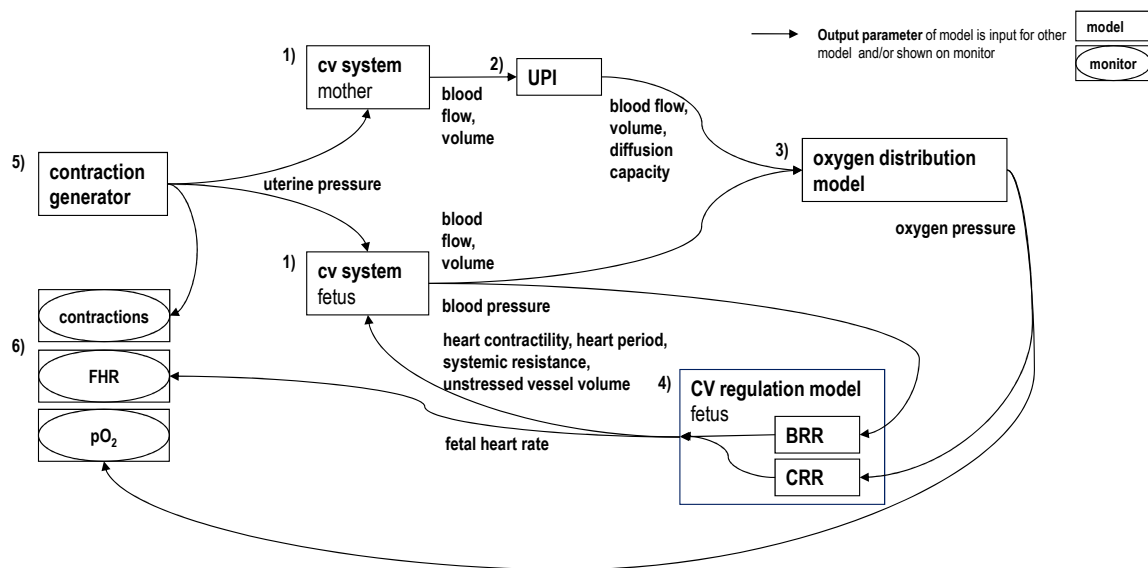


Figure 1.2: Block diagram of the feto-maternal model. 1) The cardiovascular (cv) system of mother and fetus are separate. 2) uteroplacental insufficiency (UPI) may affect uteroplacental blood flow and volume and placental diffusion capacity via parameters in the maternal cv model and/or the oxygen distribution model. 3) Oxygen distribution in mother and fetus is determined by fetal oxygen consumption, blood flow and volume, oxygen exchange in the placenta and arterial oxygen level in the mother. 4) Blood pressure and oxygen pressures in the fetus are monitored by the baro- and chemoreceptor reflexes (BRR and CRR respectively), and may evoke changes in cardiovascular parameters, including fetal heart rate (FHR). 5) Changes in uterine pressure (from uterine contractions) may alter blood pressure and flow in the fetal or maternal circulation, since these exert an external pressure on the intra-uterine blood vessels. 6) The cardiogram follows from the individual signals. The model also provides information on oxygenation, which is not clinically available.

to induce uterine pressure. The model has to be completed with a feto-maternal circulation model to describe cardiac function, blood flows and blood pressure in the fetal and maternal systemic circulation, the uterine, umbilical and fetal cerebral circulation.

The model is stepwise designed and tested. In **Chapter 2** the model is introduced with a contraction generator, feto-maternal cardiovascular system, oxygen distribution [108] and vagal nerve feedback towards the FHR [122]. The oxygen distribution model of Sá Couto et al. [108] is extended with a compartment for cerebral oxygen content. Normal values for cardiovascular output are compared to literature data. The model is tested with the scenario of caput compression during fetal descent in the first stage of labor. This causes local hypoxemia, and directly affects the vagal nerve. A preliminary validation study is used to evaluate the quality of the modeled CTGs.

In **Chapter 3**, the model is extended with cardiovascular feedback from the chemo- and baroreceptor, scaled from an adult model [122]. The model is tested with the scenario of uterine flow interruption during uterine contractions, which leads to a second type of FHR decelerations [39]. Hence during labor contractions, the blood pool in the intervillous space is refreshed poorly, and thus the amount of oxygen delivered to the fetus is reduced, which leads to fetal hypoxemia. The chemoreceptor responds with an increase in vagal and sympathetic activity to heart and blood vessels. This may lead to a secondary blood pressure response that activates the baroreceptor. Different scenarios for uteroplacental insufficiency are simulated during labor.

In **Chapter 4** the umbilical circulation in the model is extended such that the umbilical vein, microcirculation and arteries are modeled separately, and are thus individually compressible. The model is tested for the third and main cause of FHR decelerations, i.e. decelerations originating from partial and/or complete umbilical cord compression in relation with uterine contractions [30, 84, 130]. This induces a simultaneous reduction in fetal oxygen delivery (hypoxemia) and an increase in fetal blood pressure. Sheep experiments have shown different responses for umbilical arterial and/or venous occlusion. Therefore these types of cord compressions are simulated. Furthermore, the influence of contraction amplitude, duration and interval is investigated.

In **Chapter 5**, the suitability of the simulated tracings from the model is evaluated by clinicians. The simulated tracings are mixed with real tracings from a labor ward database and presented to clinicians. The evaluation concerns two research questions, regarding the origin of each tracing (computer-generated or real) and the suitability of each tracing for use in simulation training. Both questions are rated on a 5-point Likert's scale.

In **Chapter 6**, the model is used as a tool to investigate the question to what extent maternal hyperoxygenation improves FHR during variable FHR decelerations [4, 63, 80]. In the model, this is tested by increasing maternal oxygen content via partial pressure increase during repetitive umbilical cord compressions. The influence of hyperoxygenation on FHR for different grades of umbilical cord compression is investigated.

Chapter 7 concludes with a general discussion and reflects on the broader perspective of the findings in this thesis. As Chapters 2 to 6 are written to be self-contained, some overlap is present in the introduction and methods sections of these Chapters.

**A mathematical model for simulation of early
decelerations in the cardiotocogram during
labor**

*M.B. van der Hout-van der Jagt, S.G. Oei and P.H.M. Bovendeerd
Published in: Medical Engineering & Physics 2012;34:579-589*

Abstract

Fetal wellbeing during labor and delivery is commonly monitored through the cardiotocogram (CTG), the combined registration of uterus contractions and fetal heart rate (FHR). The CTG gives an indication of the main determinant of the acute fetal condition, namely its oxygen state. However, interpretation is complicated by the complex relationship between the two.

Mathematical models can be used to assist with the interpretation of the CTG, since they enable quantitative modeling of the cascade of events through which uterine contractions affect fetal oxygenation and FHR. We developed a mathematical model to simulate “early decelerations”, i.e. variations in FHR originating from caput compression during uterine contractions, as mediated by cerebral flow reduction, cerebral hypoxia and a vagal nerve response to hypoxia.

Simulation results show a realistic response, both for fetal and maternal hemodynamics at term, as for FHR variation during early decelerations.

The model is intended to be used as a training tool for gynaecologists. Therefore 6 clinical experts were asked to rate 5 real and 5 model-generated CTG tracings on overall realism and realism of selected aspects. Results show no significant differences between real and computer-generated CTG tracings.

2.1 Introduction

In current clinical practice, the main modality for intrapartum fetal monitoring in high risk pregnancies is the cardiotocogram (CTG), the combined registration of fetal heart rate (FHR) and uterine contractions. The interpretation of the CTG is based on several aspects. FHR is evaluated on baseline level, short-term variability, long term variability, accelerations and decelerations. Contractions are evaluated on frequency, duration and strength. The integral interpretation of these aspects provides valuable information on fetal welfare.

Ideally, fetal welfare would be expressed in terms of fetal tissue oxygenation and acid-base state. Although near-infrared spectroscopy seems to be a promising tool [61, 88], intrapartum measurement of these parameters is currently not available in daily clinical practice. Fortunately, fetal oxygen status is reflected in the fetal heart rate: in the body, the oxygen level is monitored by the chemoreceptor that tends to economize oxygen consumption in hypoxia by amongst others lowering FHR via the chemoreflex [14, 30, 43, 84]. However, FHR is also affected by another regulatory mechanism, the baroreflex, that serves to maintain blood pressure [14, 30, 84]. During labor and delivery, deviations in blood pressure (and thus FHR) are caused among others by variations in intrauterine pressure, induced by uterine contractions, or changes in tissue resistance due to autoregulation following fetal movements [84]. In addition, FHR is also influenced by catecholamines [84] and by the metabolic state of the heart itself [14, 30, 84]. Hence evaluation of fetal welfare from the fetal heart rate signal is far from straightforward.

Mathematical models can be used to assist with the interpretation of the CTG, since all sub-systems that contribute to heart rate regulation can be investigated individually. To study the relation between physiologic processes, hypoxia and the CTG, a model of feto-maternal cardiovascular function is needed, combined with the fetal regulatory feedback mechanisms (baro- and chemoreceptor) and the intrauterine pressure from uterine contractions. Such a model could not only be used for individual training on CTG physiology, it can also be used to drive mannequin reactions during team training of labor and delivery scenarios.

In this study a mathematical model is presented for the simulation of early decelerations in labor. Early decelerations are periodical heart rate decelerations of > 15 bpm whose nadirs coincide with the top of the uterine contractions, mirroring the contraction signal on the CTG. They originate from caput compression during uterine contractions, and are believed to be induced through a vagal stimulus mediated by the chemoreceptor in the brain that lowers the fetal heart rate instantaneously [14, 30, 84]. Although the clinical relevance of early decelerations is limited, they provide a suitable scenario for the first step towards a mathematical model for studying the CTG, since only the chemoreceptor is involved. Future research may include the more clinically relevant late and variable decelerations which also involve the baroreceptor.

2.2 Materials & Methods

2.2.1 Physiology of early decelerations

We adopted the most likely mechanism for early decelerations [30, 84, 130]: during labor, contractions may exert pressure on the fetal caput, thereby hindering cerebral circulation, and thus the supply of oxygen towards the brain [30, 84, 118]. This causes local hypoxemia, which stimulates the nervus vagus and will decrease fetal heart rate [30, 84, 92]. Once the contraction diminishes, cerebral flow will restore and oxygen level in the blood will normalize [118]. This will also restore vagal nerve fire rate to normal value and FHR will correspondingly return to baseline level [14].

The interactions on physiologic level that influence the CTG are shown in Figure 2.1. In the current work, baroreceptor influence on heart rate is neglected, since the baroreceptor is not involved in heart rate regulation in early decelerations.

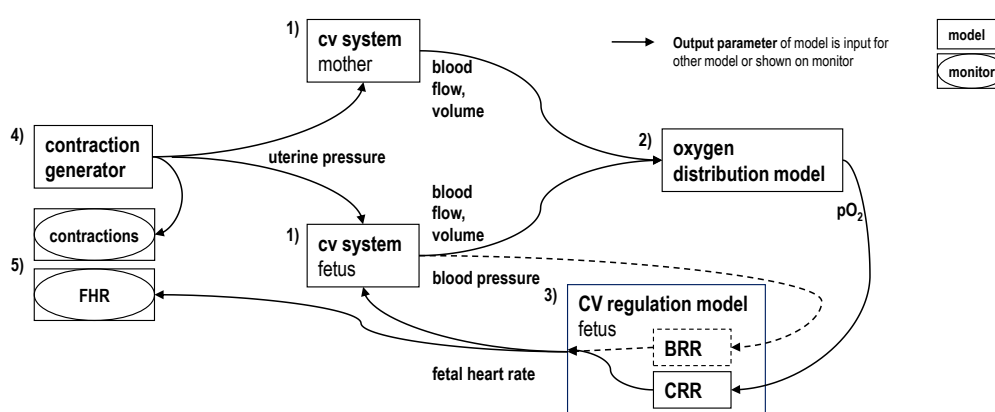


Figure 2.1: Block diagram of the feto-maternal model. 1) The cardiovascular (cv) system of mother and fetus are separate. 2) Oxygen distribution in mother and fetus is determined by fetal oxygen consumption, blood flow and volume, oxygen exchange in the placenta and arterial oxygen level in the mother. 3) Blood pressure and oxygen pressures in the fetus are monitored by the baro- and chemoreceptor (BRR and CRR respectively), and may evoke changes in cardiovascular parameters, including FHR. 4) Changes in uterine pressure (from uterine contractions) may alter blood pressure and flow in the fetal or maternal circulation, since these exert an external pressure on the intra-uterine blood vessels. 5) The cardiotocogram follows from the individual signals.

2.2.2 Model of cardiovascular hemodynamics

The cardiovascular model is visualized in Figure 2.2. The model describes the relation between blood pressure, blood flow, and cardiac performance. Properties that determine local flow and

pressure are inertance, vascular resistance and compliance. In the maternal system, the circulation is lumped into two parallel circuits (uterine and systemic (remaining) circulation). In the fetal circulation, the pulmonary circulation is of minor importance and shunted to the systemic circulation through the ductus arteriosus and the foramen ovale. We modeled the fetal heart as a combined ventricle, and also combined the pulmonary and systemic circulation. We explicitly modeled the umbilical and cerebral circulation while lumping the remaining circulation. All arterial vessels are lumped within “systemic arteries”, assuming average blood pressure and arterial pO_2 for all arterial vessels. Microcirculation and veins are modeled per circuit, and allow local changes. The compliance in between the microcirculation and the venous system represents the blood storage capacity of the microcirculation, and is needed for the calculation of oxygen distribution. Inertance is only taken into account in the systemic arteries, since it only plays a role in larger vessels with high blood acceleration.

Compliances and resistances are modeled in all compartments. For the vascular elements, the following relations between pressure, volume and flow hold:

$$\begin{aligned}\Delta p &= Rq, \\ \Delta p &= L\frac{\partial q}{\partial t}, \\ p &= \frac{1}{C}(V - V_0),\end{aligned}\tag{2.1}$$

with Δp [kPa] the blood pressure difference over the vessel, q [ml/ms] blood flow, R [kPa · ms/ml] the vessel resistance, L [kPa · ms²/ml] blood inertance and C [ml/kPa] vessel compliance. Unstressed vessel volume V_0 [ml] represents the volume of blood in the vessel above which pressure starts to build up, V [ml] represents total vessel blood volume. Furthermore, the arterial and venous resistances R are multiplied with valve parameter c_{valve} to model the open and closed state of the heart valves:

$$q_{valve} = \frac{\Delta p}{c_{valve}R},\tag{2.2}$$

with:

$$c_{valve} = \begin{cases} 1, & \Delta p > 0 \\ 10^6, & \Delta p \leq 0 \end{cases}.\tag{2.3}$$

The valves are thus open in case of a positive pressure difference over the resistance and closed in case of a negative pressure difference to prevent backflow.

The cardiac function is described with the one-fiber model that relates ventricular pressure and volume to myofiber properties [5]. For the relation between myofiber stress σ_f [kPa], ventric-

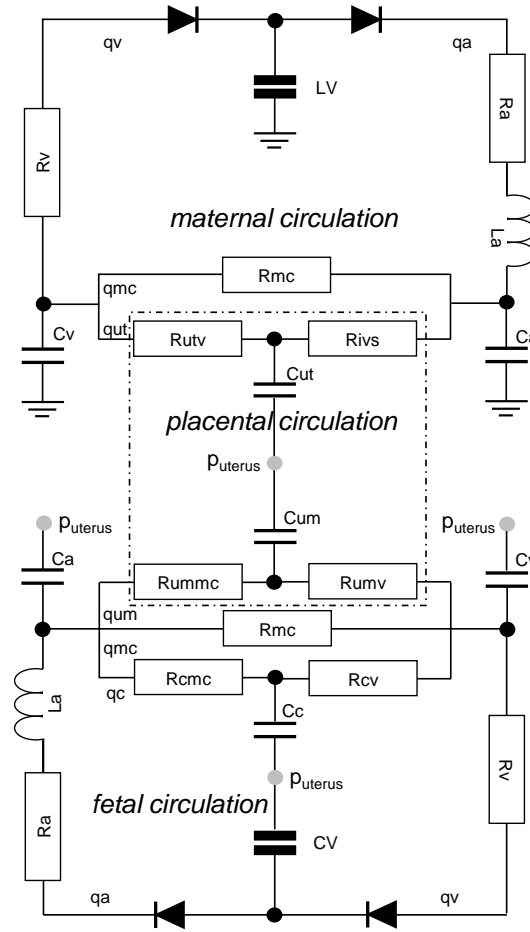


Figure 2.2: Electric analog of the feto-maternal model. The maternal left ventricle (LV) pumps blood towards the arteries (a, with resistance R, inertance L and compliance C), from where a part is directed towards the uterine circulation (ivs and utv: intervillous space and uterine veins) and the remainder to the systemic microcirculation (mc). The venous compartment (v) collects both flows and directs them towards the heart. Two valves prevent retrograde flow in the heart, both in the maternal and fetal circulation. In the fetus, the combined ventricle (CV) pumps the blood towards the arteries (a), from where it is divided over the cerebral (cmc, cv), umbilical (ummc, umv), and systemic circulation (mc). The venous compartment (v) collects these flows before redirecting them to the heart. The uterine and all fetal compliances experience external uterine pressure (p_{uterus}).

ular pressure p_{lv} [kPa], ventricular volume V_{lv} [ml] and (constant) ventricular wall volume V_w [ml] it holds [6, 12]:

$$\frac{\sigma_f}{p_{lv}} = \left(1 + 3 \frac{V_{lv}}{V_w}\right). \quad (2.4)$$

Uniaxial cardiac fiber stress σ_f consists of a passive and an active stress σ_p [kPa] and σ_a [kPa],

according to:

$$\sigma_f = \sigma_a(l_s, \dot{l}_s, t_a) + \sigma_p(l_s). \quad (2.5)$$

Passive stress σ_p is the contribution of the passive muscle to the total myofiber stress. The length dependency of σ_p is given by:

$$\sigma_p(l_s) = \begin{cases} 0 & l_s \leq l_{sp0} \\ \sigma_{p0}(e^{c_p(l_s - l_{sp0})} - 1) & l_s > l_{sp0} \end{cases}, \quad (2.6)$$

σ_{p0} [kPa] represents the scaling parameter for passive stress, c_p [-] the curvature parameter for passive stress-length relation and l_{sp0} [m] the sarcomere length at zero passive stress. Active stress σ_a originates from the stress generated by the sarcomeres. It can be modeled as function of sarcomere length l_s , time elapsed since activation t_a , and sarcomere shortening velocity \dot{l}_s . Length dependence, time dependence and velocity shortening dependence are described with:

$$\sigma_a(l_s, \dot{l}_s, t_a) = f(l_s)g(l_s, t_a)h(\dot{l}_s), \quad (2.7)$$

with length dependency modeled as:

$$f(l_s) = \begin{cases} 0 & l_s \leq l_{sa0} \\ \sigma_{a0} \tanh^2(c_a(l_s - l_{sa0})) & l_s > l_{sa0} \end{cases}. \quad (2.8)$$

In this formula, σ_{a0} [kPa] is a scaling parameter for active stress, c_a [m^{-1}] a curvature parameter for active stress-length relation and l_{sa0} [m] the sarcomere length at zero active stress. The time dependency in (2.7) is given by [6, 12]:

$$g(l_s, t_a) = \begin{cases} 0 & t_a < 0 \\ \sin^2\left(\frac{\pi t_a}{2\tau_r}\right) & 0 \leq t_a < \tau_r \\ 1 - \sin^2\left(\frac{\pi(t_a - \tau_d)}{2\tau_d}\right) & \tau_r \leq t_a < \tau_r + \tau_d \\ 0 & t_a \leq \tau_r + \tau_d \end{cases},$$

$$\tau_r = \tau_{r1} + a_r(l_s - l_{s,0}),$$

$$\tau_d = \tau_{d1} + a_d(l_s - l_{s,0}). \quad (2.9)$$

The increase in sarcomere activation takes place in time interval τ_r [μ s], while the decay takes place during time interval τ_d [s], and starts directly after τ_r . The reference τ_r and τ_d are respectively τ_{r1} and τ_{d1} , based on a reference sarcomere length $l_{s,ref}$. The length dependencies of τ_r and τ_d are described with the constants a_r [μ s/ μ m] and a_d [μ s/ μ m] respectively. Note that activation is initiated at a frequency equal to the heart rate via t_a . Shortening velocity \dot{l}_s is defined as:

$$\dot{l}_s(t) = -\frac{dl_s}{dt}. \quad (2.10)$$

The dependency of σ_a on l_s is:

$$h(\dot{l}_s) = 1 - \left(\frac{\dot{l}_s(t)}{\dot{l}_{s,0}} \right). \quad (2.11)$$

The shortening velocity at zero stress is represented by $\dot{l}_{s,0}$ [$\mu\text{s}/\mu\text{m}$]. The relation between sarcomere length and ventricle volume is defined as [12]:

$$\frac{l_s}{l_{s,0}} = \left(\frac{1 + 3\frac{V_{lv}}{V_w}}{1 + 3\frac{V_{lv,0}}{V_w}} \right)^{\frac{1}{3}}. \quad (2.12)$$

To obtain a complete system of equations, the constitutive equations are completed with equations of conservation of mass. Assuming blood to be incompressible, for each ventricle and all compliances it holds:

$$\frac{dV}{dt} = q_{in}(t) - q_{out}(t), \quad (2.13)$$

where q_{in} [ml/ms] and q_{out} [ml/ms] represent inflow and outflow.

2.2.3 Contraction generator

Uterine contractions are responsible for uterine pressure p_{uterus} in the hemodynamic system. Contractions are modeled with several variables linked to clinical observable aspects in the contraction signal: contraction duration T_{con} [s], peak strength p_{con} [kPa], interval T_{inter} [s] (difference between initiation moment (t_{con} [s]) of two subsequent contractions) and baseline level p_{rest} [kPa]. Except for p_{rest} , these variables vary per contraction. A sine quadratic function was used to model time dependence:

$$p_{uterus}(t) = \begin{cases} p_{rest} + p_{con} \sin^2\left(\frac{\pi(t-t_{con})}{T_{con}}\right), & t_{con} < t < t_{con} + T_{con} \\ p_{rest}, & else \end{cases}. \quad (2.14)$$

This pressure p_{uterus} [kPa] is the external pressure applied to the uterine vessels and all fetal vessels (see also section 2.2.2). On top of this overall effect of p_{uterus} , it was assumed that, during uterine contraction, the fetal caput was pressed into the maternal pelvis, leading to an increase in cerebral resistance $R_{cmc,0}$. This was modeled with a sigmoidal function [31, 104] according to:

$$R_{cmc} = \frac{R_{cmc,0} + (1 + c_{R,1} \cdot W_{ed}) R_{cmc,0} e^{\left(\frac{p_{uterus} - p_0}{c_{R,2} \cdot p_0}\right)}}{1 + e^{\left(\frac{p_{uterus} - p_0}{c_{R,2} \cdot p_0}\right)}}. \quad (2.15)$$

In clinical practice, not all contractions lead to early decelerations; furthermore, deceleration depth is not related to absolute uterine pressure. Therefore parameter W_{ed} [-] can be set by the user to generate a deceleration depth between 0 and 30 bpm by setting W_{ed} between 0 and 1. Parameter $c_{R,1}$ [-] is responsible for the maximum increase in resistance, while the steepness of the response in the physiological working point p_0 [kPa] is determined by $c_{R,2}$ [-]. All parameter values can be found in the appendix.

2.2.4 Model for oxygen distribution

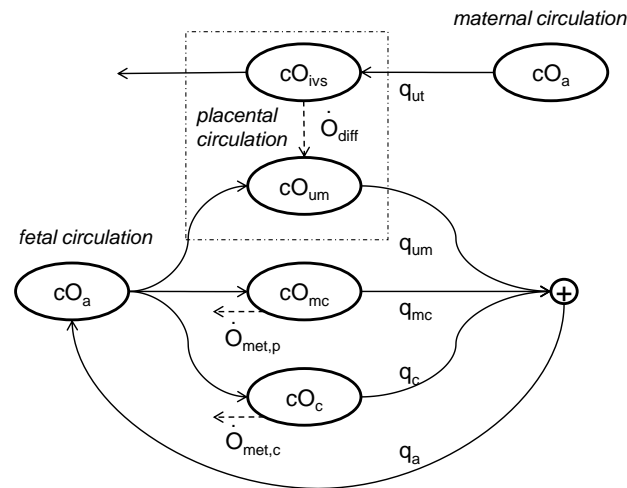


Figure 2.3: Conceptual model of the oxygen distribution model. The maternal arteries supply new oxygen to the intervillous space (ivs). In the intervillous space, oxygen diffuses towards the fetal umbilical (um) circulation. From the umbilical circulation, oxygen-rich blood is forwarded to the central circulation and is mixed with venous blood before entering the arterial (a) system. From the arterial system, blood is divided over the umbilical, cerebral (c) and peripheral (mc) circulation. Oxygen is consumed in the fetal peripheral circulation and in the cerebral circulation. The venous oxygen content is the mix of peripheral and cerebral blood entering the venous system before mixture with blood from the umbilical vein.

Oxygen distribution calculation was done similarly as in the work of Sá Couto et al. [108]. Oxygen distribution between the different vessel compartments is determined by the interplay between convective and diffusive transport and metabolic uptake. Convective transport takes place in all blood vessels, diffusion in the placenta (intervillous space and villous capillaries), and metabolic uptake in all microcirculation compartments, see also Figure 2.3. The change in oxygen amount in a single compartment can be represented by the general equation:

$$\frac{d(cO \cdot V)}{dt} = q(cO_{in} - cO) - \dot{O}_{diff} - \dot{O}_{met}. \quad (2.16)$$

Here oxygen concentration is given as cO [$\text{m}^3 \text{O}_2/\text{m}^3$ blood], the blood volume of the compartment as V [m^3], the flow through the compartment as q [m^3/s], oxygen exchange between compartments as \dot{O}_{diff} [$\text{m}^3 \text{O}_2/\text{s}$], and metabolic oxygen consumption as \dot{O}_{met} [$\text{m}^3 \text{O}_2/\text{s}$]. Oxygen diffusion in the placenta is determined by the oxygen pressure difference in the intervillous space (ivs) and the umbilical microcirculation (um) according to:

$$\dot{O}_{diff} = D(pO_{2,ivs} - pO_{2,um}), \quad (2.17)$$

where D [$\text{m}^3 \text{O}_2/\text{s}/\text{mmHg}$] is the placental diffusion capacity and pO_2 [mmHg] the partial oxygen pressure. Metabolic uptake is constant during normoxia, but is reduced when oxygen concentration cO drops below a threshold concentration cO_{th} [108]:

$$\dot{O}_{met} = \begin{cases} \dot{O}_{met,0} & cO \geq cO_{th} \\ \dot{O}_{met,0} + K_f(cO - cO_{th}) & \text{else} \end{cases}. \quad (2.18)$$

Oxygen content is calculated for all fetal volume compartments (at compliances) and in the intervillous space. Oxygen concentration in the maternal arterial circulation is fixed at normoxia level, thereby assuming that maternal oxygenation in the lungs is constant and sufficient.

In the blood, the majority of oxygen is bound to hemoglobin and only a small fraction is solved and thus responsible for the partial oxygen pressure. The following relations hold for the maternal and fetal oxygen concentration in blood cO [54, 111]:

$$cO = \frac{\alpha Hb \cdot S(pO_2)}{100} + \beta pO_2. \quad (2.19)$$

Here α [$\text{m}^3 \text{O}_2/\text{g Hb}$] represents the maximum binding capacity of hemoglobin, Hb [$\text{g Hb}/\text{m}^3$ blood] the hemoglobin concentration and β [$\text{m}^3 \text{O}_2/\text{m}^3$ blood/ mmHg] the content of dissolved oxygen as function of partial pressure. $S(pO_2)$ [%] represents the saturation as function of partial pressure:

$$S(pO_2) = \frac{100}{1 + \frac{c_1}{pO_2^3 + c_2 \cdot pO_2}}. \quad (2.20)$$

For the fetus, this curve is steeper and more shifted to the left [81], as determined by parameters c_1 [mmHg^3] and c_2 [mmHg^2]. All other equations can be found in the paper of Sá Couto et al. [108]. Since our model has an additional compartment for the cerebral circulation, fetal arterial oxygen content $cO_{a,f}$ [$\text{m}^3 \text{O}_2/\text{m}^3$ blood] now consists of the mix of blood from three compartments:

$$cO_{a,f} = \frac{cO_{mc} \cdot q_{mc} + cO_c \cdot q_c + cO_{um} \cdot q_{um}}{q_{mc} + q_c + q_{um}}. \quad (2.21)$$

Parameter settings can be found in the appendix.

2.2.5 Regulation model

The chemoreceptor monitors pO_2 in the arterial blood. Changes in pO_2 evoke sympathetic and parasympathetic nerve response. During caput compression in labor, arterial blood pO_2 is unchanged, while in the brain pO_2 levels will decrease due to diminished cerebral flow [118]. In response, the parasympathetic nerve (vagal nerve) will directly increase its fire rate, thereby lowering fetal heart rate [14].

Heart period T [s] is modeled according to Ursino et al. [122], as a result of vagal and sympathetic contribution to heart period (ΔT_s [s] and ΔT_v [s] respectively):

$$T = T_0 + \Delta T_s + \Delta T_v, \quad (2.22)$$

where T_0 [s] is an offset term. ΔT_v is determined by vagal fire rate f_v according to:

$$\frac{d\Delta T_v(t)}{dt} = \frac{1}{\tau_{T,v}} \cdot (-\Delta T_v(t) + G_{T,v} \cdot f_v(t - D_{T,v})), \quad (2.23)$$

where $\tau_{T,v}$ [s] are respectively the time constant, $G_{T,v}$ [s²] the gain and $D_{T,v}$ [s] the delay of the vagal system. We added to the model of Ursino et al. [122] a description of the dependence of the vagal nerve fire rate f_v on the partial pressure in the brain $pO_{2,c}(t)$ [mmHg] according to:

$$f_v = f_{v,0} + f_{vh} \left(1 - \frac{pO_{2,c}}{pO_{2,c,0}} \right). \quad (2.24)$$

During normoxia, when partial oxygen pressure equals $pO_{2,c,0}$ [mmHg], fire rate equals the baseline fire rate $f_{v,0}$ [s⁻¹]. Hypoxia-related change in fire rate f_{vh} [s⁻¹] is the maximum increase of the fire rate obtained at zero oxygen pressure.

T_0 , f_{vh} and $pO_{2,c,0}$ were set to fetal values (see appendix), the remaining parameters were adopted from Ursino et al. [122]. Since arterial blood pressure and arterial pO_2 do not change during early decelerations, ΔT_s was effectively constant.

2.2.6 Numerical implementation

The model was implemented in Matlab 2008a, with a time step of 1 ms for the cardiovascular model and a time step of 1 fetal heart period for the oxygen distribution and regulation models.

The latter models thus work with average flow and pressure over the cardiac cycle.

2.2.7 Validation method

For evaluation of the modeled CTG tracings, 6 gynaecologists-perinatologists were requested to validate (in Dutch) a series of 10 CTG tracings with early decelerations. From the 10 tracings, 5 were computer-generated by the model and 5 were obtained from the hospital database (these tracings were two years old to prevent possible recognition). Since short-term variability is not provided by the model, short-term variability from real CTGs was isolated and added to the modeled trace to enhance validation by clinical experts. The imposed variability is based on a fourier analysis of variability of a real CTG (bandwidth of 10 bpm; 5 zero crossings per minute). The same was done for the contraction signal.

The raters were asked to rate realism of the following aspects in the CTG tracing: fetal heart rate baseline and variability; early decelerations delay, duration, depth and morphology; uterine rest tone level and morphology; uterine contractions amplitude, frequency, duration and morphology. The rating levels for each of the items were: *realistic*, *fairly realistic* or *not realistic*. All raters were also asked to classify the 10 tracings as *real*, *computer-generated* or *not distinguishable*, the number of classified tracings was thus 60.

2.3 Results

2.3.1 Basic condition

For the basic condition, cardiovascular output is given in Table 2.1. Both fetal and maternal hemodynamics are according to normal human values obtained from literature. Fetal blood pressure target data were obtained from estimations with a mathematical model [116] instead of measured data. Oxygen pressures in the feto-maternal circulation are similar to those measured, except for placental oxygen pressures, which are slightly higher than reported (44 (vs. 23.3-39.9) and 32 (vs. 24.6-29.3) mmHg for intervillous space and umbilical vein). Fetal and maternal cardiac performance are shown in Figure 2.4 (respectively left and right panel), where the relation is shown between ventricle volume and pressure (upper panel) and between sarcomere length and stress in the myocardium (lower panel) during the cardiac cycle. Although fetal and maternal cardiac volumes differ a factor ten, sarcomere length is in the same range. Cardiac pressures and stresses differ approximately a factor two.

Table 2.1: Model target values and results.

Variable	Target value	Unit	N	Reference
Maternal parameters				
Systolic pressure	95 ± 2 103.8 ± 10 118.0 ± 8.3 97	mmHg	19 34 12	[62] [33] [106] model
Diastolic pressure	50 ± 2 58.9 ± 11 68.5 ± 12.8 49	mmHg	19 34 12	[62] [33] [106] model
Cardiac output	6.37 ± 1.48 8.56 ± 0.51 7.35 ± 1.25 5.88 ± 1.96 7.15	l/min	50 19 34 12	[90] [62] [33] [106] model
Ejection fraction	0.73 ± 0.01 0.67 ± 0.06 0.74 ± 0.08 0.62	ml	19 34 12	[62] [33] [106] model
Uterine artery flow	500 – 700 830 ± 284 712	ml/min	NA 18	[48] [66] model
Intervillous space pressure	15 15	mmHg	NA	[48] model
Intervillous space pO_2	29.2(28 – 33.9) 33.1 ± 5.35 23.3(18 – 29) 37.5(24.0 – 72.0) 39.9(27.5 – 53.7) 44	mmHg	9 30 4 NA 25	[66] [128] [100] [98] [113] model
Venous pressure	1 – 7 3 – 8 6	mmHg	NA NA	[84] [110] model
Fetal parameters				
Heart rate	135 135	bpm	-	- model
Systolic pressure	58 60	mmHg	–	[116] model
Diastolic pressure	26 26	mmHg	–	[116] model
Mean arterial pressure	45 40	mmHg	–	[116] model
Combined cardiac output	425 – 450 454	ml/min/kg	NA	[82] model
Ejection fraction	0.66 ± 4 0.66	–	50	[109] model
Umbilical artery flow	300 255 – 270 273	ml/min	252 NA	[36] [64] model
Umbilical artery pO_2	19.2 ± 4.8 18.3 18	mmHg	33 178	[73] [113] model
Umbilical vein pO_2	24.6 ± 6.5 29.3 32	mmHg	33 178	[73] [113] model
Systemic microcirculation pO_2	1 – 15 15	mmHg	3	[121] model
Cerebral flow	43.0 ± 20.0 45	ml/min/kg	81	[65] model
Cerebral microcirculation pO_2	NA 15	mmHg	NA	- model
Venous pressure	1 – 14 3	mmHg	29	[59] model

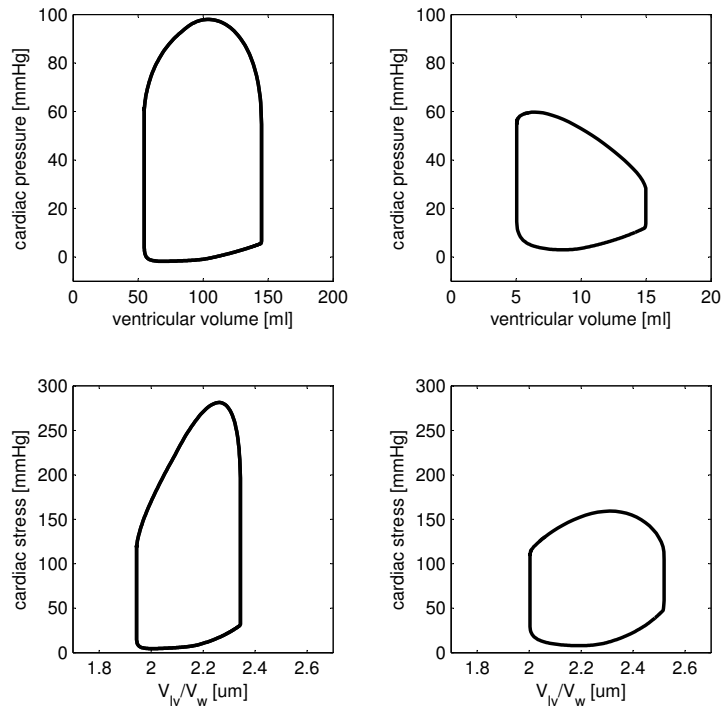


Figure 2.4: Fetal and maternal cardiac performance during normal heart cycle. The left side provides maternal cardiac performance: the heart performs at approximately double pressure according to fetal values, with approximately a tenfold increase in ventricular volume, ejection fraction thereby remaining the same. Cardiac stress as function of sarcomere length shows that maternal cardiac stress is approximately doubled while sarcomere length is more or less similar for mother and child. The right side shows fetal cardiac performance: the upper panel represents a normal pressure-volume loop with an ejection fraction of 0.66 and a stroke volume of 10 ml. Cardiac pressure is between 3 and 60 mmHg, respectively central venous and arterial systolic pressure. The lower panel shows cardiac stress (σ_f) in the sarcomeres with corresponding myofiber length (l_s) during the heart cycle.

2.3.2 Early decelerations

Early decelerations are the result of a cascade (see Figure 2.5) where the uterine contraction increases cerebral resistance, thus reducing cerebral flow, which results in diminished oxygen delivery to the vagal nerve in the brain which leads to a reduction in fetal heart rate. The model predicts that the deceleration delay predominantly originates from the delay in reduction of cerebral pO_2 following cerebral flow reduction, which is achieved in a few seconds. Only a few variables changed during caput compression: cerebral flow (-58%), cerebral pO_2 (-20%) and fetal heart rate (-30 bpm). Furthermore only a small reduction in mean arterial pressure could be seen (-3 mmHg) as a consequence of reduced cardiac output. A small increase in pO_2 was observed in the fetal microcirculation (+0.5 mmHg) since less oxygen was extracted in the fetal brain. During contractions without caput compression ($W_{ed} = 0$), no hemodynamical

effect was seen, other than a slight increase in uterine blood pressure (+3%) in the first half of the contraction, followed by a decrease (-3%) in the second half of the contraction, which led to uterine flow changes of respectively -0.4% and +0.4%. Hence no (early) decelerations occur.

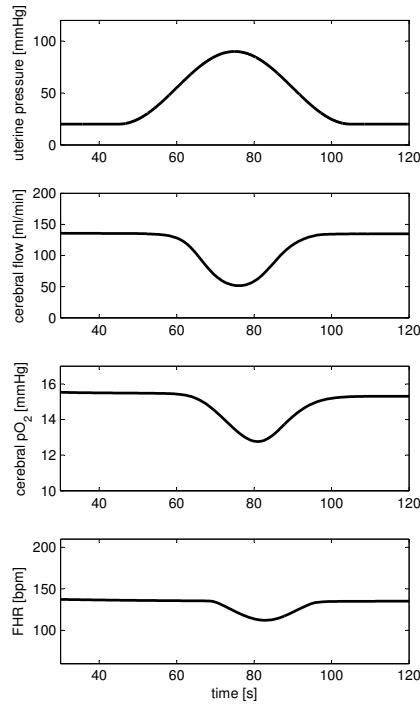


Figure 2.5: Cascade leading to early decelerations. The uterine contraction diminishes cerebral flow and thus oxygen delivery to the brain. Fetal pO_2 in the brain reduces, which evokes an FHR reduction by the vagal nerve. Once the contraction diminishes, flow restores and oxygen in the brain is quickly restored to baseline level. FHR is restored shortly after the contraction has ended.

2.3.3 Validation

The validation study consisted of two parts: the rating of the 12 items in each of the 10 CTG tracings; and a classification on origin (computer-generated/real/not distinguishable) per CTG. Figure 2.6 shows an example of a CTG with early decelerations as given by the model and the same CTG with added FHR variability and variations in contraction signal. Only 5 out of 6 raters participated in part one. A few items were not rated, the total of rated items was therefore 581 instead of 600. All 6 raters participated in part two and classified all 10 CTG tracings. Validation results are given in Table 2.2. As can be seen, no statistical difference can be detected between (rated) items in real and computer-generated tracings. Most items in both real and computer-generated tracings were found to be realistic or fairly realistic. Only 6 out of 581 items were seen as unrealistic, mostly in computer-generated tracings: especially one tracing got comments on deceleration delay being too long and a contraction morphology

that trembled too heavily. The P-value indicates that it is unlikely that there is a statistical significance between real and computer-generated tracings, but this needs to be confirmed with more data, since statistical power is too small with this number of rated *not realistic* items.

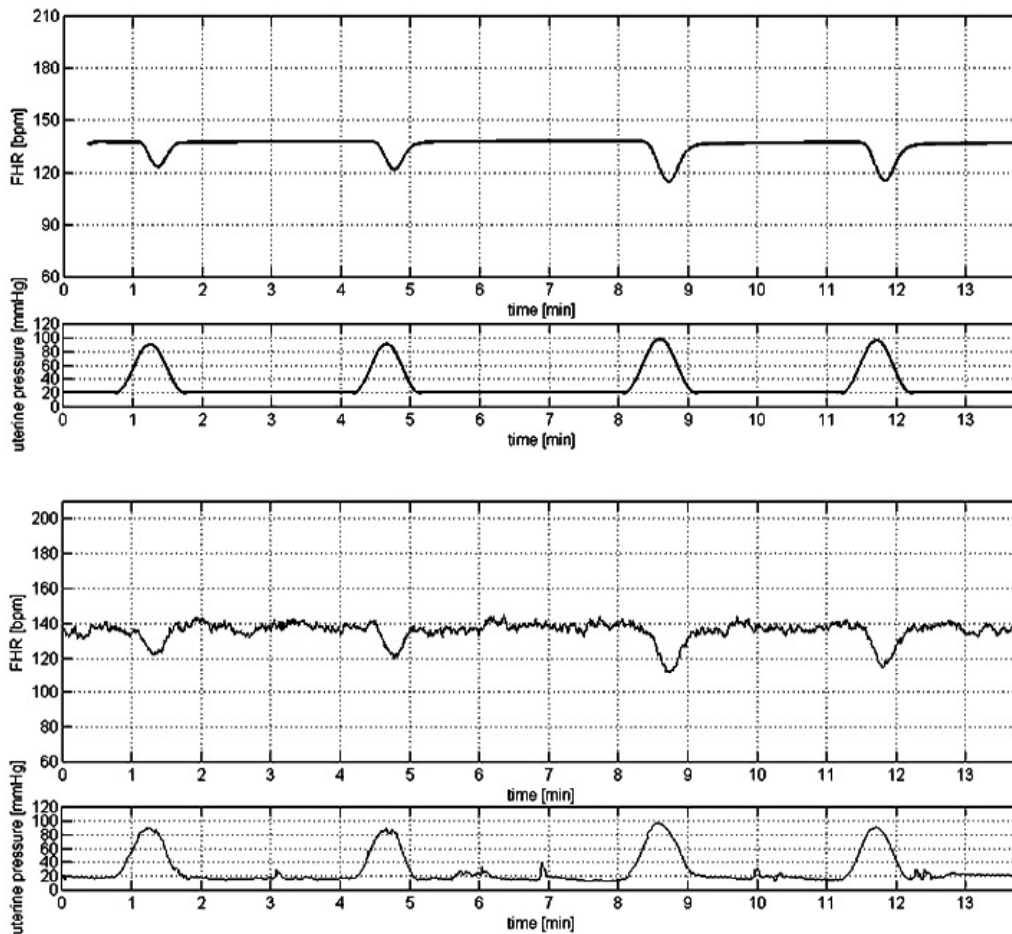


Figure 2.6: CTG signal as calculated with the model. Upper CTG: The fetal heart rate (FHR) is shown as function of time in relation to the uterine pressure, decelerations follow from vagal nerve hypoxia. Lower panel: for clinical evaluation, heart rate variability is added to the calculated heart rate signal from the model. Pressure variation is also added to the uterine pressure signal to obtain a more realistic tracing.

2.4 Discussion & conclusion

The model aims to link physiologic insights to heart rate changes during caput compression in labor as much as possible. The combination of contractions, hemodynamics, oxygen distribution and chemoreceptor reflex enables the study of the effect of maternal or fetal (local) cardiovascular changes on fetal hemodynamics and oxygen distribution.

Table 2.2: Validation results. *The number of not realistic marked items is too small for statistical analysis on this section.

	Real CTG tracings		Computer-generated CTG tracings		P-value
	[N]	[%]	[N]	[%]	
Rated items	N=285		N=293		
Realistic	201	[34.6]	204	[35.1]	0.48
Fairly realistic	83	[14.3]	87	[15.0]	0.46
Not realistic	1	[0.2]	5	[0.9]	* 0.34
Classification of CTG's	N=30		N=30		
Real	16	[26.6]	12	[20.0]	0.40
Computer-generated	9	[15.0]	10	[16.7]	0.56
Not distinguishable	5	[8.3]	8	[13.3]	0.44

Several models of the fetoplacental circulation have been published before. Some of these models have been developed to study doppler velocity waveforms in the fetal circulation to help to interpret clinical data from hemodynamical monitoring [15, 40, 96, 120]. The model of Pennati et al. [96] can be used for the investigation of pressure and flow rates in the complete arterial and venous circulation. Huikeshoven et al. [51, 52] were the first to develop a model of the fetoplacental circulation of the lamb, including oxygen distribution. Still the latter model lacks cardiovascular reflex control, and thus the ability to reproduce the CTG.

In our modeling approach of the cardiovascular system, we assumed that local differences in blood flow, pressure and pO_2 between other organs than the explicitly modeled uterine, umbilical and cerebral compartments are not important. Therefore these organs were lumped in one compartment: the systemic circulation. If other (patho)physiology is studied, the vascular tree might need to be modeled in more detail, e.g. in case of cardiac hypoxia or congenital cardiovascular anomalies. Furthermore, in the model maternal arterial oxygen concentration is kept constant, assuming sufficient oxygen supply towards the placenta. However, once maternal arterial oxygen concentration changes - e.g. due to inadequate breathing technique and/or oxygen administration - inclusion of the lung circulation and gas exchange in the lungs and tissues is necessary.

Even though we use average flow rates in the oxygen distribution model, we simulate the pulsatile character of cardiovascular hemodynamics using the one-fiber model. The parameters in this model have a clear physiological meaning, enabling for example a straightforward translation of changes in cardiac contractility and FHR into changes in flow. In addition, since the model distinguishes between geometric and material properties, as opposed to the often used time-varying elastance model [117], we can account directly for the effect of heart size. Finally, the one-fiber model predicts cardiac function not only at organ level (pressure, volume), but also at tissue level (stress, strain). Since tissue load is a stimulus for adaptation, the one-fiber model can help to study developmental changes in both the fetal and maternal circulation throughout pregnancy.

Model parameters are related as much as possible to physiology and are therefore scalable. Hence it was possible to obtain maternal hemodynamics from the non-pregnant situation by applying only three principles: 1) a scaling of volume related quantities ((unstressed) volumes, cardiac wall volume, compliances, inertances) to mimic the effect of physiologic blood volume and cardiac output increase by 40% [62], 2) a reduction of peripheral resistance by 20% [33], 3) and an increase of heart rate [33, 62, 106]. Further details can be found in the appendix. Fetal cardiac parameters were obtained from scaling as well: since fetal heart rate is approximately doubled in comparison with normal adult heart rate, all time-related parameters were divided by a factor two. Furthermore, fetal mean blood pressure is approximately 50% of adult blood pressure, hence cardiac stress level parameters were also divided by a factor two. Combined with literature data on fetal flow- and volume distribution, it was possible to obtain representative fetal term hemodynamics. Since blood pressure values were not available from human fetal measurements, we adopted the estimations of Struijk [116]. This seems reasonable, since their blood pressure estimations are in accordance with fetal sheep data [24].

The relation between uterine pressure and cerebral resistance (2.15) is central to the simulation of early decelerations. The contraction generator is a phenomenological description of contraction-induced uterine pressure, similar to the one proposed by Bastos et al. [10]. The model variables can be user-set to generate contractions of any length, amplitude and interval. Since no experimental data is available for the relation between uterine pressure and cerebral resistance, we modeled this relation according to the findings of Fung [31] and Rodbard [104] for soft-walled vessels and tuned the parameters for maximum response to a reference uterine contraction (see also the appendix).

The results show that the hemodynamics of mother and fetus can be represented with a relatively simple model. All output variables are close to the target data. As expected, during contractions with caput compression, only cerebral flow, cerebral pO_2 and FHR changed, thus representing the physiologic cascade leading to early decelerations. Placental baseline oxygen pressures are higher than reported in normal full term fetuses, despite normal fetal oxygen pressures and a flow distribution in accordance with measured data. However, it should be noted that oxygen pressure data - especially intervillous space oxygen pressure - differ considerably between individuals and are only scarcely available (see Table 2.1). Unfortunately there is no complete data set available of a fetus which reports all flow and oxygen values at different cardiovascular sites. The high oxygen pressures in the placenta may be caused by the neglect of shunt flow in our model. Parer [93] reports that only 70-90% of uterine blood flow and 80% of fetal umbilical flow partake in oxygen exchange. These high shunt flows will not only lead to lower placental, but also fetal pO_2 values. We did not attempt to improve model output by incorporating shunt flow, in view of the scarcity of experimental validation data.

Validation of the model was performed on two levels: internal variable validation (e.g. blood pressures, flows, etc.) and CTG validation. For basic condition, internal variables meet measured data, as follows from Table 2.1. However, it is not possible to validate each (internal)

variable change during early decelerations, since changes in hemodynamics, oxygenation and vagal nerve fire rate have not been measured under these circumstances. The majority of input parameters could be chosen on physiologic grounds (e.g. via scaling, see appendix), other parameters were set to match patient data from literature. However, these data are not from the same patient which may lead to discrepancies between model and (general) patient data.

The second validation method was done via experts' opinion. We used three rating levels: *realistic*, *fairly realistic* and *not realistic*. With two realistic and one non-realistic level, there is a risk of bias towards realism. However, the risk is the same for both computer-generated and real CTG's. The overall judgement of the clinical experts showed that there was no significant difference between real tracings and computer-generated tracings with respect to realism for each of the evaluated items. The experts also had difficulties to distinguish real tracings from computer-generated tracings. This suggests that the modeled CTG with early decelerations can be used in simulated scenarios to represent real CTG tracings with early decelerations.

The implementation of early decelerations in the model is a first step towards a training tool for understanding the CTG. Future applications should include late and variable decelerations that are more relevant clinically. Since all model parameters can be adapted at any time during a scenario, the model can be part of an educational training program, as it provides a lot of opportunities for studying and reproducing the manifestation of fetal welfare in the CTG.

In conclusion, we developed a mathematical model that predicts a realistic CTG during early decelerations in labor, based on a physiologic cascade consisting of uterine contraction, increased cerebral resistance, reduced cerebral flow, vagal nerve hypoxia and reduced fetal heart rate.

Appendix: Parameter assignment

The uterine pressure signal from the contraction generator provides a realistic master curve that varies per contraction in length T_{con} , strength p_{con} and interval T_{inter} by means of a random generator with a normal distribution. Parameter values of each contraction are thus based on a mean (which is the value for the first contraction) and a standard deviation. Parameter settings for the relation between uterine pressure and cerebral resistance (equation 2.15) could not be derived directly from experimental data. Instead we tuned the parameters to obtain a maximum response of -30 bpm for a contraction of 60 seconds and amplitude of 80 mmHg. This response can be user-reduced by decreasing W_{eff} . Table 2.3 represents the values used in this study for the contraction generator as used in Figure 2.6. The parameters are based on real CTG's with early decelerations (different than the CTG's used for the validation study).

All maternal model parameters (see Table 2.4) are based on pregnancy related changes in the vascular system as reported in literature. Parameter values for blood volume, arterial and venous

Table 2.3: Contraction parameters. The parameter values belong to the CTG from Figure 2.6.

Parameter	Value	Unit
p_{rest}	2.66	kPa
p_{con}	7.98 ± 0.67	kPa
T_{con}	50 ± 5	s
T_{inter}	210 ± 10	s
$c_{R,1}$	5	–
$c_{R,2}$	0.1	–
p_0	13.3	kPa
W_{ed}	0.67	–

Table 2.4: Maternal cardiovascular parameters.

Parameter	Value	Unit	Parameter	Value	Unit
V_w	196	ml	V_{total}	7000	ml
$V_{iv,0}$	$V_w/3$	ml	$V_{a,0}$	700	ml
$l_{s,0}$	2.0	μm	$V_{v,0}$	4200	ml
$l_{s,a0}$	1.5	μm	$V_{ut,0}$	500	ml
$l_{s,a1}$	2.0	μm	R_a	7	kPa · ms/ml
$\sigma_{f,0}$	0.6	kPa	R_{mc}	60	kPa · ms/ml
$\sigma_{r,0}$	0.15	kPa	R_v	3	kPa · ms/ml
$\sigma_{a,0}$	150	kPa	R_{pvs}	450	kPa · ms/ml
c_f	12	μm^{-1}	R_{utv}	90	kPa · ms/ml
c_c	1	μm^{-1}	C_a	42	ml/kPa
$\tau_{r,1}$	150	μs	C_v	840	ml/kPa
$\tau_{d,1}$	250	μs	C_{ut}	0.8	ml/kPa
a_r	100	$\mu\text{s}/\mu\text{m}$	L_a	42	kPa · ms ² /ml
a_d	400	$\mu\text{s}/\mu\text{m}$	$l_{s,0}$	0.01	$\mu\text{m}/\mu\text{s}$
			HR_0	0.5	1/s

compliances, unstressed arterial and venous blood volumes, and arterial and venous inertances were scaled from non-pregnant adult values with a volume factor of 1.4 to mimic 40 % cardiac output and blood volume increase [62] in pregnancy. Heart rate was increased from 65 bpm to 80 bpm [33, 62, 106]. Vascular resistance was decreased with 20 % [33]. The ratio between placental and systemic flow used was 1:9, based on a term cardiac output of 11.7 % [28]. Cardiac parameters were adopted from Bovendeerd et al. [12] only ventricular wall volume has been increased with the volume factor 1.4 to achieve a maternal term heart.

All fetal cardiovascular parameters (see Table 2.5) are set according to human values for a 3 kg fetus as available from literature, or else for the sheep fetus. Cardiac output was aimed at 425-450 ml/min/kg [82], with a stroke volume of 10 ml at an ejection fraction of 0.67 and heart rate of 135 bpm. Fetal cardiac parameters were scaled for pressure and time with respect to adult values for blood pressure and heart rate. Thus passive and active stress level parameters σ_{p0} and σ_{a0} were lowered by a factor 2; rise and decay time dependencies in active stress were shortened by a factor 2, while reference heart rate was increased with a factor 2. Total vascular compliance value (6.6 ml/mmHg or 50 ml/kPa) was adopted from Huikeshoven et al.

Table 2.5: Fetal cardiovascular parameters.

Parameter	Value	Unit	Parameter	Value	Unit
V_w	15	ml	V_{total}	330	ml
$V_{lv,0}$	$V_w/3$	ml	$V_{a,0}$	20	ml
$l_{s,0}$	2.0	μm	$V_{v,0}$	100	ml
$l_{s,a0}$	1.5	μm	$V_{um,0}$	90	ml
$l_{s,a1}$	2.0	μm	$V_{c,0}$	7.2	ml
$\sigma_{f,0}$	0.30	kPa	R_a	6.0	kPa · ms/ml
$\sigma_{c,0}$	0.07	kPa	R_{mc}	200	kPa · ms/ml
$\sigma_{a,0}$	75	kPa	R_v	30	kPa · ms/ml
c_p	12	μm^{-1}	R_{ummc}	698	kPa · ms/ml
c_a	1	μm^{-1}	R_{umv}	2	kPa · ms/ml
$\tau_{r,1}$	75	μs	$R_{cmc,0}$	1398	kPa · ms/ml
$\tau_{d,1}$	125	μs	R_{cv}	2	kPa · ms/ml
a_r	50	$\mu\text{s}/\mu\text{m}$	C_a	2.0	ml/kPa
a_d	200	$\mu\text{s}/\mu\text{m}$	C_v	35	ml/kPa
b_d	0.07	s^2	C_{um}	11	ml/kPa
HR_0	1.0	1/s	C_c	0.57	ml/kPa
$\dot{l}_{s,0}$	0.05	$\mu\text{m}/\mu\text{s}$	L_a	2	kPa · ms ² /ml

[51] including placental compliance. Arterial compliance was set to achieve a realistic arterial pressure rise with a stroke volume of 10 ml, and was one third higher than the original value of Huikeshoven et al. [51]. Cerebral compliance value was adopted from Pennati et al. [96]. The remainder was used for the venous compliance. Total blood volume was set at 110 ml/kg, [60, 67], of which one third is in the umbilical circulation [132]. During the normal heart cycle, the other two third was divided over the brain (8-11 ml, based on 12-17% fetal brain weight from total body weight [16, 47] and 2.22 ml/100g blood volume [131]), the heart (5-15 ml during heart cycle: 10 ml stroke volume at an ejection fraction of 0.67), the arteries (14% [41]) and the veins (remainder). Unstressed volumes were set to meet fetal blood pressure as estimated by Struijk [116]. Vascular resistance was divided according to a cardiac output distribution of 70% systemic, 20% umbilical [64] and 10% cerebral [66].

Oxygen model parameters (see Table 2.6) are adopted from Sá Couto et al. [108]. Total fetal oxygen consumption was divided over 12% cerebral [107] and 88% systemic consumption. Unfortunately this is a fetal lamb value, since no human data was available. Since oxygenation changes tremendously after birth [105], we did not adopt human neonatal values. Fetal cerebral oxygen consumption threshold was, similarly as peripheral consumption threshold, set at a half of normal value.

Regulation model parameters (see Table 2.7) are adopted from the adult regulation model of Ursino et al. [122]. For the majority of the parameters, a steady state was calculated and used in our implementation of the model. Fetal regulation parameters were scaled with respect to normal fetal arterial oxygen pressure and blood pressure.

Table 2.6: Oxygen distribution parameters.

Parameter	Value	Unit
D	$2.83 \cdot 10^{-8}$	$\text{m}^3 \text{O}_2/\text{s}/\text{mmHg}$
$cO_{a,m}$	$1.6 \cdot 10^{-1}$	$\text{m}^3 \text{O}_2/\text{m}^3 \text{blood}$
$cO_{mc,th}$	$6.8 \cdot 10^{-2}$	$\text{m}^3 \text{O}_2/\text{m}^3 \text{blood}$
$cO_{c,th}$	$3.9 \cdot 10^{-2}$	$\text{m}^3 \text{O}_2/\text{m}^3 \text{blood}$
$\dot{O}_{met,mc}$	$3.08 \cdot 10^{-7}$	$\text{m}^3 \text{O}_2/\text{s}$
$\dot{O}_{met,c}$	$4.20 \cdot 10^{-8}$	$\text{m}^3 \text{O}_2/\text{s}$
K_f	$9.33 \cdot 10^{-6}$	$\text{m}^3 \text{blood}/\text{s}$
α	$1.34 \cdot 10^{-6}$	$\text{m}^3 \text{O}_2/\text{g Hb}$
β	$3.1 \cdot 10^{-2}$	$\text{m}^3 \text{O}_2/\text{m}^3 \text{blood}/\text{mmHg}$
Hb_m	$12 \cdot 10^4$	$\text{g Hb}/\text{m}^3 \text{blood}$
Hb_f	$17 \cdot 10^4$	$\text{g Hb}/\text{m}^3 \text{blood}$
$c_{1,m}$	$2.34 \cdot 10^4$	mmHg^3
$c_{2,m}$	150	mmHg^2
$c_{1,f}$	$1.04 \cdot 10^4$	mmHg^3
$c_{2,f}$	150	mmHg^2

Table 2.7: Regulation parameters.

Parameter	Value	Unit
$f_{v,0}$	5.85	s^{-1}
$pO_{2,c,0}$	14.8	mmHg
f_{vh}	5	s^{-1}
$\Delta T_{,s}$	-0.3	s
T_0	0.21	s
$\tau_{T,v}$	1.5	s
$G_{T,v}$	0.09	s^2
$D_{T,v}$	0.2	s

**Simulation of reflex late decelerations in labor
with a mathematical model**

*M.B. van der Hout-van der Jagt, S.G. Oei and P.H.M. Bovendeerd
Published in: Early Human Development 2013;89:7-19*

Abstract

Fetal wellbeing during labor and delivery is commonly monitored through the cardiotocogram (CTG), the combined registration of uterus contractions and fetal heart rate (FHR). From the CTG, the fetal oxygen state is estimated as the main indicator of the fetal condition, but this estimate is difficult to make, due to the complex relation between CTG and oxygen state.

Mathematical models can be used to assist in interpretation of the CTG, since they enable quantitative modeling of the flow of events through which uterine contractions affect fetal oxygenation and FHR. We propose a mathematical model to simulate reflex “late decelerations”, i.e. variations in FHR originating from uteroplacental flow reduction during uterine contractions and mediated by the baroreflex and the chemoreflex.

Results for the uncompromised fetus show that partial oxygen pressures reduce in relation to the strength and duration of the contraction. Above a certain threshold, hypoxemia will evoke a late deceleration. Results for uteroplacental insufficiency, simulated by reduced uterine blood supply or reduced placental diffusion capacity, demonstrated lower baseline FHR and smaller decelerations during contraction. Reduced uteroplacental blood volume was found to lead to deeper decelerations only. The model response in several nerve blocking simulations was similar to experimental findings by Martin et al. [78], indicating a correct balance between vagal and sympathetic reflex pathways.

3.1 Introduction

For the monitoring of fetal wellbeing during labor and delivery, ideally oxygenation status should be available. However, in current clinical practice only fetal heart rate and uterine contractions can be monitored continuously. The combined record of these signals is called the cardiotocogram (CTG). As oxygenation status is reflected in the fetal heart rate, the CTG is often used to monitor fetal welfare.

A clinically important case of reduced oxygenation occurs in uteroplacental insufficiency (UPI), where oxygen delivery to the fetus cannot satisfy demand, e.g. due to decreased uterine blood flow or decreased transport across the placental membrane [30]. UPI can affect FHR at different levels: it can reduce FHR baseline and variability, but also evoke uniform periodic changes in FHR, the so-called late decelerations [29, 30, 44, 78, 94]. Late decelerations in the FHR signal appear as a gradual decrease and return to FHR baseline, that is delayed (>30 seconds) with regard to the contraction signal [76, 103]. In current clinical practice, late decelerations on the CTG are classified as *abnormal* according to internationally accepted guidelines [2, 29, 76, 103]. There are two known mechanisms that lead to late decelerations: myocard hypoxemia and reflex feedback [44, 78, 91]. In the case of myocard hypoxemia FHR decreases because of lack of oxygen delivery to the heart. In the case of *reflex* late decelerations the reduction of FHR is caused through chemo- and baroreceptor activation following transient reduction of oxygen delivery to the fetus during contractions [44, 78, 91].

Clinical use of the CTG requires insight into the relation between oxygenation and heart rate. Animal experiments have provided qualitative insight in this relation. Martin et al. [78] proposed a conceptual model that depicts the different pathways that lead to reflex late decelerations in fetal sheep (see also Figure 3.1). During labor, contractions are believed to reduce uteroplacental flow [39], thereby reducing oxygen diffusion over the placental membrane. In non-compromised fetuses, oxygen reserves are sufficient to compensate for this temporary reduction of oxygen delivery. In fetuses with uteroplacental insufficiency, the contraction will lead to transient hypoxemia that triggers the chemoreceptor. This receptor activates the vagal and sympathetic centers that affect four effectors, i.e. heart rate, contractility, peripheral resistance and venous unstressed volume. These changes in cardiac and vascular parameters result in changes in blood pressure that trigger the baroreceptor. This receptor in turn also activates the vagal and sympathetic centers, again leading to changes in the four effectors. In addition to this central reflex mechanisms, local autoregulation mechanisms, e.g. in the brain, cause local vasodilation that also affect oxygen pressure and blood pressure levels. The final change in FHR depends in the balance between the various feedback mechanisms.

The extent to which arterial oxygen level and blood pressure are restored provides information on the reflex mechanisms. With regard to the baroreceptor feedback Martin et al. [78] reported increased arterial blood pressure during late decelerations, but the subjects in a study by Parer et al. [91] had either identical, increasing or decreasing blood pressure. Itskovitz et al. [53] did

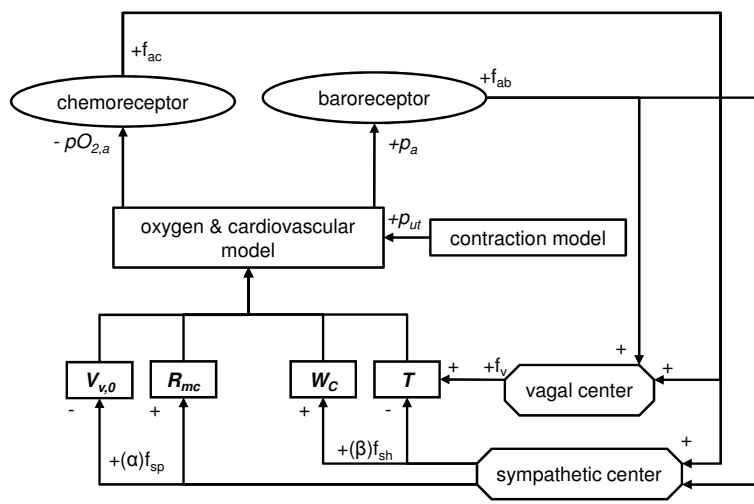


Figure 3.1: Block diagram of the role of the nervous system in late decelerations. A late deceleration is triggered by a uterine contraction that is converted into an increase of the uterine pressure p_{ut} reduces blood flow and oxygen transport to the fetus. Reduced arterial oxygen pressure ($pO_{2,a}$) triggers the chemoreceptor to stimulate the vagal and sympathetic centers via an afferent fire rate (f_{ac}). The efferent vagal fire rate f_v induces an increase in heart period T , whereas the efferent sympathetic fire rate to the heart $(\beta)f_{sh}$ induces a counteracting decrease in heart period, along with an increase in cardiac contractility W_C . The efferent sympathetic fire rate to the vessels $(\alpha)f_{sp}$ induces an increase in peripheral resistance R_{mc} and a decrease in venous unstressed volume $V_{v,0}$. These changes in cardiac and vascular parameters result in a change in arterial blood pressure p_a that triggers the baroreceptor to stimulate the vagal and sympathetic centers via an afferent fire rate f_{ab} . An increase in blood pressure leads to an increase in heart period, through both the vagal and sympathetic pathway. In addition, it leads to a decrease in contractility, a decrease in peripheral resistance and an increase in venous unstressed volume through the sympathetic pathway. Fetal heart rate, the inverse of the heart period, follows from vago-sympathetic balance.

not observe significant changes in blood pressure. To better understand the relative contribution of the individual components of the fetal cardiovascular regulatory mechanism, Martin et al. [78] also investigated the effect of selectively blocking various neuronal pathways. Yet, our insight in the complex relation between oxygenation and heart rate remains incomplete, making interpretation of the CTG to determine fetal oxygen state a difficult task.

Mathematical models can be used to assist in interpretation of late decelerations in the CTG, since all subsystems that contribute to heart rate regulation can be investigated individually. Previously, we used a mathematical model to investigate early decelerations [124] that are mediated by the chemoreceptor reflex only. In the current study, we extend this model with the baroreceptor reflex and use it to reproduce and study the reflex pathways involved in late de-

celerations. Therefore we investigate both the normal situation and various scenarios of UPI. Additional simulations are performed with blocked neuronal pathways to validate model outcome with experimental data from Martin et al. [78]. In its current state, the model serves as a research tool to understand better the complex relation between oxygenation and FHR. When extended with a user interface, either screen based or in the form of a mannequin, it might be used for individual and team training. The model also serves as a basis for a decision support tool in obstetric practice.

3.2 Materials & Methods

3.2.1 Mathematical model

The model consists of several modules, describing cardiovascular function, uterine contraction, oxygen delivery and cardiovascular regulation. Figure 3.2 gives an overview of the modules. The first three modules have been presented in detail before [124], see also Figure 3.3, and will be briefly described here and in the appendix. The regulation module is described in more detail.

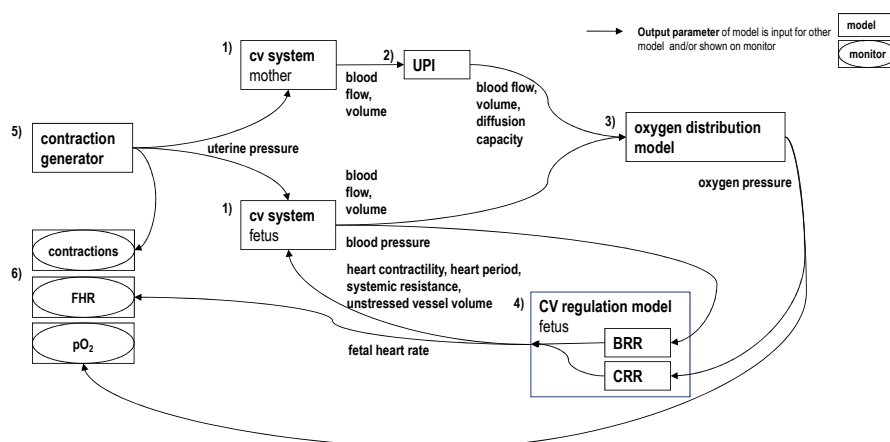


Figure 3.2: Block diagram of the feto-maternal model. Block diagram of the feto-maternal model. (1) The cardiovascular (cv) system of mother and fetus is separate. (2) Uteroplacental insufficiency affects maternal parameters in the circulation and/or in the placenta. (3) Oxygen distribution in mother and fetus is determined by fetal oxygen consumption, blood ow and volume, oxygen exchange in the placenta and arterial oxygen level in the mother. (4) Blood pressure and oxygen pressures in the fetus are monitored by the baro- and chemoreceptor reflexes (BRR and CRR respectively), and may evoke changes in cardiovascular parameters, including fetal heart rate. (5) Changes in uterine pressure (from uterine contractions) may alter blood pressure and ow in the fetal or maternal circulation, since these exert an external pressure on the intra-uterine blood vessels. (6) The cardiotocogram follows from the individual signals. Partial oxygen pressure provides additional information. Adapted from [124].

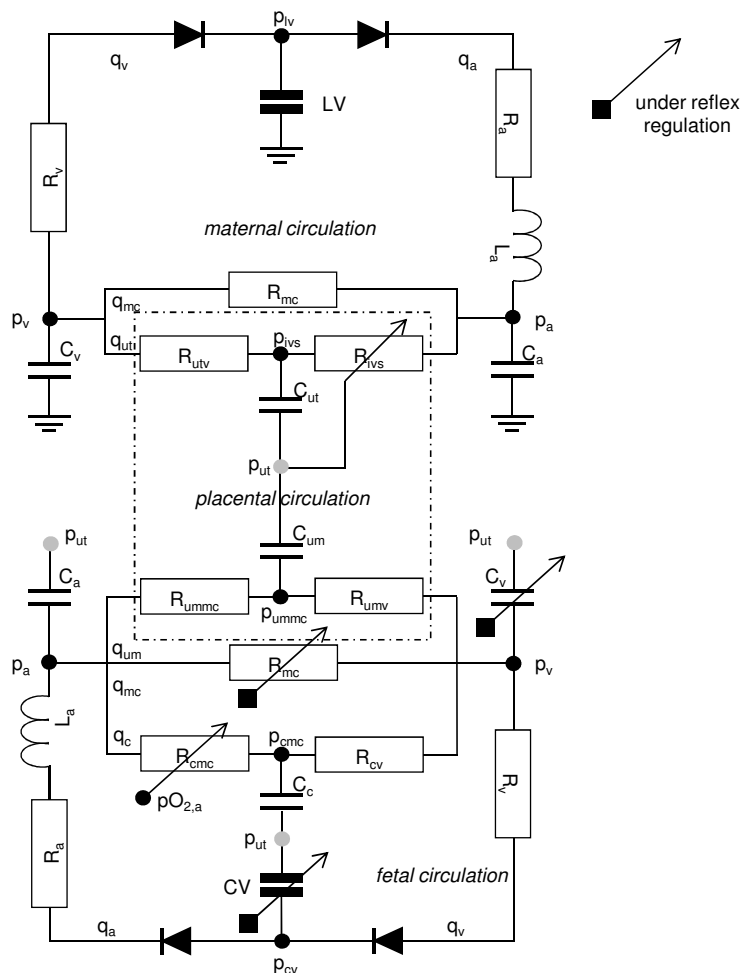


Figure 3.3: Electric analog of the feto-maternal cardiovascular model to compute pressures p and flows q . The maternal arteries (subscript a, with resistance R , inertance L and compliance C) receive blood from the left ventricle (LV). The uterine circulation (ivs and utv: intervillous space and uterine veins) and the remainder of the systemic microcirculation (mc) run in parallel and fuse in the venous circulation (v). Retrograde ow in the heart is prevented via valves. Intervillous space resistance R_{ivs} is dependent on uterine pressure p_{ut} . In the fetus, the combined ventricle (CV) forwards blood towards the arteries (a). Three compartments run in parallel: the cerebral (cmc, cv), umbilical (ummc, umv), and systemic circulation (mc). They all fuse in the venous compartment (v). Fetal cerebral microcirculation resistance is dependent on arterial pO_2 through local autoregulation. Venous compliance and volume, systemic resistance in the microcirculation, cardiac contractility and heart period are all under reflex regulation. The uterine and all fetal compliances experience external uterine pressure (p_{ut}). Adapted from [124].

3.2.1.1 Cardiovascular function

The vascular tree is modeled separately for mother and fetus, both with a systemic circulation in parallel to the placental circulation (see Figure 3 for an electrical analog). For the fetus, the

cerebral tree is also explicitly modeled (in parallel). Properties of the (blood in the) vascular tree are represented by discrete elements. A resistance R accounts for the characteristic impedance of the large arteries and veins and the viscous pressure loss in the small vessels. An inertia L accounts for resistance of the blood to acceleration in the arterial compartments. A capacitance C accounts for the ability of the large vessels to store blood, where pressure starts to build up once vascular volume exceeds the (unstressed) volume V_0 . The valves are modeled as ideal diodes.

Maternal cardiac function is modeled with the left ventricle, for the fetus a combined ventricle is used. The one-fiber model [5] is used to relate cardiac pressure p and volume V to myofiber stress via sarcomere length. Myofiber stress consists of an active part, related to cross-bridge formation and a passive part, related to matrix formation. Active stress is proportional to a contractility parameter W_C , where $W_C = 1$ represents normal contractility. It is initiated every heartbeat at a cycle time T .

The cardiovascular model is subject to influences from uterine contractions and regulation. As shown in Figure 3.3, uterine contractions affect hemodynamics of mother and fetus through changes in uterine pressure p_{ut} , that acts as an external pressure to the uterine vessels and all fetal vessels and the fetal heart. It may also affect the resistance R_{ivs} of the vessels in the intervillous space. As shown in Figures 3.1 and 3.3, the baroreflex and the chemoreflex affect three components in the cardiovascular model, the heart (through changes in contractility W_C and heart period T), the peripheral vessels (through changes in the peripheral resistance R_{mc}) and the veins (through changes in the unstressed venous volume $V_{v,0}$). In addition, cerebral autoregulation causes cerebral resistance R_{cmc} to vary in response to cerebral arterial oxygen content.

3.2.1.2 Uterine contraction

The effect of uterine contractions is modeled through changes in uterine pressure p_{ut} with a sine quadratic function to mimic the contraction shape. The interval, duration and contraction strength can be varied from contraction to contraction. Uterine contractions are responsible for uterine flow reduction through an increase of the resistance of the vessels in the intervillous space [39, 71]. We used a sigmoidal function [31, 104] to describe this increase. Parameters were chosen such that the transition from minimum to maximum resistance occurs for uterine pressures between 35 and 65 mmHg [71].

3.2.1.3 Oxygen distribution

The model for oxygen distribution is based on the work of Sá Couto et al. [108] and was described before [124]. In short, oxygen concentration in a vessel compartment is determined by the interplay between metabolic uptake and diffusive and convective transport. Convective transport represents oxygen delivery through blood flow, and thus takes place in all blood

vessels. Diffusion takes place in the placenta only (intervillous space and villous capillaries). Metabolic uptake, i.e. oxygen consumption, takes place in all microcirculation compartments. It is modeled as constant during normoxia, but reduces linearly with oxygen content once this content drops below a threshold value [108, 124].

In the present study we simulate the condition of uteroplacental insufficiency (UPI), that leads to a decrease in oxygen diffusion over the placental membrane. This diffusive transport \dot{O}_{diff} is determined by the difference in oxygen pressure pO_2 between the intervillous space and the umbilical microcirculation. In turn, the oxygen pressure in the intervillous space is determined from the balance between convective and diffusive transport to the intervillous space. The blood volume in the intervillous space is taken as 35% from the total uteroplacental blood volume. The relation between oxygen concentration and partial oxygen pressure is described with the oxygen dissociation curve which is different for mother and fetus [54, 111]. Reduced oxygen supply during UPI can be due to reduced diffusion capacity (DC), placental flow (q_{ut}), uteroplacental blood volume (V_{ut}) or maternal oxygenation status (pO_2 and cO).

3.2.1.4 Regulation

The regulation model is based on the work of Ursino et al. [122]. Deviations in arterial blood pressure and oxygen pressure are sensed by the receptors, processed in the central nervous system in the sympathetic and vagal centers and result into changes of cardiac contractility, heart period, resistance of the peripheral vessels and unstressed volume of the veins.

The first step in the regulation process involves the receptors (see appendix for mathematical details). The baroreceptor responds to rise of arterial pressure p_a above a reference pressure $p_{a,n}$ through an increase in its afferent fire rate f_{ab} . The arterial oxygen pressure level is translated into three fire rates. As a main effect, the arterial chemoreceptor responds to a decrease in arterial oxygen pressure pO_2 through an increase in its afferent fire rate f_{ac} . In addition, the central nervous system may respond to a decrease in pO_2 by changing the threshold fire rates for sympathetic activity to heart $f_{sh,o}$ and vessels $f_{sp,o}$. These threshold fire rates are constant during normoxia, but decrease when arterial oxygen pressure drops below a threshold values $pO_{2,n,sh}$ and $pO_{2,n,sp}$, for activity to the heart and the vessels, respectively. Finally, cerebral hypoxia may lead to an increase in vagal offset $f_{v,o}$. This offset fire rate is zero during normoxia, but increases when cerebral oxygen pressure drops below a threshold value $pO_{2,n,c}$.

The second step involves the central nervous system, where the afferent and threshold fire rates are processed by the sympathetic and vagal centers (see appendix). The vagal center increases its efferent fire rate f_v in response to increases in the baroreceptor fire rate f_{ab} , the chemoreceptor fire rate f_{ac} and the offset vagal fire rate $f_{v,o}$. The sympathetic center has two efferent pathways, the alpha-sympathetic pathway that affects the vessels and the beta-sympathetic pathway that affects the heart. Both pathways increase their fire rate with increasing chemoreceptor fire rate f_{ac} , decreasing baroreceptor fire rate f_{ab} , and decreasing threshold fire rates $f_{sh,o}$ or

$f_{sp,o}$.

The third step involves the effect of the vagal and sympathetic fire rates on heart and vessels (see appendix). An increase of the vagal fire rate f_v leads to an increase of the heart period T . An increase of the beta-sympathetic fire rate f_{sh} leads to a decrease of the heart period T and an increase of cardiac contractility W_C . An increase of the alpha-sympathetic fire rate f_{sp} leads to a decrease of the venous unstressed volume $V_{v,0}$ and an increase of peripheral resistance R_{mc} .

Apart from the central regulation, cerebral autoregulation is included, through which cerebral resistance R_{cmc} varies between a minimum and maximum depending on cerebral arterial oxygen content (see appendix).

Many input-output relations in the regulatory model are nonlinear, this is detailed in the appendix. In addition both the receptor and the effector models include low-pass filtering and delay times, at a typical time scale of 0.2-5 s.

The overall effect of the regulation model is that an increase in blood pressure evokes a baroreceptor response that leads to a decrease in heart rate and contractility, a decrease in vascular resistance and an increase in venous unstressed volume. This will lower the blood pressure. A decrease in oxygen pressure evokes a somewhat contradictory response. Through the vagal pathway it leads to a decrease in heart rate, thus lowering blood pressure and cardiac output. Through the beta-sympathetic pathways it leads to an increase in heart rate and contractility, thus increasing blood pressure and cardiac output. Through the alpha-sympathetic pathways it leads to a decrease in venous unstressed volume, which increases blood pressure and cardiac output, and an increase in peripheral resistance, which increases blood pressure but reduces cardiac output. The final effect in terms of changes in blood pressure, cardiac output, oxygen state and heart rate depends on the balance between these individual effects.

Parameter settings for all modules can be found in the appendix.

3.2.2 Simulation protocol

The cascade following contraction-induced hypoxemia in a term fetus is investigated with simulations with an intact nervous system and simulations with blocked neuronal pathways.

3.2.2.1 Model simulations with intact nervous system

Simulations with intact nervous system are performed to investigate the overall model response during late decelerations. This is done both for fetuses with and without UPI. Parameter settings per simulation can be found in Table 3.1.

Uncompromised fetus

Table 3.1: Settings for simulations with intact nervous system. For the UPI simulations, only the parameter values that differ from the reference situation are given.

Parameter	Uncompromised	UPI			Unit
	$p_{ut,ref}$	UPI-BUF	UPI-DIF	UPI-FLOW	
$V_{ut,0}$	500	250			ml
DC	$2.83 \cdot 10^{-8}$		$1.42 \cdot 10^{-8}$		$m^3 O_2/s/mmHg$
$R_{ivs,0}$	450			990	kPa · ms/ml

The uncompromised fetus is simulated with a reference contraction with a duration of 60 s and an amplitude of 70 mmHg, which is referred to as $p_{ut,ref}$. This is a reference situation with maximal effect on uterine flow reduction to investigate model response to uterine contractions without UPI.

UPI

As opposed to the simulation with the uncompromised fetus, uteroplacental insufficiency is simulated by changing one of three oxygen supply-related parameters with a factor two. Firstly, in simulation UPI-BUF, where uteroplacental blood volume is reduced by 50% to reduce the oxygen buffer function of the placenta. Secondly, in simulation UPI-FLOW the uteroplacental resistance is doubled (where R_{ut} is the sum of R_{ivs} and $R_{ut,v}$), to reduce convective oxygen transport to the placenta by 50%. Thirdly, in simulation UPI-DIF the placental diffusion capacity is decreased by 50% to reduce diffusive transport of oxygen. Parameter settings are listed in Table 3.1.

Contraction variations

To investigate the relation between contraction strength, duration and interval on oxygenation and fetal heart rate in the uncompromised fetus, a series of contractions is simulated based on the reference contraction. The series consists of three contractions with half the amplitude of the reference contraction, followed by three reference contractions, then three reference contractions with a doubled interval (4 minutes instead of 2), and finally three contractions with double duration of the reference contraction. To enhance clinical interpretation, artificial FHR variability and high frequency variations in the uterine contraction signal are added to the CTG as described before [124].

3.2.2.2 Model simulations with blocked neuronal pathways

To investigate model response on the level of neuronal pathways, simulations are performed in which the three pathways are blocked one at a time. Blocking of the alpha receptors is simulated by fixing alpha-sympathetic nerve fire rate f_{sp} at its normal level. Hence the effectors unstressed venous vessel volume ($V_{v,0}$) and peripheral resistance (R_{mc}) cannot respond to alpha activity following chemo- and baroreceptor activation. Blocking of the beta receptors was done via fixed beta-sympathetic nerve fire rate f_{sh} . Cardiac contractility (W_C) and heart period (T)

Table 3.2: Fixed fire rates used in model simulations with blocked neuronal pathways.

Blockade type	Parameter	Value	Unit
alpha	f_{sp}	25	s^{-1}
beta	f_{sh}	10.7	s^{-1}
vagal	f_v	5.8	s^{-1}

cannot respond to chemo- and baroreceptor activation, as they are the effectors of beta activity. The vagal nerve was blocked via a fixed vagal nerve fire rate f_v . Hence the effector heart period (T) cannot respond to chemo- and baroreceptor activation. Parameter settings for the blocking studies can be found in Table 3.2. Model outcome is compared to experimental data from Martin et al. [78], who invoked hypoxemia by directly by periodic occlusion of the maternal hypogastric artery. In our model this protocol was mimicked by varying uterine resistance R_{ivs} according to the reference contraction ($p_{ut,ref}$), while keeping the uterine pressure p_{ut} acting upon the fetus constant.

3.3 Results

3.3.1 Intact nervous system

3.3.1.1 Uncompromised fetus

The results of the reference contraction are shown in the left panel of Figure 3.4. It can be seen that the reference uterine contraction leads to a reduction of uterine flow to zero and transient arterial hypoxemia. Mean arterial pressure (MAP) is hardly affected, but FHR reduces with 15 bpm. FHR deceleration delay with respect to the uterine pressure signal mainly originates from the delay in arterial pO_2 following uterine flow reduction (31 seconds between both nadirs, 33 seconds after the top of the contraction). The nadir of the FHR coincides approximately with the nadir of pO_2 reduction indicating that the delay in the regulation process is minor.

In the oxygen distribution graph (Figure 3.5) it can be seen (left panel) that pO_2 reduces at all sites of the fetoplacental circulation. In the cerebral microcirculation, pO_2 reduction is less than in the systemic circulation, due to autoregulation in the brain and reflex vasoconstriction in the systemic circulation. The change in cerebral and peripheral resistance leads to a redistribution of flow, increasing flow in the brain at the expense of systemic flow (see lower left graph). The umbilical flow remains constant.

3.3.1.2 UPI

Results of UPI simulations are shown in the right panel of Figure 3.4. Reduction of uteroplacental blood volume $V_{ut,0}$ (UPI-BUF) reduces the oxygen buffer function of the placenta.

While arterial oxygen pressure is not affected at baseline, it is reduced more in response to the contraction (-0.5 mmHg) when compared to the reference contraction. There is no extra effect on MAP, but FHR is reduced with an additional 4 bpm.

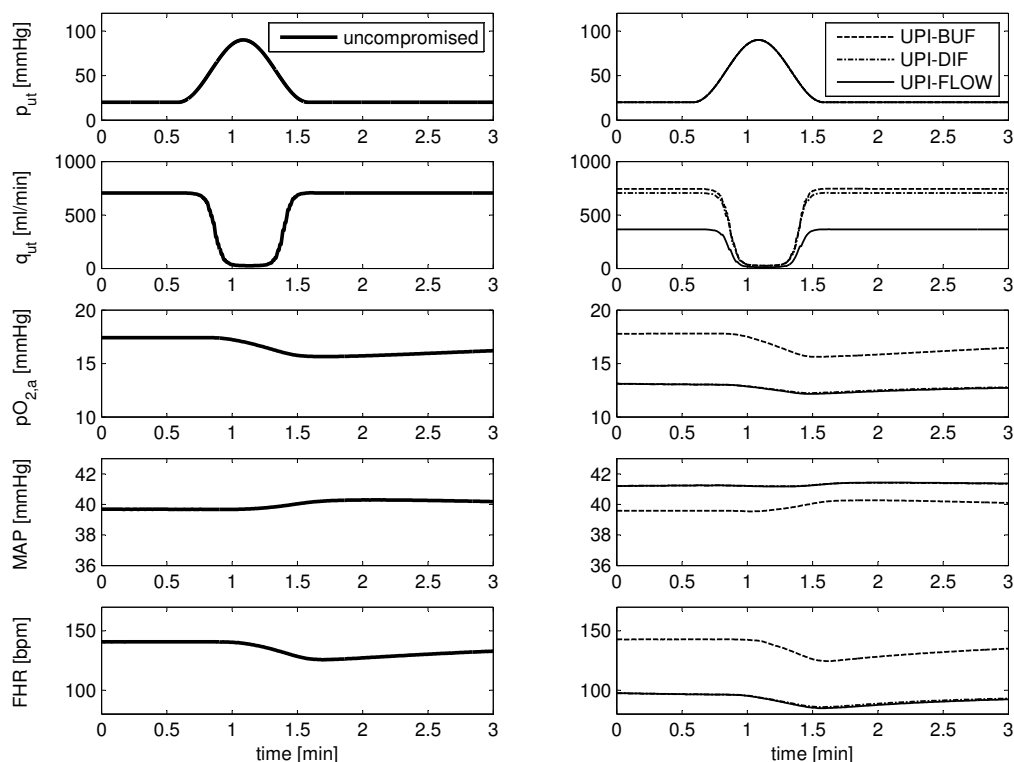


Figure 3.4: Simulation results for normal labor and UPI. Left: With the reference contraction $p_{ut,ref}$, uterine flow q_{ut} reduces to zero. Arterial oxygen pressure pO_2 reduces by 2 mmHg, mean arterial pressure MAP increases with 1 mmHg and FHR drops by 10 bpm. Right: In the UPI simulations, reduced oxygen supply (via reduction in diffusion capacity (UPI-DIF) and flow (UPI-FLOW)) leads to baseline decrease of pO_2 and FHR, and minor response of pO_2 and FHR during the contraction. Reduced oxygen buffer (UPI-BUF) does not affect baseline values, but leads to faster and stronger reduction of pO_2 and FHR during the contraction.

A 50% reduction in either baseline uterine blood flow (UPI-FLOW) or placental diffusion capacity (UPI-DIF) leads to the same hypoxic response. With respect to the non-UPI reference contraction, oxygen pressure is reduced already in baseline situation with 4 mmHg. In response to the contraction, oxygen pressure reduces only by a little extra (-1 mmHg). The corresponding MAP is slightly increased at baseline level (+1.5 mmHg) and hardly affected during the contraction. Baseline FHR is reduced with 44 bpm with respect to the reference situation. The deceleration depth is only 11 bpm.

In UPI, the nadir of both pO_2 reduction and FHR deceleration is achieved somewhat earlier

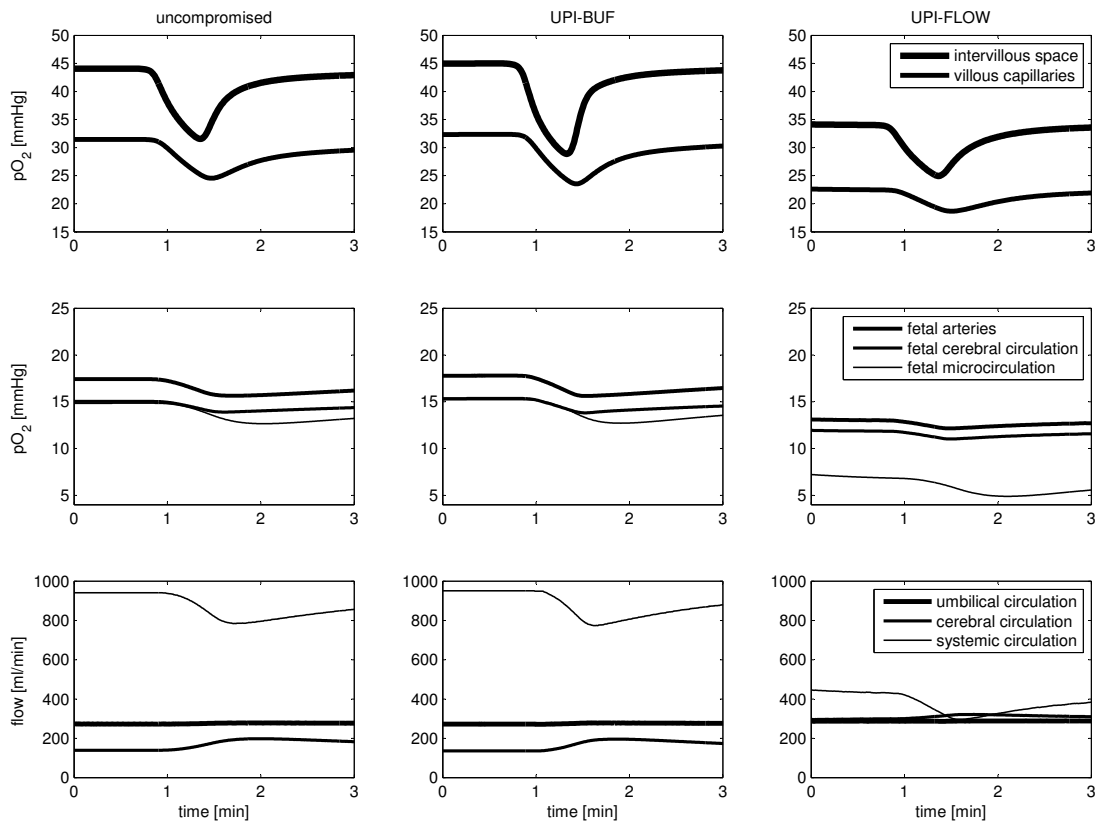


Figure 3.5: Partial oxygen pressures and flow redistribution. All partial oxygen pressures (pO_2) reduce during a uterine contraction. Left: Uncompromised fetus. Temporary pO_2 reduction in the intervillous space (due to the contraction) leads to reduction in pO_2 in the umbilical circulation. This influences the pO_2 in the fetal arterial and microcirculation, where the cerebral microcirculation is less affected than the systemic circulation due to flow redirection, as demonstrated in the bottom panel. Middle: uteroplacental volume reduction to 50% (UPI-BUF). Changes in pO_2 are more pronounced and more steep; pO_2 in the systemic microcirculation is even more reduced while pO_2 in the cerebral microcirculation is hardly changed in comparison with the reference situation. Baseline levels are not affected. Flow redistribution is earlier achieved (bottom panel). Right: Uteroplacental flow reduction of 50% (UPI-FLOW). Baseline pO_2 is reduced at all sites; in the cerebral microcirculation pO_2 is almost equal to arterial pO_2 , while systemic microcirculation pO_2 is even further reduced as a result of flow redistribution (bottom panel). Additional response to the contractions is less steep and deep than for the reference situation.

(10 seconds) than without UPI. As can be seen from the right panel in Figure 3.4, the level of FHR is directly related to the arterial pO_2 level: baseline reduction of pO_2 leads also to FHR baseline reduction, while transient reduction in pO_2 leads to a FHR deceleration.

The oxygen and flow distribution graph (Figure 3.5) shows that uteroplacental volume reduction leads to flow redistribution during contractions, but not in between them. In contrast, reduced oxygen supply, either through an increased uterine resistance or a decreased diffusion capacity, leads to flow redistribution in between contractions already. The absolute minimum of cerebral pO_2 is only slightly lower for cases with pre-existing hypoxemia. Partial oxygen pressures for the case of reduced diffusion capacity (not shown) are virtually identical to those of increased resistance.

3.3.1.3 Contraction variations

Results of contraction variations on oxygenation and FHR are shown in Figure 3.6. It can be seen that small contractions lead to small reductions in pO_2 that barely evoke a FHR deceleration. With the series of the reference contractions, pO_2 baseline level is not achieved before the next contraction and thus leads to deteriorating pO_2 . An increase in contraction interval allows baseline to restore and leads to identical decelerations for each subsequent contraction. However, with longer contractions, pO_2 is not restored to baseline anymore before the next contraction. Fetal heart rate follows the shape of the pO_2 signal almost instantaneously: the decelerations are deeper when oxygen level is more reduced and longer when pO_2 baseline is not yet achieved.

3.3.2 Neuronal blocking

Results for the neuronal blocking simulations are shown in Figure 3.7.

3.3.2.1 Alpha blockade

Alpha blockade leads to a slightly more pronounced reduction in pO_2 following a contraction (see first column in Figure 3.7). As peripheral vasoconstriction and venous unstressed volume changes are blocked, MAP reduces slightly during hypoxemia (-1 mmHg). The late deceleration is only slight and followed by a “late acceleration” (both 2 bpm change from baseline) as the vagal component from the baroreceptor is not activated.

3.3.2.2 Beta blockade

During beta blockade, the response of pO_2 to uterine flow reduction is similar to that without blockade (see second column in Figure 3.7). MAP and FHR response are virtually identical.

3.3.2.3 Vagal blockade

Vagal blockade also does not affect pO_2 response (see third column in Figure 3.7). As cardiac stimulation via the vagal center is blocked, MAP cannot be maintained during hypoxemia and

increases further due to the lack of cardiodeceleration. A “late acceleration” (+3 bpm) is seen in response to hypoxemia, as vagal cardiodecelerative effects are blocked. FHR is also slightly increased in baseline (+3 bpm).

3.4 Discussion & conclusion

We developed a model that can be used to reproduce reflex late decelerations in uteroplacental insufficiency. The model response of the reflex pathways is in accordance with the conceptual model of Martin et al. [78]. In the model, contractions evoke a cascade of events that lead to late decelerations. The depth of the deceleration depends on the balance between counteracting cardioaccelerative and cardiodecelerative effects from the vagal and sympathetic centers, induced by inputs from the chemoreceptor and the baroreceptor (Figure 3.1). During the contraction, arterial blood pressure is hardly affected, indicating the effectiveness of the baroreflex mechanism. Oxygen pressure is reduced, but cerebral oxygen pressure is maintained fairly well, due to a redistribution of blood flow in response to vasodilation of the cerebral vessels and vasoconstriction of the peripheral vessels. The delay between the uterus contraction and the change in FHR is dominated by the delay in the drop of fetal oxygen pressure.

Our model simulations for the uncompromised fetus show the results for complete uterine flow interruption during uterine contractions. In general, the depth of the deceleration will be dependent of the amplitude, duration and frequency of contractions [39]. As an example, we varied the contraction amplitude to detect the threshold leading to a minimal deceleration, that would be just above the detection limit in clinical practice. This detection limit was chosen as a deceleration depth of -3 bpm. The corresponding contraction amplitude was found to be 32 mmHg. This contraction reduces uterine blood flow with 50%, which leads to a decrease in fetal arterial pO_2 of 0.7 mmHg. This reduction hardly triggers the vagal nerve and hence maximum FHR reduction is 3 bpm. This threshold contraction indicates that with a contraction duration of 60 s, a contraction amplitude of more than 32 mmHg leads to a late deceleration.

Three mechanisms of uteroplacental insufficiency were included: reduced uteroplacental blood volume, reduced placental flow via resistance increase and reduced placental diffusion capacity. During simulations with uteroplacental volume reduction, oxygen buffer diminished in the placenta, and thus led to a quicker and more pronounced reflex response with a deeper and slightly earlier deceleration (Figure 3.4). There are no baseline effects, as the buffer function becomes relevant only during contractions. Simulations with a decrease in placental diffusion capacity gave a similar effect as a decrease in placental blood flow. Already at baseline an effect is present that follows from a continuous oxygen deficiency: f_{ac} is thus continuously higher and in the upper saturation of the sigmoidal curve that relates f_{ac} to oxygen content. Hence flow redistribution has already taken place (Figure 3.5) and baseline FHR is lower than without UPI (Figure 3.4). These responses to reduced uterine blood flow are also observed in fetal sheep [57, 114, 115]. A further reduction in oxygen due to the contraction thus has a small additional

effect only, as saturation restricts further response. Blood pressure effects are not present in our simulations, although in sheep blood pressure is slightly increased, but not always significantly [114, 115]. In our simulations the maximum reduction of FHR is achieved earlier during UPI than during normal conditions. This finding is in agreement with results from a study by Itskovitz et al. [53], who found a shorter delay in the onset of bradycardia for sheep fetuses if pO_2 was lowered already. Their explanation is that this delay represents the time necessary for pO_2 to fall below the threshold for chemoreceptor activation. Our simulations show that the shorter delay results either from a lower baseline level pO_2 , caused by a reduced baseline uterine flow or placental diffusion capacity, or from a smaller oxygen buffer, due to a reduced uteroplacental blood volume. Since we do not account for the transit time of umbilical blood to the peripheral and cerebral circulation [3], our lag times are likely to underestimate real lag times.

The simulation with contraction variations shows the influence of contraction interval, strength and duration on arterial oxygen level and fetal heart rate (Figure 3.6). The contraction sequence gives an indication of the possibilities of the model to respond to different contractions. By prescribing the contraction-related variables (duration, interval strength) and by adding FHR variability and high-frequency variation in the contraction signal, numerous CTG tracings with late decelerations can be generated for use in a simulated clinical environment and for educational purposes.

Where the overall reaction to oxygen reduction during uterine contractions can be studied with an intact nervous system [53, 78, 91], insight into the individual contribution of these pathways can be increased with the neuronal blocking studies [78]. These experiments provide an opportunity to validate the internal response of our mathematical model. Reproduction of the blocking studies in the mathematical model confirms the delicate balance between cardioaccelerative and -decelerative effects of the pathways. During alpha-sympathetic blockade, FHR is almost unchanged, as the reduced cardiodecelerative effect is almost canceled out by the cardioaccelerative effect of beta-sympathetic response. This can be seen in the biphasic response: the late deceleration is followed by a late acceleration. Minor changes in neuronal response may thus lead to different effects due to this balance. Whereas blood pressure was hardly affected in simulations with an intact nervous system, it could not be maintained when the alpha-sympathetic or vagal pathway was blocked. This is in accordance with the studies of Martin et al. [78], Parer et al. [91], and Itskovitz et al. [53], as they all found differences in MAP per fetal sheep: Martin's subjects had increased MAP while in Parer's subjects it was sometimes a little increased, decreased or unchanged. Itskovitz et al. [53] did not find significant changes in MAP.

Due to lack of fetal data, many parameter settings in the fetal model had to be derived from animal data and human adult data. Relations between blood flow and oxygen pressure were based on sheep data from Peeters et al. [95]. As cardiac output distribution differs between the human and sheep fetus [107], we adopted their relations and scaled them for normal flow rates and oxygen pressures in the human fetus.

We used an adult cardiovascular regulation model, proposed by Ursino et al. [122] and scaled only a few blood- and oxygen pressure-dependent parameters to create a fetal model. The scaling was based on differences in average oxygen pressure and blood pressure levels between the adult and the fetus. Furthermore we included vagal nerve hypoxia as described in our previous publication [124]. These model adaptations were sufficient to evoke the physiological cascade leading to late decelerations. However, it is not unlikely that the balance of the neuronal pathways differs in the fetus compared to the adult, as it is known that central nervous system maturation is an ongoing process after birth. This means that quantitative analysis of our simulation results should be undertaken with caution.

Unfortunately, animal experiments that investigate the mechanism of late decelerations are limited in number and go back to the late 1970s and early '80s [53, 58, 78, 91]. In the review of Jensen et al. [58] it becomes clear that different experimental protocols result in different effects on FHR, flow distribution and oxygenation. To test our model of late decelerations, we only used data from animal experiments that investigated intermittent oxygen delivery reduction to the intervillous space (either from maternal aorta compression or uterine blood flow reduction) to mimic uterine blood flow reduction during contractions [53, 58, 78, 91]. Furthermore, we used sheep experiments with graded (chronic) uterine flow reduction [57, 114, 115] to test our model predictions for UPI.

To allow investigation of the “pure” reflex pathways we did not include beat-to-beat heart rate variability in these simulations. However, for the simulation with variable contractions, FHR variability and high-frequency contraction variations to the FHR and contraction signals are added in a postprocessing step, merely to approximate the clinical appearance of these signals (Figure 3.6). It is clear that heart rate variability needs to be included in more fundamental way, e.g. as a result of fetal breathing, sucking or other movements [84] or due to vagal and sympathetic nerve activity, to obtain realistic CTG tracings when the model would be used in a simulated clinical environment.

Furthermore, the model was restricted to reflex late decelerations. This implies that other mechanisms that directly or indirectly may alter FHR, like myocard depression [78, 91] and blood pressure regulation via catecholamines and humoral effects [72, 77, 78], are not taken into account. These mechanisms require additional model components, such as myocard oxygenation, acid/base status of the fetus and humoral regulation.

In conclusion, we present a mathematical model that can be used to study and reproduce hemodynamics during reflex late decelerations in term labor. Not only is the model able to reproduce late decelerations, it also replicates the contribution of the neuronal pathways as derived from sheep experiments [78, 91]. Incorporated in a screen-based simulator, the model can be a useful tool for individual training for obstetricians to obtain insight into the complex physiology behind the FHR. Furthermore, incorporated as simulation engine in a mannequin, it can be used to drive mannequin reactions during obstetric team training. For both applications, the

model should be extended with a graphical user interface to enhance manipulation of model parameters.

Acknowledgements

We gratefully acknowledge Germaine Jongen for her assistance with the simulations and the European Union for the Stimulus grant we received from the European Fund for Regional Development.

Appendix

Additional model equations

Many model equations and parameters are described in our previous publication [124]. Unless otherwise stated, additional model equations given in this appendix are based on the adult regulation model of Ursino et al. [122]. An overview of the regulation pathways is shown in Figure 3.8.

UPI

During a contraction, the uteroplacental resistance is increased due to the transmural pressure of the contraction. This is modeled with a sigmoidal function, according to:

$$R_{ivs} = \frac{R_{ivs,min} + R_{ivs,max} e^{\left(\frac{p_{ut} - p_{ut,n}}{k_{ivs}}\right)}}{1 + e^{\left(\frac{p_{ut} - p_{ut,n}}{k_{ivs}}\right)}}. \quad (3.1)$$

At resting tone, vessel resistance in the intervillous space is about equal to $R_{ivs,min}$ [kPa · ms/ml], while $R_{ivs,max}$ [kPa · ms/ml] is the maximum value. The slope of the response in the physiological working point $p_{ut,n}$ [kPa] is determined by k_{ivs} [kPa⁻¹]. Parameters were chosen such that the transition from minimum to maximum resistance occurs for uterine pressures between 35 and 65 mmHg [71].

Uteroplacental insufficiency (UPI), leads to a decrease in oxygen diffusion over the placental membrane. This diffusive transport \dot{O}_{diff} [m³ O₂/s] is determined by the difference in oxygen pressure pO_2 [mmHg] between the intervillous space (ivs) and the umbilical microcirculation (um):

$$\dot{O}_{diff} = DC(pO_{2,ivs} - pO_{2,um}), \quad (3.2)$$

where DC [m³ O₂/s/mmHg] is the placental diffusion capacity. In turn, the oxygen pressure in

the intervillous space is determined from the balance between convective and diffusive transport to the intervillous space:

$$\frac{d(cO_{ivs} \cdot V_{ut})}{dt} = q_{ut}(cO_{a,m} - cO_{ivs}) - \dot{O}_{diff}. \quad (3.3)$$

Here oxygen concentration in the maternal arterial circulation and intervillous space is given as $cO_{a,m}$ and cO_{ivs} [$\text{m}^3 \text{O}_2/\text{m}^3 \text{blood}$] respectively, the blood volume of the compartment as V_{ut} [m^3], and the flow through the compartment as q_{ut} [m^3/s]. In the model, UPI is modeled through an increase in placental resistance R_{ivs} (UPI-FLOW), a decrease in uteroplacental blood volume V_{ut} (UPI-BUF), or a decrease in placental diffusion capacity DC (UPI-DIF).

Baro- and chemoreceptor

The receptors, that translate blood pressure and oxygen pressure levels into afferent fire rates that are input for the CNS, in general consist of 1) a comparator, 2) a transfer function and 3) a low pass filter, see also Figure 3.3. We will discuss the receptor model for a generic input parameter x , that is translated in a fire rate f_x [s^{-1}]. First the input x is translated into a deviation Δx by comparing it to a normal value x_n :

$$\Delta x = x - x_n. \quad (3.4)$$

Second, the deviation is processed to an intermediate fire rate f_x^* using a sigmoidal transfer function:

$$f_x^* = \frac{f_{x,\min} + f_{x,\max} \cdot e^{\left(\frac{\Delta x}{k_x}\right)}}{1 + e^{\left(\frac{\Delta x}{k_x}\right)}}. \quad (3.5)$$

Here $f_{x,\min}$ [s^{-1}] and $f_{x,\max}$ [s^{-1}] are constant fire rates that are achieved for deviations $\Delta x \rightarrow -\infty$ and $\Delta x \rightarrow +\infty$, respectively. According to equation 3.5 the fire rate for $\Delta x = 0$ equals $\frac{1}{2}(f_{x,\min} + f_{x,\max})$. The parameter k determines the slope of the response. Finally, the intermediate fire rate f_x^* is translated into the actual fire rate f_x through a low pass filter, written as a first order differential equation:

$$\frac{df_x}{dt} = \frac{1}{\tau_x} \cdot (f_x^* - f_x). \quad (3.6)$$

Here the time constant τ_x [s] determines to what extent high frequency variations in Δx the are passed into the actual fire rate f_x . In the extreme case $\tau_x \rightarrow 0$ no filtering takes place. The parameters settings for the various receptors in Figure 3.3 are given in Table 3.3.

Table 3.3: Receptor parameters.

	f_{vh}	f_{ab}	f_{ac}	$f_{sh,o}$	$f_{sp,o}$	
Parameter	Value	Value	Value	Value	Value	Unit
$f_{x,min}$	0	2.52	1.16	-49.38	7.33	s^{-1}
$f_{x,max}$	2.5	47.78	17.07	3.59	13.32	s^{-1}
x_n	11	40	11	11.36	7.52	mmHg
k_x	1.7	4.09	7.24	6	2	mmHg
τ_x	-	-	2	30	30	s

CNS

Vagal nerve

We slightly adapted the models proposed by Ursino et al. [122]. The vagal fire rate f_v [s^{-1}] is modeled according to:

$$f_v = W_{b,v} \frac{f_{ev,min} + f_{ev,max} \cdot e^{\left(\frac{f_{ab} - f_{ab,n}}{k_{ev}}\right)}}{1 + e^{\left(\frac{f_{ab} - f_{ab,n}}{k_{ev}}\right)}} + W_{c,v} f_{ac} - W_{p,v} f_{ap} + f_{vh}, \quad (3.7)$$

with:

$$f_{vh} = \frac{f_{vh,min} + f_{vh,max} \cdot e^{\left(\frac{pO_{2,c} - pO_{2,n,c}}{k_{vh}}\right)}}{1 + e^{\left(\frac{pO_{2,c} - pO_{2,n,c}}{k_{vh}}\right)}} - f_{v,o}, \quad (3.8)$$

and $f_{ev,min}$ [s^{-1}], $f_{ev,max}$ [s^{-1}], $f_{ab,n}$ [s^{-1}], k_{ev} [s^{-1}], $f_{vh,min}$ [s^{-1}], $f_{vh,max}$ [s^{-1}], $f_{v,o}$ [s^{-1}], k_{vh} [$mmHg^{-1}$] and $pO_{2,n,c}$ [$mmHg$] as constants. Weight factors $W_{b,v}$ [-], $W_{c,v}$ [-] and $W_{p,v}$ [-] determine the relative importance of baro-, chemo- and pulmonary stretch receptor fire rates. The fire frequency of the lung stretch receptor f_{ap} [s^{-1}], that is included in the original model by Ursino, is kept constant in our model.

Sympathetic nerves

Fire rate for sympathetic innervation of the peripheral circulation and the heart ($y = sp$ and $y = sh$ respectively), is calculated according to a generic formula:

$$f_y = \begin{cases} f_{es,\infty} + (f_{es,0} - f_{es,\infty}) \cdot e^{(k_{es} \cdot (-W_{b,y} \cdot f_{ab} + W_{c,y} \cdot f_{ac} - W_{p,y} \cdot f_{ap} - f_{y,o}))} & f_y < f_{es,max} \\ f_{es,max} & f_y \geq f_{es,max} \end{cases}, \quad (3.9)$$

with $f_{es,max}$ [s^{-1}], $f_{es,0}$ [s^{-1}], $f_{es,\infty}$ [s^{-1}] and k_{es} [s] as constants. Weight factors $W_{b,sp}$ [-], $W_{c,sp}$ [-] and $W_{p,sp}$ [-] are used for baro-, chemo- and pulmonary stretch receptor fire rates. Again f_{ap} is kept constant. Hypoxic offset $f_{y,o}$ [s^{-1}] creates a threshold for sympathetic response:

$$\frac{df_{y,o}}{dt} = \frac{1}{\tau_{isc}} \cdot (f_{y,o}^* - f_{y,o}), \quad (3.10)$$

with:

$$f_{y,o}^* = \frac{f_{y,min} + f_{y,max} \cdot e^{\left(\frac{pO_{2,a} - pO_{2,n,y}}{k_{isc,y}}\right)}}{1 + e^{\left(\frac{pO_{2,a} - pO_{2,n,y}}{k_{isc,y}}\right)}}, \quad (3.11)$$

where $f_{y,o}^*$ is the unfiltered hypoxic offset and τ_{isc} [s], $f_{y,min}$ [s^{-1}], $f_{y,max}$ [s^{-1}], $pO_{2,n,y}$ [mmHg] and $k_{isc,y}$ [mmHg $^{-1}$] are constants. Parameter settings for the vagal and sympathetic nerves are given in Table 3.6.

Effectors

Contractility, venous unstressed volume and systemic vascular resistance

The function that translates the vagal and sympathetic fire rates into an effect on heart and vessels in general consist of 1) a time delay, 2) a transfer function and 3) a low pass filter. We will discuss the receptor model for a generic input fire rate f_z [s^{-1}], that is translated into an effect z . The effector value z is given by the sum of a baseline value z_0 and regulation based change Δz :

$$z = z_0 + \Delta z. \quad (3.12)$$

First the input fire rate f_z is translated into a unfiltered change of the effector Δz^* . In most cases a logarithmic function is used:

$$\Delta z^* = \begin{cases} G_z \cdot \ln\left(\frac{f_z(t-D_z) - f_{es,min} + f_{s,1}}{f_{s,1}}\right) & f_z \geq f_{es,min} \\ 0 & f_z < f_{es,min} \end{cases}. \quad (3.13)$$

Here the parameter D_z [s] describes the time delay of the response and the fire rate $f_{es,min}$ [s^{-1}] describes the input fire rate below which no effect is generated and $f_{s,1} = 1$ [s^{-1}] ensures continuity. The parameter G_z governs the steepness of the response.

In case of the systemic vascular resistance a sigmoidal function is used:

$$\Delta z^* = \frac{z_{min} + z_{max} \cdot e^{\left(\frac{f_z(t-D_z) - f_{z,n}}{k_z}\right)}}{1 + e^{\left(\frac{f_z(t-D_z) - f_{z,n}}{k_z}\right)}}. \quad (3.14)$$

Here the parameter D_z [s] again describes the time delay of the response, the parameter k_z governs the steepness of the response and the fire rate $f_{z,0}$ [s^{-1}] represents a reference fire rate at which the effect is equal to $\frac{1}{2}(z_{min} + z_{max})$.

Finally, the unfiltered effect Δz^* is translated into the actual effect Δz through a low pass filter, written as a first order differential equation:

$$\frac{d\Delta z}{dt} = \frac{1}{\tau_z} \cdot (\Delta z^* - \Delta z). \quad (3.15)$$

Here the time constant τ_z [s] determines to what extent high frequency variations in input fire rate f_z are passed into the actual effect Δz . Parameter values can be found in Table 3.5.

Heart period

The vagal and sympathetic contribution to heart period T [s], is given by:

$$T = T_0 + \Delta T_v + \Delta T_s, \quad (3.16)$$

where T_0 [s] is the basal heart period, and ΔT_v [s] and ΔT_s [s] are the change in heart period from the vagal and sympathetic nerve respectively, filtered through a low pass filter:

$$\begin{aligned} \frac{d\Delta T_v}{dt} &= \frac{1}{\tau_{T_v}} \cdot (-\Delta T_v + \Delta T_v^*) \\ \frac{d\Delta T_s}{dt} &= \frac{1}{\tau_{T_s}} \cdot (-\Delta T_s + \Delta T_s^*), \end{aligned} \quad (3.17)$$

with:

$$\Delta T_s^* = \begin{cases} \Delta T_v^* = G_{T_v} \cdot f_v(t - D_{T_v}) \\ G_{T_s} \cdot \ln \left(\frac{f_{sh}(t - D_{T_s}) - f_{es,min} + f_{s,1}}{f_{s,1}} \right) & f_{sh} \geq f_{es,min} \\ 0 & f_{sh} < f_{es,min} \end{cases}. \quad (3.18)$$

Change in contribution to heart period is thus governed by time constants τ_{T_v} [s] and τ_{T_s} [s], delays D_{T_v} [s] and D_{T_s} [s], and gains G_{T_v} [s] and G_{T_s} [s]. Parameter values can be found in Table 3.5.

Cardiac contractility

Myofiber stress is a function of active (σ_{act} [Pa]) and passive (σ_{pas} [Pa]) stress that in turn depend on sarcomere length (l_s) and shortening velocity (\dot{l}_s [m/s]), time t [s] and heart period T [s]:

$$\sigma_f = W_C \cdot \sigma_{act}(l_s, \dot{l}_s, t, T) + \sigma_{pas}(l_s). \quad (3.19)$$

Cardiac contractility is governed with scaling factor W_C [-] for active stress, where $W_C = 1$ represents normal contractility.

Table 3.4: Uterine and cerebral resistance parameters.

Parameter	Value	Unit
$\tau_{R_{cmc}}$	10	s
$R_{cmc,0}$	1398	kPa · ms/ml
$R_{cmc,min}$	$R_{cmc,0}/3$	kPa · ms/ml
$R_{cmc,max}$	$3 \cdot R_{cmc}$	kPa · ms/ml
$cO_{a,n}$	0.12	$\text{m}^3 \text{O}_2/\text{m}^3 \text{ blood}$
k_{cmc}	0.018	$\text{m}^3 \text{ blood}/\text{m}^3 \text{O}_2$
$R_{ivs,0}$	450	kPa · ms/ml
$R_{ivs,min}$	450	kPa · ms/ml
$R_{ivs,max}$	18000	kPa · ms/ml
$p_{ut,n}$	10	kPa

Autoregulation in the brain

In sheep, the relation between cerebral flow q_c [m^3/s] and arterial oxygen content cO_a [$\text{m}^3 \text{O}_2/\text{m}^3 \text{ blood}$] has been determined [95]. From that data, we determined the following relation between steady state cerebral resistance R_{cmc} [kPa · ms/ml] and cO_a . The temporal response was based on Ursino et al. [122].

$$\frac{dR_{cmc}}{dt} = \frac{1}{\tau_{R_{cmc}}} \cdot (-R_{cmc} + R_{cmc}^*), \quad (3.20)$$

with:

$$R_{cmc}^* = \frac{R_{cmc,min} + R_{cmc,max} \cdot e^{\left(\frac{cO_a - cO_{a,n}}{k_{cmc}}\right)}}{1 + e^{\left(\frac{cO_a - cO_{a,n}}{k_{cmc}}\right)}}. \quad (3.21)$$

Here $\tau_{R_{cmc}}$ [s] represents the time constant, $cO_{a,n}$ [$\text{m}^3 \text{O}_2/\text{m}^3 \text{ blood}$] a constant normal arterial oxygen content, while $R_{cmc,min}$ and $R_{cmc,max}$ represent minimum and maximum resistance values, based on measured data from Konje et al. [65]. The steepness of the curve is determined via k_{cmc} [$\text{m}^3 \text{ blood}/\text{m}^3 \text{O}_2$]. Parameter values can be found in Table 3.4.

Parameter assignment

In general, parameter settings are identical to those in our previous publication [124], unless otherwise mentioned. The setting of the majority of the regulation parameters is adopted from Ursino (see Table 3.3 and 3.6), and scaled where applicable to normal fetal arterial oxygen pressure and blood pressure levels. The gain for cardiac contractility and unstressed volume was set at the same fraction as for the adult. Parameters for cerebral autoregulation during hypoxemia (see Table 3.4) are based on the work of Peeters et al. [95] and Konje et al. [65]. Parameters related to uterine resistance are based on the descriptive relation between uterine contraction pressure and vascular resistance in the intervillous space [71], see Table 3.4.

Table 3.5: Effector parameters.

	T_s	T_v		W_c		$V_{v,0}$		R_{mc}	
Parameter	Value	Value	Unit	Value	Unit	Value	Unit	Value	Unit
z_0	0.25	0.25	s	75	kPa	100	ml	200	kPa · ms/ml
z_{min}	-	-	-	-	-	-	-	160	kPa · ms/ml
z_{max}	-	-	-	-	-	-	-	1000	kPa · ms/ml
$f_{es,min}$	-	2.66	s ⁻¹	2.66	s ⁻¹	2.66	s ⁻¹	-	-
$f_{z,n}$	-	-	-	-	-	-	-	12	s ⁻¹
k_z	-	-	-	-	-	-	-	1.44	s
τ_z	1.5	2	s	8	s	20	s	6	s
G_z	0.09	-0.13	s ²	10.2	kPa · s	-15.09	ml · s	-	-
D_z	0.2	2	s	2	s	5	s	2	s
$f_{s,1}$	-	1	s ⁻¹	1	s ⁻¹	1	s ⁻¹	-	-

Table 3.6: CNS parameters.

	f_v	f_{sh}	f_{sp}	
Parameter	Value	Value	Value	Unit
$f_{es,0}$	-	16.11	16.11	s ⁻¹
$f_{es,\infty}$	-	2.1	2.1	s ⁻¹
$f_{es,max}$	-	60	60	s ⁻¹
k_{es}	-	0.0675	0.0675	s
$f_{ev,min}$	3.2	-	-	s ⁻¹
$f_{ev,max}$	6.3	-	-	s ⁻¹
$f_{ab,n}$	25	-	-	s ⁻¹
k_{ev}	7.06	-	-	mmHg ⁻¹
$f_{v,o}$	-0.68	-	-	s ⁻¹
$W_{b,y}$	1	1	1	-
$W_{c,y}$	0.2	1	5	-
$W_{p,y}$	0.103	0	0.34	-

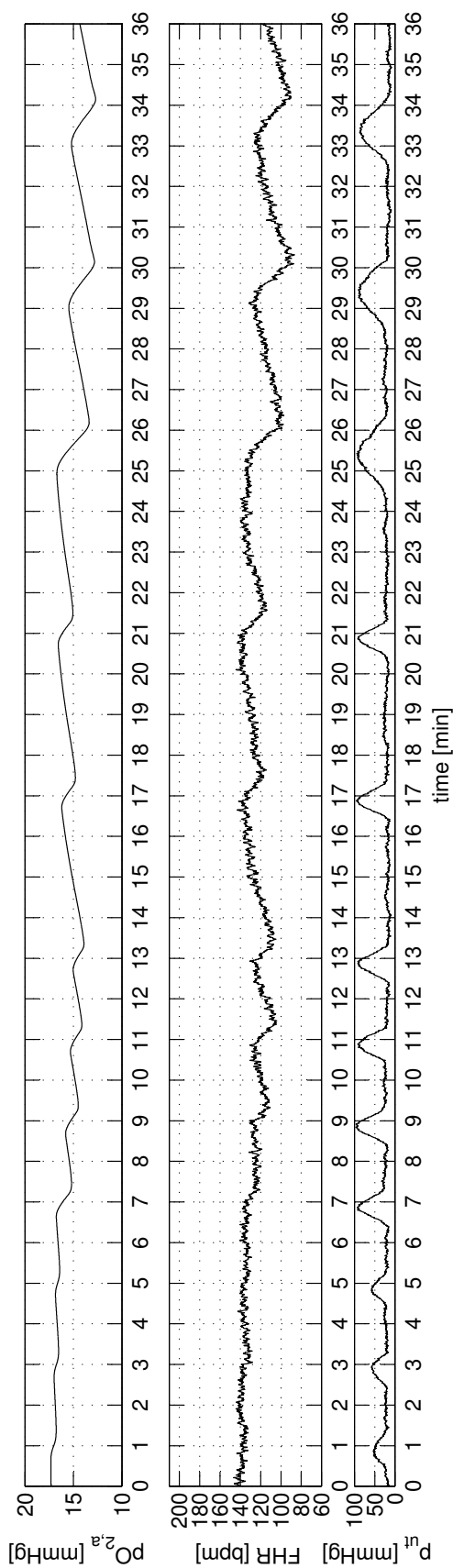


Figure 3.6: Simulation results for contraction variations. The relation between arterial oxygen pressure and the cardiogram is shown. Reduction of oxygen pressure depends on the contraction length, strength and interval. A series of contractions with half the amplitude of the reference contraction evokes almost no dips in pO_2 . A series of reference contractions with the same interval (2 min) leads to deeper hypoxemia and pO_2 does not return to the baseline in between contractions. A series of reference contractions with a larger interval (4 min) allows oxygen level to return to the baseline after the contraction. However, by increasing the duration of the contraction (2 min instead of 1 min), oxygen level falls deeper and does not return to the baseline before the next contraction. Fetal heart rate follows oxygenation levels: lower pO_2 leads to lower FHR decelerations. FHR variability and high-frequency contraction variations are added to approximate clinical appearance.

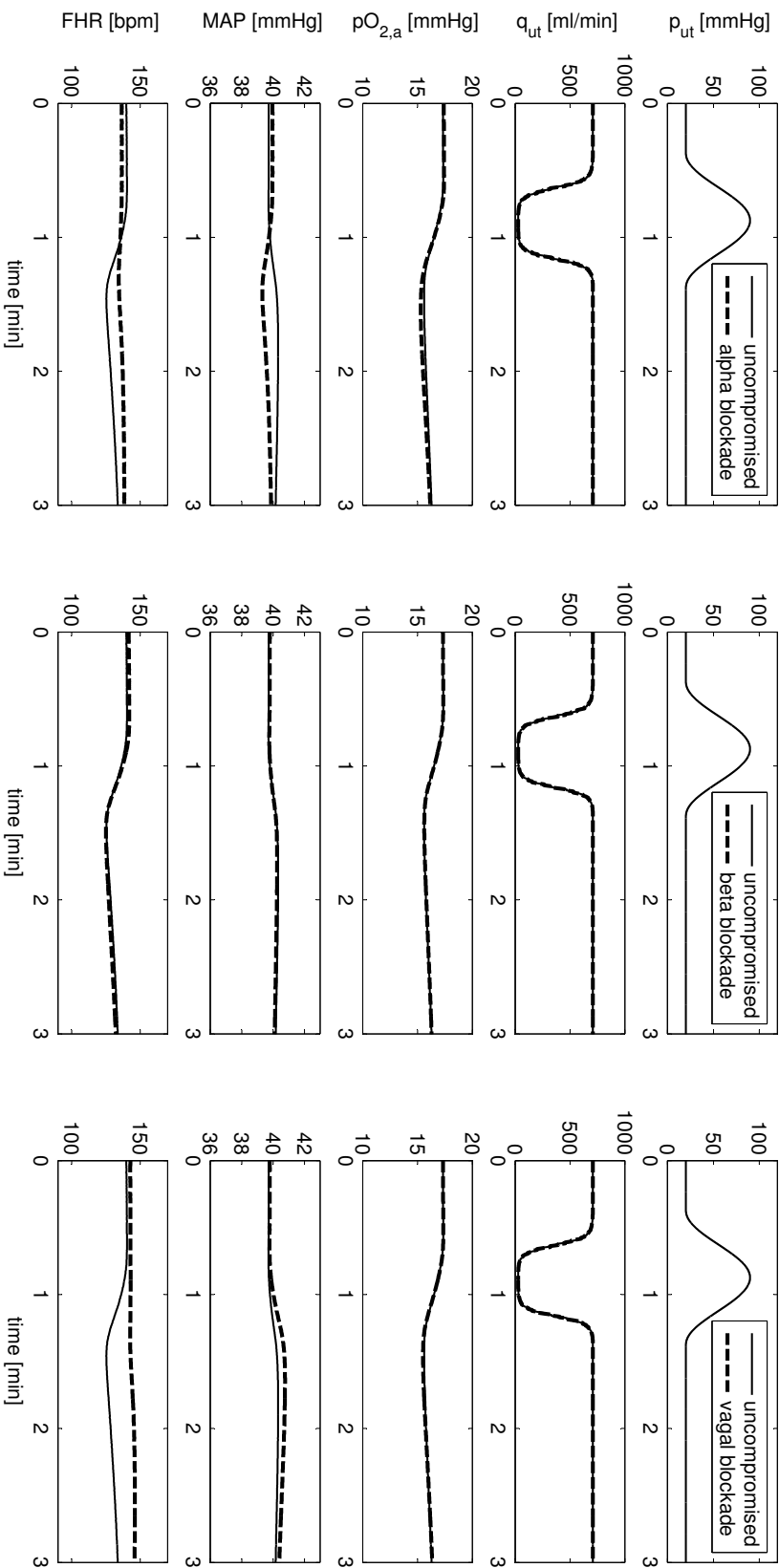


Figure 3.7: Simulation results for normal labor and blocking simulations. First column: with alpha blockade, the regulatory system fails to maintain MAP during hypoxemia. FHR decelerates in response to hypoxemia, but less pronounced than without blockade. Second column: with beta blockade, MAP is slightly decreased but can be maintained during hypoxemia. FHR baseline is also slightly reduced and the deceleration depth is slightly deeper due to blocked cardioacceleration. Third column: with vagal blockade, MAP cannot be maintained during hypoxemia and is increased. FHR increases as cardiodecelerative effects are blocked, this results in late acceleration.

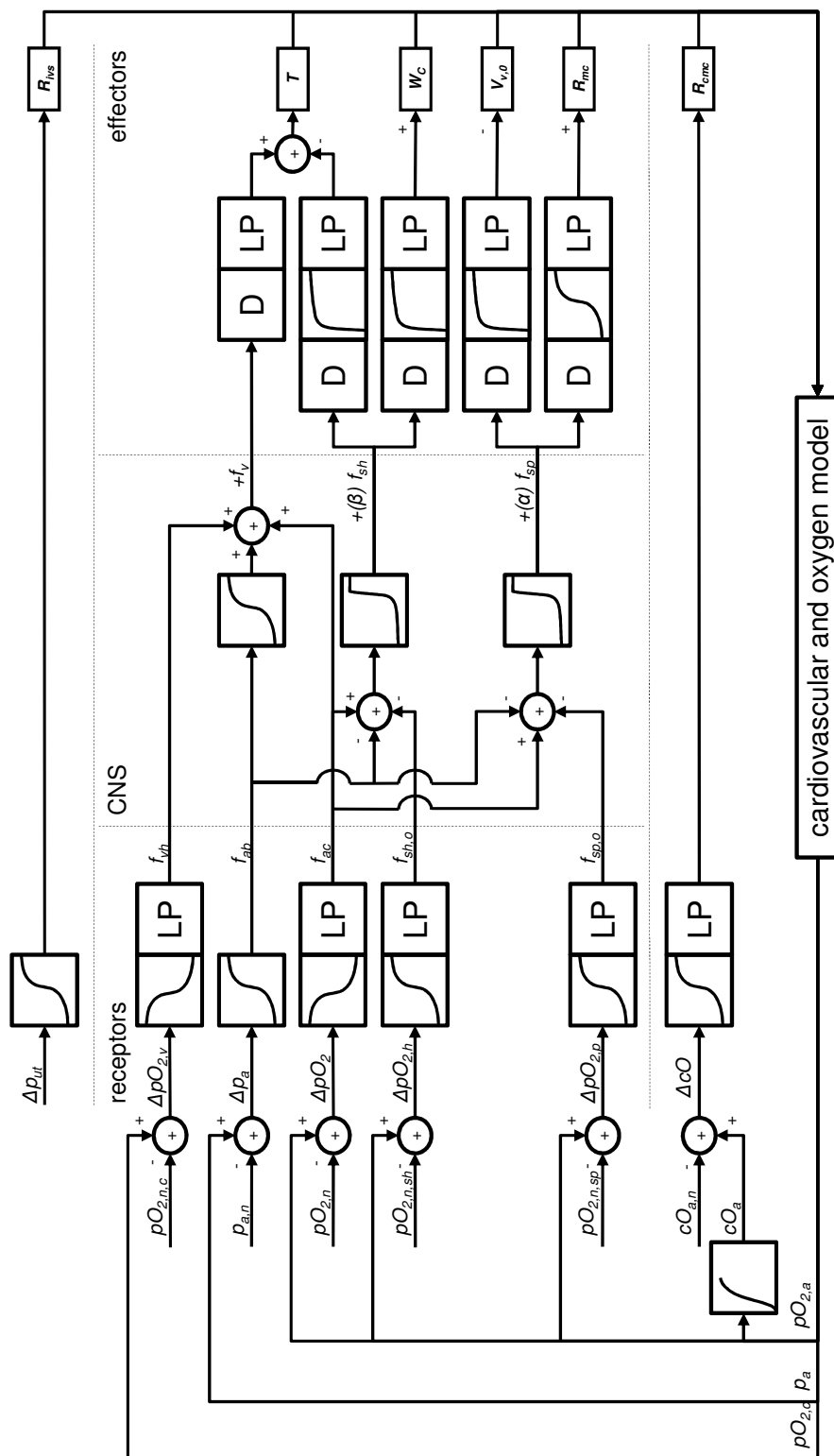


Figure 3.8: Block diagram of the regulatory model with details of modeled variables. Input are deviations in uterine pressure, blood pressure, oxygen content, and partial oxygen pressures (arterial pO_2 compared to respectively normal vagal nerve value ($\Delta pO_{2,v}$), normal chemoreceptor value (ΔpO_2), hypoxic threshold for the sympathetic fibers working on the heart ($\Delta pO_{2,h}$) and hypoxic threshold for the sympathetic fibers working on the periphery ($\Delta pO_{2,p}$)). These deviations give a sigmoidal response, that may be filtered with a low pass filter (LP). Increase in p_{ut} leads to an increase in R_{lvs} in a direct mechanistic way. Other functions used are exponential (used in the sympathetic center), linear (vagal nerve hypoxia) and logarithmic (for the effector response). The variables regulated by the CNS are heart period T , contractility factor W_c , unstressed vessel volume $V_{v,0}$ and peripheral resistance R_{mc} . These are modeled with a delay (D), a logarithmic or sigmoidal function and a low pass filter.

Insight into variable fetal heart rate decelerations from a mathematical model

M.B. van der Hout-van der Jagt, G.J.L.M. Jongen, P.H.M. Bovendeerd and S.G. Oei
Available online: *Early Human Development*,
<http://dx.doi.org/10.1016/j.earlhumdev.2012.12.001>

Abstract

During labor and delivery, variable decelerations in the fetal heart rate (FHR) are commonly seen on the cardiotocogram (CTG) that is used to monitor fetal welfare. These decelerations are often induced by umbilical cord compression from uterine contractions. Via changes in oxygenation and blood pressure, umbilical cord compression activates the chemo- and baroreceptor reflex, and thus affects FHR. Since the relation between the CTG and fetal oxygenation is complex, assessment of fetal welfare from the CTG is difficult.

We investigated umbilical cord compression-induced variable decelerations with a mathematical model. For this purpose, we extended our model for decelerations originating from caput compression and reduced uterine blood flow with the possibility to induce umbilical venous, arterial and total cord occlusion. Model response during total occlusion is evaluated for varying contractions (duration and amplitude) and sensitivity of the umbilical resistance to the uterine pressure. A clinical scenario is used to simulate a labor CTG with variable decelerations.

Simulation results show that fetal mean arterial pressure increases during umbilical cord occlusion, while fetal oxygenation drops. There is a clear relation between these signals and the resulting FHR. The extent of umbilical compression and thus FHR deceleration is positively related to increased contraction duration and amplitude, and increased sensitivity of the umbilical resistance to uterine pressure. No relation is found between contraction interval and FHR response, which can probably be ascribed to the lack of catecholamines in the model.

The simulation model provides insight into the complex relation between uterine pressure, umbilical cord compression, fetal oxygenation, blood pressure and heart rate. The model can be used for individual learning, and incorporated in a simulation mannequin, be used to enhance obstetric team training.

4.1 Introduction

During labor and delivery, umbilical cord blood flow is often disturbed due to temporary compression of the umbilical cord induced by uterine contractions. The temporary reduction in blood flow and oxygen delivery induces changes in fetal blood pressure and oxygen pressure, thereby activating the baro- and chemoreceptor reflexes [7]. These reflexes are responsible for a sudden decrease in fetal heart rate (FHR) that can be recognized as a variable deceleration on the cardiotocogram (CTG). The variable character of these decelerations is thought to result from the varying location of the umbilical cord in the uterus throughout labor.

Animal experiments have provided qualitative insight into the relation between umbilical cord compression and fetal heart rate. Barcroft [8] suggested that the rapid onset of the FHR deceleration following cord occlusion was due to a vagal response. Sheep experiments have confirmed a central role for the vagal nerve in variable decelerations. Several studies indicate that this response is due to changes in both blood pressure [11, 19, 55, 70] and oxygen pressure [11, 89, 102]. As the umbilical circulation represents a significant part of the fetal circulation, umbilical cord occlusion causes a rapid increase of fetal blood pressure, thereby evoking a baroreceptor response. Furthermore, with no or little umbilical flow, oxygen pressures in the fetus will drop rapidly and thus activate the chemoreceptor reflex. Both reflexes activate the vagal and sympathetic nerves, resulting in an apparently dominant vagal stimulus to the fetal heart [7]. In addition, the sympathetic stimulus induces systemic peripheral vasoconstriction, that, together with cerebral autoregulation results in flow redistribution from the periphery towards the heart, brain and adrenals to economize oxygen consumption [56, 93, 101, 102].

Different types of occlusion may induce different effects on blood pressure [7, 26, 55]. With partial venous occlusion alone, fetal blood can still be pumped into the umbilical circulation, but exit this circulation to a limited extent. This leads to a reduced blood volume in the fetal body and consequently to a reduced blood pressure in the fetal circulation. Partial venous occlusion is therefore sometimes associated with a baroreflex induced increase of FHR, also recognized as shoulders that accompany a variable deceleration [7, 130]. With increasing intrauterine pressure, not only the umbilical vein, but also the arteries become occluded and further inflow of fetal blood into the umbilical circulation is blocked. Despite the reduction of fetal body blood volume, blood pressure is increased during complete venous or total umbilical occlusion, due to increased fetal cardiac afterload [7]. Occlusion type and degree not only affect blood pressure, and thus the baroreceptor response, but also fetal oxygen pressure, and thus the chemoreceptor response. Together, the baro- and chemoreceptor reflex determine the actual FHR. In experimental setting, also the influence of (partial) arterial occlusion alone has been investigated. Although this will never occur in clinical practice, this experiment provides valuable insight into cardiovascular processes during cord occlusion.

Besides the type of the occlusion, also occlusion duration and interval are known to play a role [19, 130] in FHR response. With increasing duration and decreasing interval, not all cardiovas-

cular responses may have returned to normal before the onset of the subsequent contraction, and in these cases FHR overshoot and baseline shift can be seen after the decelerations [54, 129].

In order to better understand the hemodynamic and oxygenation changes during umbilical cord compression, we use a mathematical model to investigate and reproduce variable fetal heart rate decelerations resulting from umbilical cord compression in the human fetus. To this end, we extended our model to investigate the relative contribution of the reflex pathways involved in early and late decelerations [124, 125]. In order to evaluate experimental findings, arterial, venous and total umbilical cord occlusion are simulated. In addition, variations in cord occlusion are induced by applying contractions with different amplitude and duration and by varying the sensitivity of the umbilical resistance response to uterine contractions. We envision the use of the model in an educational setting, both for individual learning and for enhancement of obstetrical team training.

4.2 Materials & Methods

4.2.1 Mathematical model

The mathematical model describes cardiovascular function, uterine contraction, oxygen delivery and cardiovascular regulation via the baro- and chemoreceptor. In previous publications, we presented the model in detail [124, 125], see also Figure 4.1 for the cardiovascular model. For the current study we made a few model extensions.

In order to investigate partial or complete umbilical cord compression, the umbilical circulation is now modeled as a serial circulation of umbilical arteries, microcirculation and vein. The arterial and venous umbilical resistances increase with uterine pressure. Compression of these vessels was achieved by modeling the relation between uterine pressure and vessel resistance with a sigmoidal function, as described by Fung [31] and Rodbard [104] for compression of collapsible tubes and used earlier in our model for compression of uterine and cerebral vessels during contractions [124, 125]. Figure 4.2 shows the relation between uterine pressure and umbilical cord resistance. At low uterine pressure levels, umbilical resistances are at baseline, representing uncompressed vessels. As the uterine pressure p_{ut} rises during a contraction, the resistances of the umbilical vein and the umbilical arteries increase, and consequently umbilical flow decreases. The resistance of the vein starts to rise at lower pressures than that of the arteries. Thus, during a contraction, the vein will occlude earlier than the arteries. The actual resistance increase is determined by four parameters: minimum umbilical cord resistance, maximum umbilical cord resistance, a reference uterine pressure ($p_{ut,v,n}$ and $p_{ut,a,n}$ for umbilical vein and arteries, respectively) at which the resistance equals the mean of the minimum and maximum value, and the slope at this reference pressure. Since in clinical practice identical contractions may lead to different grades of umbilical cord compression, a parameter W_{VD} is introduced to model the variable sensitivity of the umbilical cord to compression due to its

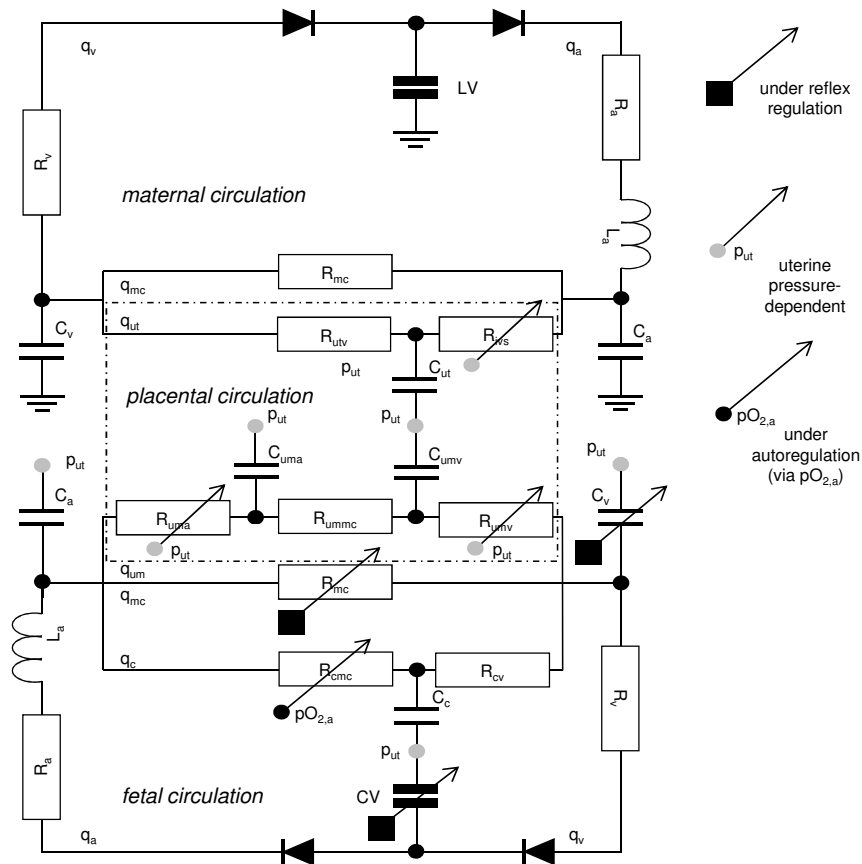


Figure 4.1: Electric analog of the feto-maternal cardiovascular model. The maternal arteries (subscript a, with resistance R , inertance L and compliance C) receive blood from the left ventricle (LV). The uterine circulation (ivs and utv: intervillous space and uterine veins) and the remainder of the systemic microcirculation (mc) run in parallel and fuse in the venous circulation (v). Retrograde flow in the heart is prevented via valves. Intervillous space resistance R_{ivs} is uterine pressure-dependent. In the fetus, the combined ventricle (CV) forwards blood towards the arteries (a). Three compartments run in parallel: the cerebral (cmc, cv), umbilical (uma, ummc, umv), and systemic circulation (mc). They all fuse in the venous compartment (v). Fetal cerebral microcirculation resistance is dependent on arterial pO_2 through local autoregulation. Venous compliance and volume, systemic resistance in the microcirculation, cardiac contractility and heart period are all under reflex regulation. The uterine and all fetal compliances experience external uterine pressure (p_{ut}). Adapted from [124].

variable location in the uterus, e.g. free or easily compressible. This parameter influences the occlusion response curve via the maximum umbilical resistance at high uterine pressure, with this maximum ranging from the minimum umbilical resistance ($W_{VD} = 0$, no compression) to the maximum umbilical resistance ($W_{VD} = 1$, complete occlusion). This thus affects the extent and the steepness of the response. Identical contractions can thus cause different umbilical compressions. Modeling details for the variable compression of the umbilical vessels can be

found in appendix 4.4.

The variable character of umbilical cord occlusions is also achieved via variation of the duration and amplitude of uterine contractions from contraction to contraction, see also [124]. Hence only the extent of the occlusion itself is influenced, the response curve remains unchanged.

In a clinical setting the umbilical arteries are never occluded without the vein. In an experimental setting, the arteries can be occluded while the vein remains open. In the model, this scenario can be achieved by setting $W_{VD} = 0$ for the umbilical vein and setting $W_{VD} \neq 0$ for the umbilical arteries.

Oxygen content in the umbilical arteries is determined by in- and outflow of oxygen (convective transport), and depends on umbilical arterial blood volume, umbilical arterial flow and oxygen concentration in the fetal arterial circulation. Modeling details of oxygen distribution in the umbilical arterial compartment can be found in appendix 4.4.

In comparison to our previous studies, we attenuated the baroreceptor gain with a factor 5. This change is based on a sheep study [18] and our previous finding that the adult-to-fetal scaled baroreceptor reflex in our model probably overestimates fetal baroreceptor function [125]. Details can be found in appendix 4.4.

4.2.2 Simulation protocol

The simulations mimic both experimental and a clinical scenarios. The experimental scenarios are used to investigate model response to variations in uterine contraction amplitude and duration, and variations in the umbilical resistance response curve. In the clinical scenario, we simulate repetitive brief umbilical cord occlusions in response to uterine contractions with a variable character.

In all simulations, the resistance response curve for the umbilical vein and the umbilical arteries is based on constant parameters for slope, reference pressure, and minimum and maximum resistance. Factor W_{VD} for the maximum response is set equal for the vein and the arteries, unless mentioned explicitly. Umbilical parameter settings can be found in Table 4.2 in the appendix and hold for all simulations where no explicit values are given.

4.2.2.1 Experimental scenarios

Occlusion type

A reference contraction of 60 s with an amplitude of 70 mmHg is used to investigate the differences in cardiovascular response to venous, arterial and total umbilical occlusion. Venous occlusion alone is achieved by setting W_{VD} for the arterial occlusion response curve to zero, hence the arterial resistance is independent of changes in uterine pressure. In a similar fashion,

during arterial occlusion W_{VD} was set zero for the umbilical venous occlusion response curve.

Contraction duration and amplitude

The contraction is varied in duration (between 50 and 90 s, increasing with 20 s steps) and amplitude (from 50 to 90 mmHg, increasing with 20 mmHg steps) to investigate the effects on cardiovascular response with total umbilical occlusion.

Umbilical resistance response curve

The effect of varying sensitivity of umbilical resistance to uterine pressure is investigated by setting W_{VD} to a value between 0.1 and 1 (with steps of 0.3, see also Figure 4.2). The reference contraction of 60 s with an amplitude of 70 mmHg is used.

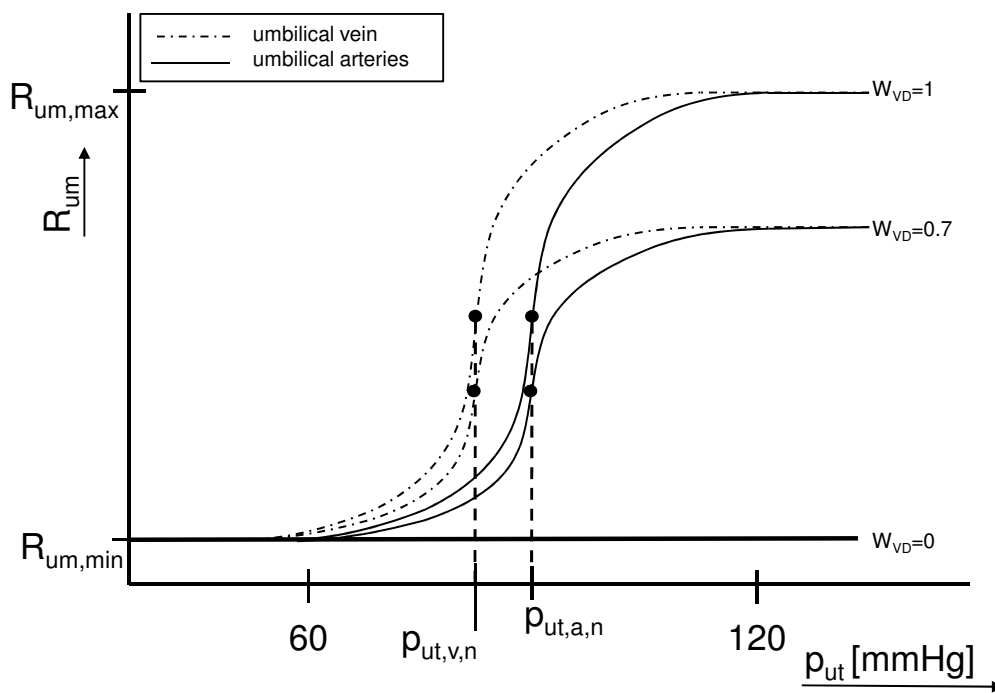


Figure 4.2: Variable response curve for umbilical resistances. The resistance in the umbilical venous and umbilical arterial circulation are uterine pressure-dependent. At low uterine pressure and/or low factor W_{VD} , umbilical resistance equals the normal minimum resistance ($R_{um,min}$), and increases sigmoidally with increasing uterine pressure and/or factor W_{VD} to the maximum resistance $R_{um,max}$. This factor determines the steepness and maximum response to a contraction and can be used to create a variable umbilical cord compression from contraction to contraction. The resistance increase is the steepest at the reference pressures $p_{ut,v,n}$ and $p_{ut,a,n}$.

4.2.3 Clinical scenario

4.2.3.1 CTG tracing with variable contractions and occlusions

A series of random uterine contractions (duration, amplitude, interval) is applied while for each contraction the occlusion response curve is varied via factor W_{VD} . The random variation in W_{VD} (0.6 ± 0.2) and contraction duration (60 ± 8 s), amplitude (60 ± 15 mmHg), and interval (150 ± 10 s) is based on a Gaussian distribution with a mean value μ and a standard deviation σ , noted as $(\mu \pm \sigma)$. To enhance clinical appearance, FHR variability and short term uterine pressure variations are added in a postprocessing step as described before [124].

4.3 Results

4.3.1 Experimental scenarios

4.3.1.1 Occlusion type

The columns in Figure 4.3 show the FHR response to umbilical occlusions originating from venous, arterial and total umbilical occlusion, respectively. For umbilical vein occlusion, venous umbilical flow reduces to zero within a few seconds, whereas umbilical arterial flow remains nonzero throughout the contraction (minimum of 49 vs. 268 ml/min in baseline). Hence an extra amount of fetal blood is pumped into the umbilical circulation (24 ml), and fetal venous volume decreases (Figure 4.3). Flow redistribution takes place after the top of the contraction has occurred, with the cerebral circulation receiving more flow at the expense of the peripheral circulation. Fetal blood pressure drops initially (37 vs. 40 mmHg in baseline), but increases in the second phase of the contraction (+15 mmHg). Oxygen pressure builds up in the umbilical vein proximal to the occlusion due to ongoing diffusion (54 vs. 31 mmHg in baseline) and is decreased in the fetal circulation due to continued oxygen consumption without new delivery (both 13 vs. 17 mmHg in the umbilical and fetal arterial circulation with respect to baseline). FHR drops biphasically, the first, major drop (from 134 to 78 bpm) is mainly caused by hypoxia, while the second, smaller drop (-15 bpm) is due to the increased blood pressure in second phase of the contraction.

During umbilical arterial occlusion, flow through the umbilical arterial and venous circulation is virtually identical, even though the umbilical vein resistance is unchanged. Almost no blood is pumped into the umbilical circulation (3 ml). Blood pressure fluctuates throughout the contraction (overall increased, with peak pressure +11 mmHg) and is determined by the product of total fetal flow and total fetal vascular resistance. During the first phase of the occlusion, blood pressure increases, as total fetal resistance increases due to the changes in the umbilical resistance. However, shortly after the first increase in blood pressure, fetal flow decreases due to a baroreceptor reflex-induced decrease of FHR. This results in a small decrease in blood

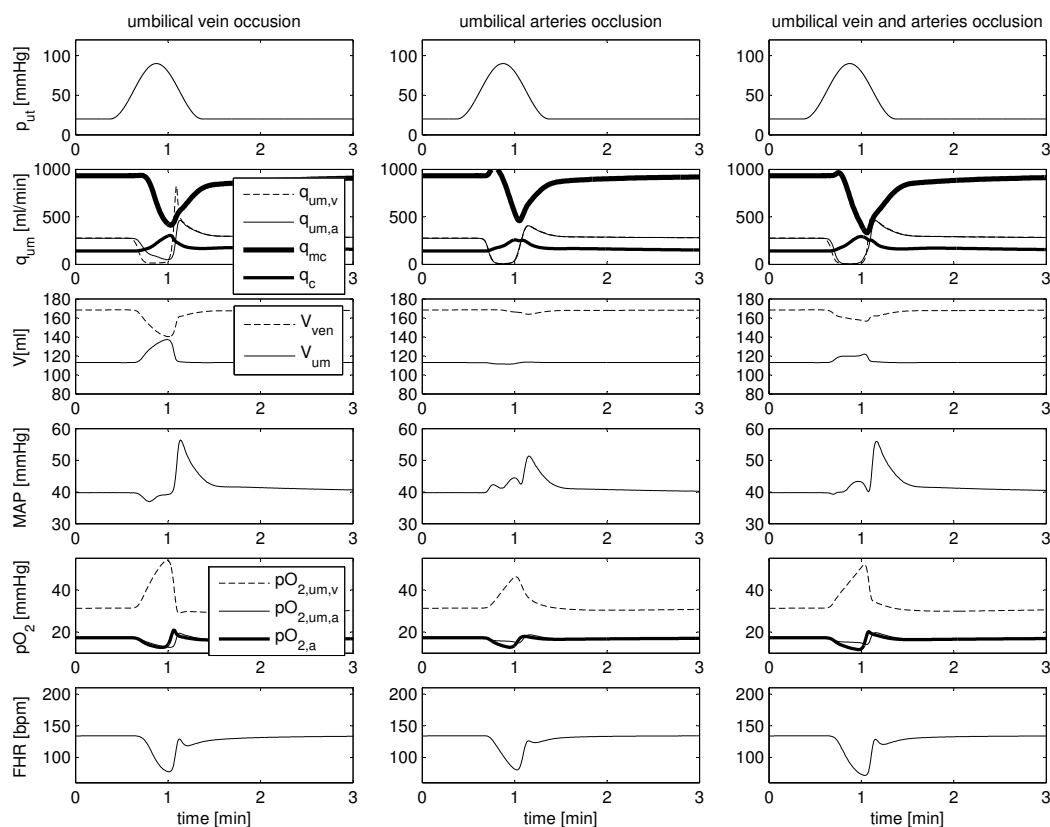


Figure 4.3: Umbilical cord occlusion. First column: Umbilical vein occlusion. Uterine contraction (p_{ut}) causes a quick decrease in umbilical venous flow ($q_{um,v}$) and a delayed reduction in umbilical arterial flow ($q_{um,a}$). Consequently, blood volume in the umbilical compartment (V_{um}) increases and decreases in the fetal venous compartment (V_{ven}). This causes an initial reduction in mean arterial pressure (MAP). Flow is redistributed from the microcirculation towards the cerebral circulation (q_{mc} and q_c , respectively). Interruption of oxygen delivery to the fetus causes an increase in umbilical venous, and a decrease in umbilical arterial and fetal arterial pO_2 ($pO_{2,um,v}$ and $pO_{2,um,a}$ and $pO_{2,a}$, respectively), which is slightly different from the fetal arterial pO_2 . The changes in fetal blood- and oxygen pressure evoke a baro- and chemoreceptor response that results in a FHR deceleration. The secondary MAP response is described in detail in the main text. Second column: Umbilical arteries occlusion. Total umbilical flow stagnates almost instantaneously, hence almost no blood is pumped into the umbilical circulation. Fetal MAP is overall increased, but fluctuates due to changes in balance between vascular resistance and FHR. Changes in oxygenation and FHR are less pronounced than during venous occlusion, due to a shorter occlusion duration. Third column: umbilical vein and arteries occlusion. The effects of umbilical vein and arteries occlusion are combined. This results in an intermediate amount of blood trapped into the umbilical circulation, a biphasic MAP response and a broader and deeper FHR deceleration and an increased flow redistribution.

pressure. The second increase is due to an increase in fetal total resistance under influence of

chemoreceptor reflex-induced peripheral vasoconstriction. After the peak of the contraction, total resistance and flow turn to normal. Firstly the decrease in total resistance is faster than the increase in total flow (FHR is still at its minimum), with a small decrease in MAP as a result. Thereafter, FHR restores quickly while the return of systemic resistance to baseline is slower. The result is a quick increase in fetal blood pressure. Blood pressure subsequently reduces to normal at the same rate as the decrease in systemic resistance. Oxygen pressures are disturbed less than during venous occlusion alone, due to the shorter occlusion time (umbilical vein: +15 mmHg, umbilical artery: -2 mmHg, fetal artery: -4 mmHg, all with respect to baseline level). The biphasic response in heart rate is less pronounced than during venous occlusion alone (-53 and -10 bpm for primary and secondary reduction respectively).

During total occlusion, the vein occludes first. Until the arteries are occluded as well, blood is pumped into the umbilical circulation, however, less blood (11 ml) is stored than during venous occlusion alone. After a minor decrease, blood pressure shows a biphasic increase (+3 and +26 mmHg above baseline) and is overall increased. The temporary decrease in MAP at the end of the occlusion is due to reduced fetal vascular resistance (re-opening of the umbilical circulation) and still reduced fetal flow (nadir in FHR). The rapid increase in FHR and the still elevated vascular resistance are responsible for the second peak in MAP. Oxygen pressures are somewhat less disturbed than during venous occlusion (umbilical vein: +20 mmHg, umbilical artery: -3 mmHg, fetal artery: -4 mmHg, all with respect to baseline level). FHR drops biphasically during the occlusion and is lower than during venous occlusion alone (-62 and -13 bpm).

4.3.1.2 Contraction duration and amplitude

The first two columns in Figure 4.4 show the results for increased contraction pressure and duration. A variation in contraction amplitude affects the extent of all cardiovascular responses. A contraction below 70 mmHg does not evoke a variable deceleration. Furthermore, a linear increase in contraction strength results in a non-linear cardiovascular response for all effectors. All responses become increasingly more pronounced with increased peak pressure. The FHR deceleration is broader and deeper with increased peak pressure.

Different results are seen for increased contraction duration, with contraction amplitude maintained at the reference pressure of 90 mmHg: a linear increase in duration leads to a fairly linear increase in effector response. Increased duration mainly affects the duration of the deceleration, and to a lesser extent the depth of the deceleration.

All hemodynamical and oxygenation changes are restored within 10-15 seconds after the end of the contraction.

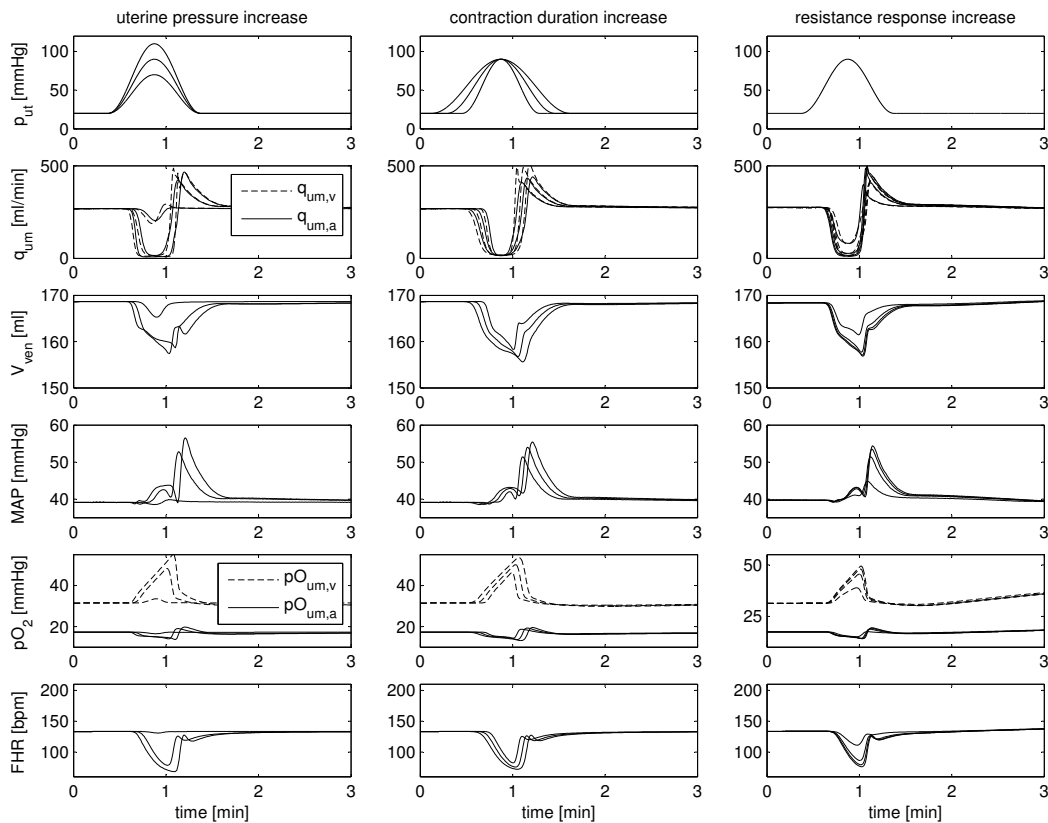


Figure 4.4: Model response to changes in uterine contraction and umbilical resistance response curve. First column: Contraction amplitude variation (50, 70 and 90 mmHg). A linear increase in uterine pressure leads to a non-linear response, characterized by longer and deeper decelerations, more reduced fetal venous blood volume (i.e. increased umbilical blood volume), increased MAP, increased umbilical vein/artery oxygen difference, and decreased FHR. Second column: Contraction duration variations (50, 70 and 90 s). An increase in contraction duration leads to a fairly linear effect in the cardiovascular responses. Especially the duration of the FHR deceleration is affected and in a lesser extent the depth of the deceleration. Third column: Umbilical resistance response variations via factor W_{VD} (0.1, 0.4, 0.7 and 1.0). A linear increase of the sensitivity of the umbilical resistance to uterine pressure has a strong effect on all effectors until $W_{VD} = 0.4$, with increasing W_{VD} , the effect saturates.

4.3.1.3 Umbilical resistance response curve

The third column in Figure 4.4 shows the simulation results due to variations of the resistance response curve. The degree of compression rises with increasing weighting factor for umbilical occlusion (W_{VD}). The influence of W_{VD} on FHR deceleration depth is non-linear: strong changes are found when W_{VD} is increased to 0.4, but the additional effect on FHR deceleration when W_{VD} is increased above 0.4 is less pronounced.

4.3.2 Clinical scenario

4.3.2.1 CTG tracing with variable contractions and occlusions

Figure 4.5 shows the CTG for a series of varying contractions and varying umbilical resistance response curves. Increased uterine pressure and contraction duration not necessarily lead to increased FHR response, since this response also depends on the maximum umbilical resistance responses that are determined by W_{VD} . However, the correspondence between FHR deceleration and both pO_2 and MAP changes remains clearly recognizable. The results per contraction are given in Table 4.1.

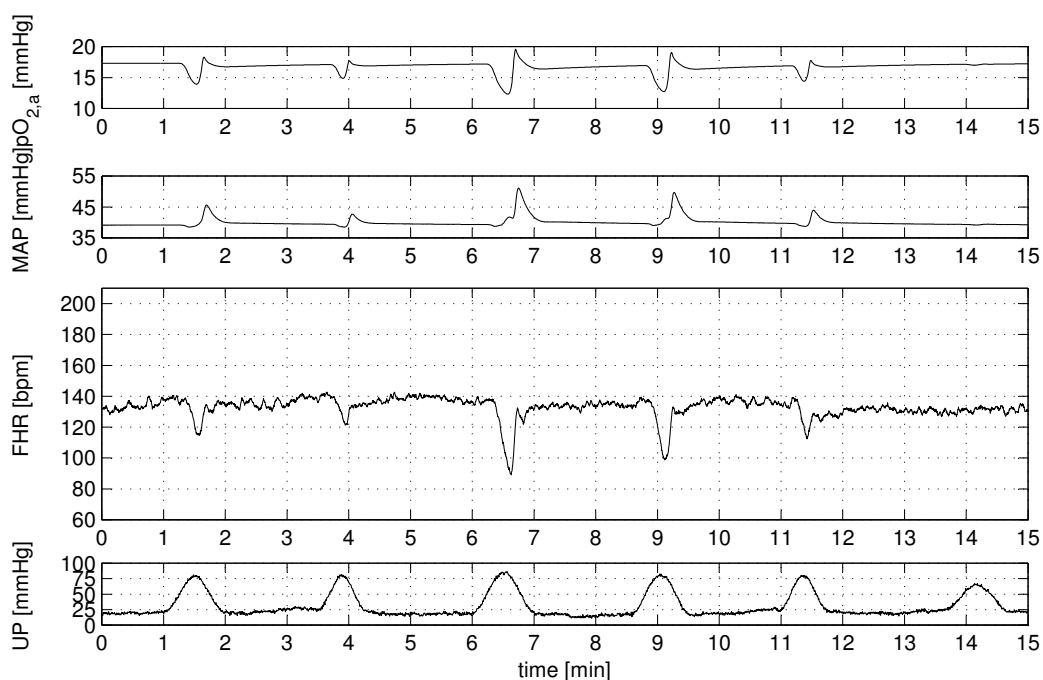


Figure 4.5: Clinical scenario: CTG with variable decelerations and corresponding arterial oxygen and MAP signal. Each contraction evokes a different FHR response, due to contraction-to-contraction changes in both uterine pressure level (UP) and duration, and in the compressibility of the umbilical cord. Characteristics of the CTG are given in Table 4.1. Overall, FHR corresponds well with changes in MAP and arterial pO_2 .

4.4 Discussion & conclusion

We developed a model that can be used to generate and investigate variable decelerations resulting from umbilical cord compression in the human fetus. Umbilical cord compression was modeled via a uterine pressure-dependent resistance for the umbilical venous and arterial compartment, taking into account that the vein will occlude first. During umbilical venous occlu-

Table 4.1: Characteristics of the CTG in Figure 4.5. Per contraction, the random variables are given: contraction duration and amplitude, and weighting factor W_{VD} for the umbilical arterial and venous resistance curve. The resulting minimum values for arterial partial oxygen pressure, MAP and FHR are also given ($pO_{2,min}$, MAP_{min} and FHR_{min} , respectively).

Contraction #	Duration [s]	Amplitude [mmHg]	W_{VD} [-]	$pO_{2,min}$ [mmHg]	MAP_{min} [mmHg]	FHR_{min} [bpm]
1	60	60	0.6000	13.9	45.6	107
2	48	56	0.6010	14.9	42.6	120
3	64	65	0.7278	12.3	51.0	85
4	60	64	0.5420	12.7	49.7	92
5	49	56	0.7770	14.4	43.9	116
6	65	43	0.7270	17.0	39.4	133

sion, blood from the fetal circulation is still pumped towards the umbilical circulation as long as the umbilical arteries are patent. This results in temporary storage of fetal blood volume in the umbilical circulation. The amount of volume stored, is dependent on the elasticity of the umbilical circulation and the time between closure of the umbilical vein and arteries. With re-opening of the umbilical circulation, a temporary umbilical peak flow occurs in all simulations (Figures 4.3 and 4.4). The extent of this peak flow is primarily determined by the amount of blood entrapped in the umbilical circulation.

The reduction in fetal blood volume leads to a reduction in blood pressure. Mean arterial blood pressure is determined by the product of total vascular resistance and total blood flow. Total vascular resistance is influenced by umbilical resistance increase (umbilical cord occlusion), systemic resistance increase (sympathetic stimulus from the chemoreceptor) and cerebral resistance decrease (autoregulation). Total blood flow depends on FHR and cardiac contractility, which in turn are determined by the baroreflex and the chemoreflex. It also depends on fetal blood volume through the Frank Starling effect, incorporated in our model through the dependence of active myocardial stress generation on sarcomere length. The balance between these effects determines the actual blood pressure. In our simulations of venous occlusion alone, this balance results in an initial decrease of MAP (Figures 4.3 and 4.4). For arterial and total occlusion, MAP does not decrease initially, but rises directly. This initial blood pressure increase is caused by the rise of total vascular resistance, despite the instantaneous reduction in cardiac output (via FHR reduction) and the reduced fetal blood volume. The secondary blood pressure increase can be ascribed mainly to flow redistribution via increased peripheral resistance under influence of sympathetic stimulation, and to the recovery of FHR, which is also reported from experimental data [26, 55].

Oxygen delivery to the fetus is blocked by the interruption of umbilical flow during cord compression. As a result, oxygen builds up in the umbilical vein, while in all other feto-umbilical vessels oxygen pressures will drop since oxygen consumption continues. The differences between umbilical arterial and fetal arterial oxygen pressure (Figure 4.3) can be explained by local changes in flow due to cord compression. The fetal pO_2 reduction activates the chemoreceptor

that in turn increases vagal and sympathetic activity. FHR drops under vagal influence, while fetal peripheral resistance increases, and flow is redistributed from the fetal systemic circulation towards the fetal umbilical and cerebral circulation. The latter is supported by decreased cerebral resistance due to cerebral autoregulation.

The fetal heart rate response is the result of vagal and beta-sympathetic stimuli from the chemo- and baroreceptor. The initial response to cord compression is a hypoxia- and hypertension-induced fetal heart rate reduction, mediated by the vagal center, in accordance with observations from animal experiments [7, 8, 130]. The secondary and smaller reduction in FHR is a compensation mechanism of the baroreceptor to the (secondary) blood pressure increase. FHR responds almost instantaneously to changes in umbilical flow, in contrast to FHR response to changes in uterine flow [35, 125]. The delay in FHR response from both uterine and umbilical flow interruptions is primarily caused by hypoxemia that triggers the vagal nerve via the chemoreceptor [125]. The main difference between umbilical and uterine flow reduction lies in the availability of a buffering placental blood pool in the latter case, and the absence thereof in the former case. Hence fetal oxygen concentration reduces more quickly during cord occlusion than during uterine flow reduction.

Comparison of model outcome to clinical data is difficult, since FHR is the only continuous signal available from human fetuses. Hence we had to compare the outcome variables with animal data. Although this makes a quantitative model validation impossible, qualitative data analysis is still useful to enhance insight into the complex balance between the different contributions to changes in heart rate, blood pressure and oxygenation.

In our venous occlusion simulation with the reference contraction, 24 ml of blood is trapped in the umbilical circulation. This amount is of the same order as the only reported value we are aware of, which is 35 ml, reported by Hasaart et al. [45]. During arterial occlusion, they observed the opposite effect, where umbilical blood was pumped into the fetal circulation. This did not occur in our simulations, probably due to the segmentation choices of the umbilical compliance in our model.

During most sheep experiments, blood pressure registrations show an increase throughout umbilical cord compression between 20 and 50% [7, 11, 26, 55, 102]. Our results for total occlusion show an increase of 43%. We note that the validity of this comparison is limited, since the umbilical circulation in the fetal sheep receives normally about 40 % of the cardiac output, whereas the human fetus receives 20% of the cardiac output [64, 93]. Thus blood pressure in the fetal sheep is more likely to rise during umbilical cord occlusion since the increase in total resistance is stronger.

Both in our model and in the sheep experiments from Richardson [102], cerebral flow increases but not sufficient to maintain cerebral oxygen delivery. However, fetal cerebral oxygen consumption is maintained due to increased fractional extraction. Fetal systemic oxygen consumption is reduced as a sparing mechanism [93]. The pO_2 reduction is dependent on the severity of

the compression (duration and grade). For a 1-minute total occlusion, Richardson [102] reports a pO_2 reduction of 34% to a value of 14 mmHg, comparable to our results, where pO_2 reduces by 25% to a value of 13 mmHg. Others report values from 25 to 50%, for cord compressions with shorter duration [26, 56].

The simulations show the dependency of the variable FHR deceleration on parameters related to the contractions (duration, amplitude) and the sensitivity of the umbilical resistance (venous and/or arterial) to uterine pressure. The longer the contraction, the longer the compression and thus the deeper the deceleration. In addition, the shape of the deceleration evolves from a V-shape into a U-shape. The amplitude of the contraction influences the degree of cord compression, and thus the depth of the deceleration. This is also reported by Itskovitz et al. [55], who reported no cardiovascular changes (MAP and FHR) with flow reduction below 50%. Also in our simulations, virtually no cardiovascular changes are seen below 50 % flow reduction.

Our simulations do not display FHR overshoot after a severe deceleration. From animal data it is known that overshoots are caused by catecholamine release during severe hypoxemia caused by short contraction intervals and/or long contractions [57, 129]. Above a certain concentration threshold, catecholamines contribute to the sympathetic stimuli to the heart and vessels, inducing peripheral vasoconstriction and increased cardiac performance [17]. We hypothesize that the absence of catecholamines in the model is responsible for the lack of overshoot in our simulations, even after severe repetitive contractions (not shown). Currently our model can thus only be used to simulate non-asphyxiated fetuses in labor, i.e. not for contraction durations of more than 1 min and/or contraction intervals shorter than 2.5 min for a longer time period [19, 129, 130].

We modeled the increase in umbilical resistance during a contraction with an umbilical resistance response curve. The response curve may vary from contraction to contraction as the cord location - and thus the sensitivity to uterine pressure - can change. The introduced weighting factor is intended to achieve this variable character in an easy manner. However, this weighting factor could instead also have been applied to the reference uterine pressure or the steepness of the curve.

During previous simulations, we reported that the baroreceptor reflex in our model is probably too effective, as almost no blood pressure changes occurred [125]. The baroreceptor reflex was adapted from an adult model [122], by scaling the pressure-related parameters to fetal blood pressure. Evidence was found that the baroreceptor is less sensitive in the fetus compared to both the newborn and the adult: Dawes et al. [18] reported sensitivity (gain) differences between fetuses and adults of 1/8, 1/5 and 1/2, depending on the method to induce blood pressure changes. We therefore attenuated our baroreceptor gain with 1/5, although we are aware that this is fragile proof of an attenuated fetal baroreceptor reflex.

In conclusion, the model is able to simulate the flow of events during umbilical cord conclusion originating from uterine contractions in the non-asphyxiated fetus. The variable character of

cord compression is achieved via both variation in strength and duration of subsequent uterine contractions and variations in the umbilical resistance response curve. The main determinants for FHR deceleration due to cord compression are the decrease in fetal oxygen pressure and the increase in blood pressure, that evoke a vagal stimulus to the heart via the baro- and chemoreceptor. For the simulation of severe contractions (with respect to duration and interval) leading to asphyxia, it is advised to include cardiovascular regulation via catecholamines.

Appendix

Model settings

Almost all model equations and parameters are described in our previous publications [124, 125]. Here we only describe the extensions to the previous models.

Compression of umbilical venous and arterial compartments

For the simulations described in this study, the model was extended with explicitly modeled umbilical arterial circulation and variable resistances in the umbilical arterial and venous compartments of the umbilical cord, see Table 4.2. These relations are modeled with sigmoidal functions as described by Rodbard [104] and Fung [31]. The relation between uterine pressure p_{ut} [mmHg] and umbilical arterial $R_{um,a}$ or venous resistance $R_{um,v}$ [kPa s/m³] respectively, is modeled as a sigmoidal curve, see also Figure 4.2:

$$R_{um,x} = \frac{R_{um,x,0} + W_{VD} \cdot R_{um,x,max} \cdot e^{\left(\frac{p_{ut} - p_{ut,x,n}}{k_{um}}\right)}}{1 + e^{\left(\frac{p_{ut} - p_{ut,x,n}}{k_{um}}\right)}}. \quad (4.1)$$

Hence there are two curves, one for the umbilical vein ($x = v$) and one for the umbilical arteries ($x = a$). During low uterine pressures and/or with $W_{VD} = 0$, $R_{um,x}$ equals the normal resistance $R_{um,x,0}$. The maximum resistance $R_{um,x,max}$ occurs only at high uterine pressure and $W_{VD} = 1$, for lower values of W_{VD} , maximum resistance is the corresponding fraction of $R_{um,x,max}$. The steepness of the response is governed by k_{um} , and identically modeled for venous and arterial occlusion. However, the reference point $p_{ut,x,n}$ differs for both responses such that the vein will occlude at a lower uterine pressure than the arteries. The parameters are chosen such that cord compression takes place in the physiological range of uterine pressure and that occlusion is complete and maximal when W_{VD} equals 1. However, these values are somewhat arbitrarily as in fact for every uterine contraction a new curve can be defined, as the sensitivity of the umbilical cord resistance to uterine pressure differs when the location of the cord changes.

Table 4.2: Umbilical circulation parameters.

Parameter	Value	Unit	Parameter	Value	Unit
$V_{um,a,0}$	10	ml	$V_{um,v,0}$	80	ml
$C_{um,a}$	0.01	ml/kPa	$C_{um,v}$	8.2	ml/kPa
$R_{um,a,min}$	10	kPa · ms/ml	$R_{um,v,min}$	2	kPa · ms/ml
$R_{um,a,max}$	30000	kPa · ms/ml	$R_{um,v,max}$	6000	kPa · ms/ml
$p_{ut,a,n}$	12	kPa	$p_{ut,v,n}$	11	kPa
k_{um}	0.5	kPa	W_{VD}	0.7	–
$R_{um,mc}$	688	kPa · ms/ml			

Oxygen distribution in the umbilical arterial compartment

Oxygen distribution in the model is based on the work of Sá Couto et al. [108]. Oxygen concentration in the umbilical arterial compartment is determined by convective transport alone. There is no oxygen diffusion nor metabolic uptake in the umbilical arteries. The change in oxygen amount in the umbilical arterial compartment can therefore be represented by the following equation:

$$\frac{d(cO_{um,a} \cdot V_{um})}{dt} = q_{um,a}(cO_a - cO_{um,a}). \quad (4.2)$$

Here oxygen concentration in the fetal arterial circulation and umbilical arteries is given as cO_a and $cO_{um,a}$ [$\text{m}^3 \text{O}_2/\text{m}^3 \text{blood}$] respectively, the blood volume of the compartment as $V_{um,a}$ [m^3] and the flow through the compartment as $q_{um,a}$ [m^3/s].

Baroreceptor gain

The baroreceptor reflex has been described before [125], but its gain is attenuated with a factor five to account for the differences between fetal and adult baroreceptor sensitivity, as described by Dawes et al. [18]. Baroreceptor activity as function of mean arterial blood pressure is modeled with a sigmoidal function and expressed as a fire rate f_{ab} that can vary between a minimal and maximal fire rate $f_{ab,min}$ and $f_{ab,max}$ [122, 125]:

$$f_{ab} = \frac{f_{ab,min} + f_{ab,max} \cdot e^{\left(\frac{MAP - MAP_n}{k_{ab}}\right)}}{1 + e^{\left(\frac{MAP - MAP_n}{k_{ab}}\right)}}. \quad (4.3)$$

The steepness is governed by k_{ab} , that is inversely related to the gain in the central point ($MAP = MAP_n$). Hence a fivefold decrease in gain is obtained by a fivefold increase in k_{ab} , see Table 4.3. All other baroreceptor-related parameters are identical to our previous publication [125]. Fire rate f_{ab} is filtered with a low pass filter (time constant set to 8 s) and forwarded to the vagal and sympathetic center. It thus influences four cardiovascular effectors: heart rate, cardiac contractility, venous unstressed blood volume and systemic vascular resistance.

Table 4.3: Baroreceptor parameters.

Parameter	Value	Unit
$f_{ab,min}$	2.52	s^{-1}
$f_{ab,max}$	47.78	s^{-1}
p_n	40	mmHg
k_{ab}	4.09 · 5	mmHg

**Validation of cardiocograms from a
mathematical model for use in simulation
training**

Abstract

Simulation of the cardiotocogram is increasingly used in educational programs that enhance insight into physiology or improve team work. We investigated whether the realism of model-generated CTG tracings is sufficient for educational purposes by means of a questionnaire. Respondents included participants from a training for obstetric emergencies in a simulation center (76/102 respondents), a workshop at ECOSIM 2011 (9/102 respondents) and a research meeting for clinicians at a labor ward (17/102 respondents).

Five real and five computer-generated CTG tracings with late decelerations were randomized. A 5-points Likerts scale was used to evaluate two research questions. First it was asked whether the clinicians classified the tracing as computer-generated or real (Likert's scale category 1 being *computer-generated* and 5 being *real*). Second, the suitability of each tracing was assessed (Likert's scale category 1 being *suitable* and 5 being *unsuitable*). The clinicians had the opportunity to provide additional feedback on the tracings via the evaluation form and during a group discussion after filling out the questionnaire.

Results show that the suitability for use in simulation training is found to be almost equal for real and computer-generated tracings, even though real tracings are more likely to be recognized correctly. The group discussions during the workshops revealed that variability and regularity of the simulated signals greatly influence the perception of a tracing and that the suitability of a particular tracing for use in simulation training mainly requires that the tracing is clear and free of physiological inconsistencies. The clinicians concluded that this was the case for all simulated and real tracings.

5.1 Introduction

During labor and delivery, the recording of the fetal heart rate (FHR) in combination with the recording of uterine contraction pressure i.e. the cardiotocogram (CTG) is the main modality for fetal monitoring. In the CTG, often transient FHR changes are seen in response to uterine contractions. They reflect the response to changes in (local) blood pressure and oxygen content due to local compression of fetal blood vessels e.g. in the umbilical cord, uterine or fetal cerebral circulation. Interpretation of the CTG is not straightforward, due to the complexity of the underlying physiological processes. Mathematical models that address this complexity can provide insight into this physiology. Once validated, these models can be used in labor and delivery educational programs.

We presented a mathematical model that can be used to simulate different types of FHR decelerations [123–125]. These decelerations are due to temporary reductions in local blood flow during a contraction, e.g. in the umbilical, uterine or cerebral circulation. The model describes the relation between uterine contractions and FHR. However, it has not yet been investigated whether these simulated CTG traces are suitable for use in simulation training. In this study we present a user evaluation of computer-generated (c) and real (r) traces for late decelerations. Two research questions are addressed: 1) Are the raters able to identify the origin of the tracing (i.e. computer-generated or real) and 2) Are the tracings suitable for use in simulation training.

5.2 Methods

5.2.1 Simulation model

The model describes fetomaternal cardiovascular function, fetal cardiovascular regulation (via baro- and chemoreceptor) and oxygen distribution. A contraction generator provides a uterine pressure signal that can influence specific intrauterine vascular resistances, and consequently placental and fetal blood flow, depending on the chosen scenario. Fetal oxygen levels are described via the relation between placental oxygen uptake, fetal oxygen consumption and distribution via blood flow in the cardiovascular system. The chemo- and baroreceptor respond to changes in partial oxygen pressure and blood pressure via activation and inhibition of the vagal and sympathetic nerve. They thus contribute to short-term regulation of FHR, cardiac contractility, and peripheral vasoconstriction in order to economize oxygen consumption and maintain blood pressure. The model is presented in detail in previous publications [123–125].

5.2.2 CTG tracings

The simulated scenario describes the response to contraction-induced uterine flow reduction. The temporary reduction in uterine flow prevents transport of maternal oxygen to the intervill-

lous space, which leads to a temporary reduction in oxygen transport (via diffusion) towards the fetal circulation. The corresponding fetal hypoxemia triggers the fetal chemoreceptor reflex that activates the central nervous system. The vagal and sympathetic centers respond with FHR reduction and flow redistribution from the peripheral to the central circulation. A secondary blood pressure response may further contribute to changes in FHR and flow redistribution via the baroreceptor reflex. Due to fetoplacental oxygen reserve, the FHR response is delayed with respect to the contraction, and is therefore known as “late deceleration”.

5.2.2.1 Computer-generated CTGs

Five CTGs with late decelerations from uteroplacental insufficiency were created with the simulation model [123–125]. Input parameter settings per computer-generated CTG can be found in Table 5.1. The CTG tracings with late decelerations were obtained by simulation of uteroplacental insufficiency via uteroplacental blood volume reduction of 50%, see also [125]. All CTGs had per contraction a random duration of $60 \pm 0-10$ s, a random interval of $\pm 0-20$ s and an amplitude of $\pm 0-5$ bpm with respect to input amplitude and interval. Figure 5.1 shows one of the computer-generated tracings used in this validation study.

Table 5.1: Input characteristics of the computer-generated CTGs. Per CTG, the input values for amplitude and interval of the first contraction is given. The subsequent contractions have random variation on these input values as described in the main text.

CTG #	Amplitude $\pm 0-20$ [mmHg]	Interval $\pm 0-5$ [s]
1	45	170
2	65	120
3	33	134
4	77	156
5	31	143

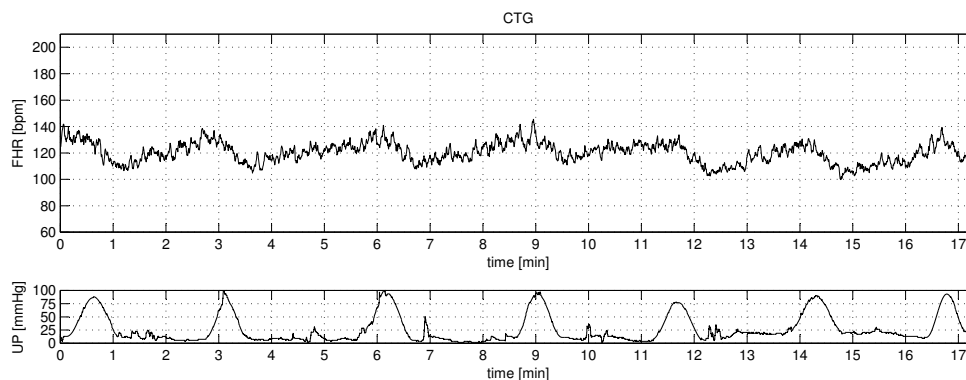


Figure 5.1: Example of a computer-generated CTG. This CTG is a computer-generated tracing with late decelerations and corresponds with #1 in Table 5.1.

5.2.2.2 Real CTGs

From the CTG database at the labor ward, the first five CTGs with late decelerations were selected. These signals were imported to Matlab (The MathWorks, release 2008a), where they were presented in a similar fashion as the CTG tracings created by the model. Figure 5.2 shows one of the real CTGs used in this validation study.

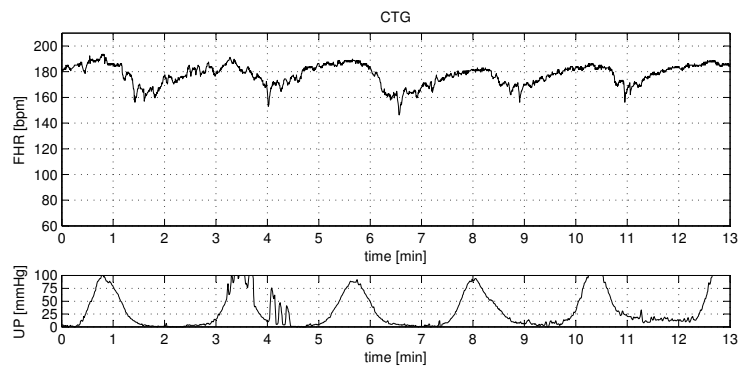


Figure 5.2: Example of a real CTG. This CTG is a real tracing obtained from the hospital database.

5.2.3 CTG validation

For validation of the CTGs, the set of five real and five computer-generated tracings was presented in the same randomized order to 102 clinicians (obstetricians, obstetric residents and midwives). The majority of these clinicians (93/102) come from different hospitals in The Netherlands and participated in an obstetric team training in a simulation center. The raters were unaware of the number of real and computer-generated tracings. The tracings have a paper speed of 2 cm/min [86]. The rating was anonymous. The raters were asked to provide their profession and the years of experience with CTG interpretation.

Ratings were collected on three occasions, one during an obstetric team training (76 raters), and two during a workshop at a conference and a hospital research meeting, respectively (17 and 9 raters).

The first group of raters, clinicians who underwent a full-day obstetric team training in a medical simulation center, filled in the questionnaire during lunch time, after a training session with 3 obstetric scenarios. The raters were asked to evaluate the tracings on a 5-points Likerts scale to determine whether they found the particular tracing:

- Computer-generated or real (1 to 5 respectively);
- Suitable or unsuitable for use in simulation training (1 to 5 respectively).

Within this paper, these two research questions are referred to as the origin and suitability of the CTGs respectively. The raters had the opportunity to give additional (voluntary) feedback on aspects in CTG, such as realism of FHR baseline, variability, deceleration depth, delay, duration and shape/appearance; contraction signal features as baseline and its shape/appearance, duration, interval, amplitude and shape/appearance of the contraction.

The second and third group of clinicians participated in two different meetings: at the Second European Conference on Simulation in Women's Health (ECOSIM 2011) and at a research meeting at a labor ward. The CTGs were presented via a beamer, the rating was on paper. After rating of all ten CTGs, a group discussion was used to obtain additional feedback on the rating. Raters were not allowed to change their rated scores once the discussion started. In the discussion, it was asked what scores each tracing was given and why, and what aspects in the CTGs determine the suitability for use in simulation training. Furthermore it was asked if there were aspects in the simulated tracings that need improvement for the use in simulation training, or how recognition of the computer-generated origin could be prevented.

5.2.4 Data analysis

5.2.4.1 Qualitative data analysis

Per CTG, the Likert's scale response frequencies (normalized) are plotted and analyzed, for both origin and suitability. Comments from the user evaluation forms and from the workshop group discussions are grouped and analyzed qualitatively.

5.2.4.2 Statistical data analysis

Quantitative data analysis was performed with Excel (Microsoft Office, 2010) and SPSS (IBM SPSS Statistics, version 20). Per trace it was investigated whether there is a trend in the rating score for the origin and suitability of the computer-generated (c) and real (r) CTGs, both with Kendall's tau test and the z-test for binominal proportions.

Origin

A low Likert's scale score indicates that the raters judge the tracing as a *computer-generated* tracing, whereas a high score indicates that the tracing is judged as *real*. Ideally, all r tracings should thus score high, i.e., raters can identify real tracings. If the raters can identify c tracings, these would get a low score in the rating. However, if they can not distinguish whether the c tracing is real or computer-generated, a high response frequency is expected for score 3, or that all scores have similar proportions.

To test the hypothesis that r tracings will show a positive trend and c tracings a negative trend, a Kendall's tau test is used for the 5-point Likert's scale. As this test has limited performance when the rating shows a stepwise response, a two-sample test for binominal proportions was

used in addition, where the data was grouped into two proportions per research question. Frequencies for scores 1-3 were grouped into category *computer-generated* and for scores 4-5 into category *real*. The z-test is performed between the two score categories within one research question, thus *computer-generated* vs. *real*.

Suitability

Data analysis for suitability is similar to data analysis for origin. For the binominal z-test, the data was grouped into *suitable* (scores 1-2) and *unsuitable* (scores 3-5), respectively. A low score represents *suitable* and a high score *unsuitable*. A negative or positive trend thus indicates that the raters judge the tracing as *suitable* and *unsuitable* for use in simulation training respectively. Tracings with no trend reflect that the raters are not unanimous about the suitability. We hypothesize that r and c tracings are equally suitable for use in simulation training, even when the origin of the tracing can be distinguished by the raters.

5.3 Results

5.3.1 Qualitative data analysis

5.3.1.1 Origin & suitability

Figure 5.3 shows the normalized frequency responses per Likert's scale score per CTG per research question (rows), for every individual CTG (left column) and for all CTGs combined (right column).

The first column in Figure 5.3 shows that the clinicians are able to recognize the origin for 4 out of 5 real tracings correctly, as the proportion increases with increasing Likert's scale. The fifth tracing shows an opposite effect: the frequency proportion reduces with increasing Likert's scale, which means that the clinicians find it more likely that this tracing is computer-generated. They had more difficulty with the origin of the c tracings: all c tracings show similar proportions for each Likert's scale category. The clinicians are thus not unanimous about the origin of the c tracings. The second column in Figure 5.3 shows that in general, r tracings are more likely to be rated as real tracing while c tracings are more likely to be rated as computer-generated tracing.

For suitability, the proportions for all of the r tracings decrease with increasing Likert's scale, indicating that the r tracings are found suitable for use in simulation training, even the tracing that was found more computer-generated than real. Although less pronounced, there seems to be a decreasing trend for some of the c tracings as well. However, a particular tracing shows the opposite trend: the majority of the raters judge this tracing as unsuitable. The general trend is that r tracings are found somewhat more suitable for use in simulation training than c tracings (see second column).

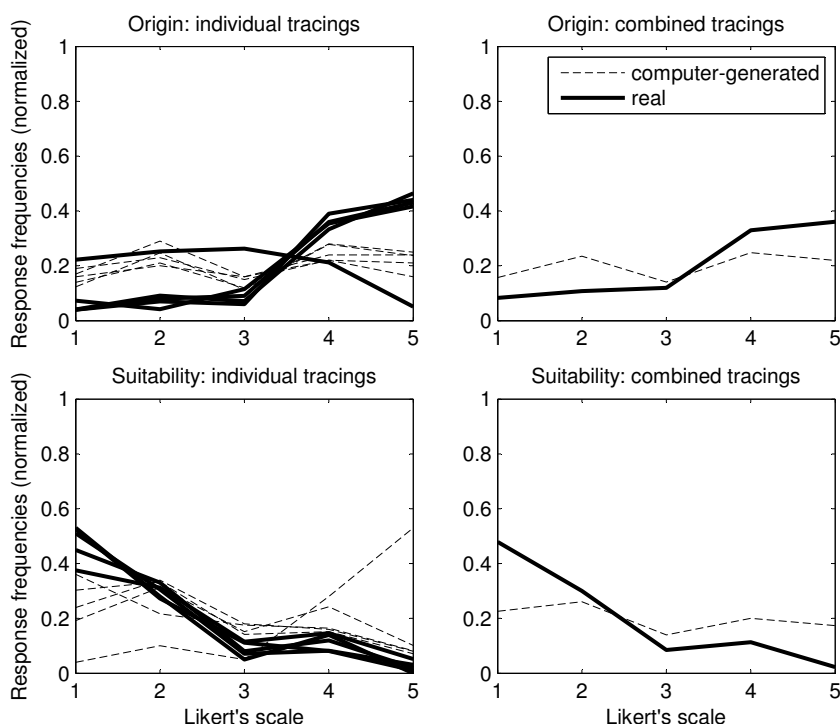


Figure 5.3: Normalized response frequencies for origin and suitability of CTGs with late decelerations. The normalized frequency response for each CTG is shown in the first column for each of the two research questions: origin and suitability (rows). Dotted lines represent computer-generated tracings, while real tracings are shown in bold lines. The second column gives the response for the combined tracings (normalized) and thus represents the mean of the first column. For origin, 1 represents *computer-generated*, 5 represents *real*. For suitability, 1 represents *suitable* and 5 *unsuitable*.

5.3.1.2 User comments on computer-generated CTGs

Although a number of experts was able to distinguish between real and computer-generated CTGs, during the discussion the experts were unanimous that the computer-generated tracings are also suitable for use in simulation training. The following remarks were made:

- The interval between contractions in some of the CTGs is too regular. In real CTGs, often more variation is seen.
- The contraction signal is too symmetric, real contractions may be skewed.
- The FHR variability seems too regular over a too long period in some of the computer-generated CTGs. Changes in variability or reduction of signal length would make the signals more realistic.

- The paper speed of the CTGs should be equal to the paper speed the clinician is used to. This speed differs from country to country and especially influences the perception of variability.
- It is difficult to distinguish between real and computer-generated tracings, one has to search for “anomalies” to find out whether the tracing is real.
- It is not a problem if it can be seen that the tracing is computer-generated, as long as the tracing is realistic, i.e., there are no physiologic inconsistencies.

5.3.2 Statistical data analysis

Table 5.2 show the statistical results for the tracings. All CTGs with late decelerations are rated by 102 clinicians on a paper form. However, sometimes a tracing in the middle of the series was skipped, for which no explanation was given.

Kendall’s tau test is used to identify a positive or negative trend for the Likert’s scale scores. A number close to 1 represents a pure monotonous relationship. From Table 5.2, it can be seen that for origin, only r1-r4 have a significant monotonous relationship, as identified by a high positive outcome for Kendall’s tau test. Hence these r tracings are recognized by the clinicians as real tracings. Kendall’s tau test is not able to identify tracings that indeed have a step response, but are not monotonous. Therefore, the z-test for binominal proportions was used to test for significant different frequency response (proportions) between the *computer-generated*- and *real*-judged tracings. Not only the tracings that were identified by Kendall’s tau, but also other tracings now reveal a distinction between the proportion of raters that judge a particular tracing as *real* or *computer-generated*. These results are in correspondence with the qualitative analysis.

Most of the c, and all of the r tracings are suitable for simulation training, according to the z-test. Two c tracings, c2 and c5, show similar proportions for the categories *suitable* and *unsuitable*, indicating that the raters are not unanimous. None of the tracings was found *unsuitable* by the majority of the raters. Although Kendall’s tau test identifies a monotonous trend for tracing c5, the binominal proportions are more or less identical. This reveals the complementary role of both tests.

5.4 Discussion

The results show that majority of the real CTGs evaluated by the clinicians is correctly identified as a real tracing. There was a number of tracings that scored equally on binominal proportions, i.e. a p-value >0.05 , indicating that the raters are not unanimous about the origin and thus cannot distinguish as a group whether the tracing is real or not.

Table 5.2: Statistics of the rated CTGs. Per research question and per CTG, Kendall's tau and the score for the binominal z-test for testing two proportions are given. Values between brackets represent the p-value for the used test, printed in bold when $p < 0.05$. A negative Kendall's tau indicates a negative relationship with increasing Likert's scale score. The proportions consists of Likert scale category 1-3 vs. category 4-5 (Origin), and Likert scale category 1-2 vs. category 3-5 (Suitability). Hence Likert's scale category 3 is grouped with the most unfavorable group: *computer(-generated)* and *unsuitable*.

	Origin				Suitability			
	Kendall's tau	<i>computer</i> [N]	<i>real</i> [N]	z-test	Kendall's tau	<i>suitable</i> [N]	<i>unsuitable</i> [N]	z-test
c1	0.20 (0.62)	47	50	(0.39)	0.32 (0.45)	57	41	(0.01)
c2	-0.32 (0.45)	62	38	(0.00)	-0.40 (0.33)	50	50	(0.56)
c3	0.67 (0.12)	52	48	(0.34)	-0.80 (0.05)	58	43	(0.02)
c4	0.40 (0.33)	47	53	(0.24)	-0.60 (0.14)	63	36	(0.00)
c5	0.00 (1.00)	57	43	(0.03)	0.80 (0.05)	48	52	(0.34)
r1	1.00 (0.00)	21	79	(0.00)	-0.53 (0.21)	78	22	(0.00)
r2	0.80 (0.05)	17	83	(0.00)	-0.20 (0.62)	81	20	(0.00)
r3	0.80 (0.05)	22	74	(0.00)	-0.80 (0.05)	67	30	(0.00)
r4	0.80 (0.05)	20	79	(0.00)	-1.00 (0.00)	79	20	(0.00)
r5	-0.40 (0.33)	73	26	(0.00)	-0.80 (0.05)	79	18	(0.00)

Almost all CTGs with late decelerations are found suitable for use in simulation training. For two computer-generated tracings, the clinicians are divided into two equal groups and thus not unanimous about the suitability of these tracings.

The composition of the group of clinicians is not homogenous, as they have different experience and responsibility in clinical practice for CTG interpretation. The majority of the raters (93/102) works in a Dutch hospital, while the remaining 9 clinicians work in European hospitals. As statistical analysis was already difficult due to small proportions, no further attempt was made to subdivide the group into different categories for profession and/or experience with CTG interpretation. However, it would be interesting to investigate the differences in rating between those groups within a larger population.

The respondents from the participants in the obstetric team training course come from groups with a similar distribution of clinicians per team (1 gynaecologist, 1 resident, 1-2 midwives and several nurses). These clinicians come from non-academic hospitals from all over The Netherlands, but train together with their own hospital team (7-9 persons at a time). The respondents from the conference were from different countries. During their group discussion it became clear that especially the perception of variability depends on paper speed. The international attendees are used to a paper speed of either 1, 2 or 3 cm/min, while the presented CTGs were printed with a paper speed of 2 cm/min, which is common in The Netherlands. Most of these clinicians agreed that changing the paper speed to the speed they use in daily practice, would probably solve the issue.

Several additional comments were made with respect to suitability of the tracings for use in simulation training, either on paper or during the group discussion in the workshops. A number

of comments was made on short-term (beat-to-beat) FHR variability, which was often perceived as artificial. As the physiologic modeling of short-term FHR variability is not within the scope of this research project, a simple black box model was used for variability. Variability is not part of the model, but added in a postprocessing step to enable validation of simulated CTGs by clinicians. Clinicians are fairly good in detecting artificial FHR variability, as one of the obstetricians commented during the single scenario workshop: “the signal is too regular and lacks anomalies, suggesting that it is computer-generated”. Another frequent remark was the regular shape of contractions on some of the r tracings. Some clinicians found it unrealistic that the contraction signal was that smooth.

From the user evaluation via the questionnaire and group discussion in workshops, it becomes clear that the perception of the tracing depends strongly on the variability and regularity of the signals. However, there is a lot of physiologic variation in both FHR and uterine contraction signals, which has the drawback that some r tracings are still perceived as *computer-generated*, but the advantage that c tracings fit in more easily in the large physiologic range of real tracings. To enhance the simulated tracings, a physiologic model of FHR variability could be incorporated that also takes into account the evolution of FHR baseline and variability changes over time.

The participants of the workshops were asked for factors in the CTGs that could be improved for use in simulation training. Two main suggestions were made, related to the variability of the FHR and the regularity of the contraction interval. The variability signal should be more irregular and evolving over time. A more irregular contraction interval would also improve the suitability of the computer-generated tracings, as real tracings often have typical irregularities. Most of the participants agreed that the presence of irregularities was also the main trigger for them to distinguish real from computer-generated tracings. However, they did not find it necessary to include irregularities on purpose to mask the origin of the signal in an educational setting.

During the workshop at the research meeting in the hospital, the clinicians agreed that CTG tracings are suitable once they are clear and lack physiologic contradictions, like severe short-term variability during late decelerations, etc. This implied that after the discussion, if they would have been allowed, they would have rated more tracings as *suitable* than *unsuitable*. However, this option was not given, as this would have resulted in a biased rating.

Simulated signals are intended to enhance simulation training, it is especially important that the tracings are suitable for use in simulation training. Therefore, category 3 in the Likert's scale was grouped within *unsuitable*. However, “suitability for use in simulation training” may be perceived differently from clinician to clinician. A shortcoming of the current set-up was that no explanation was given on what was meant with this phrase. However, all participating clinicians are familiar with obstetric simulation training, either from the team training day at the simulation center (CTGs were provided during the scenarios) or as participants of the ECOSIM

conference. The clinicians at the research meeting at the labor ward have several years of experience with simulation-based training. As a result, they may have different notions on the suitability of CTG tracings for simulation-based training.

At the end of the group discussion at the international conference, all experts agreed that the computer-generated CTG traces as presented to them can be used for simulation training. The participants at the hospital research meeting agreed that -when no physiologic inconsistencies are present- simulated tracings may even be more suitable for simulation training than real tracings, which often are less clear.

Acknowledgements

We gratefully acknowledge Koo Rijpkema for his advice with the statistical analysis.

**Intrauterine resuscitation by maternal
hyperoxygenation evaluated in a simulation
model**

*L. Bullens, M.B. van der Hout-van der Jagt, P.J. van Rinnard Heimeel and S.G. Oei
Submitted to: Early Human Development*

Abstract

Uterine contractions influence fetal hemodynamics and oxygenation status which, via complex pathways, affects fetal heart rate (FHR). When fetal distress is suspected due to nonreassuring FHR, maternal hyperoxygenation may be useful as an intrauterine resuscitation technique. In this study we simulated the effect of maternal hyperoxygenation on FHR and fetal pO_2 in a mathematical model.

First, we simulated variable decelerations during maternal normoxia level (98 mmHg). Second, we simulated variable decelerations during maternal hyperoxia by increasing maternal pO_2 gradually to 475 mmHg. We simulated the effect of hyperoxygenation on variable FHR decelerations and pO_2 in the umbilical cord, placenta and fetus, caused by contractions of different strength.

Depending on the contraction amplitude, deceleration depth during maternal normoxia was between -32 and -62 beats per minute (bpm). Deceleration duration varied between 109 and 140 seconds. During maternal hyperoxygenation, deceleration depth decreased and varied between -9 and -50 bpm. Deceleration duration varied between 22 to 60 seconds. In all placental and fetal compartments, pO_2 increased during maternal hyperoxygenation.

6.1 Introduction

One of the main tasks of obstetricians is to monitor fetal wellbeing during labor and prevent fetal hypoxemia and asphyxia [38]. Therefore, fetal heart rate (FHR) is monitored during labor, generally by the use of the cardiotocogram (CTG) that registers FHR in relation to uterine contractions. Intrauterine pressure influences fetal hemodynamics and oxygenation status which, via complex pathways, affects FHR [7, 14, 30, 78, 84, 130]. Therefore it is important to monitor both uterine pressure and FHR in relation to each other. Ideally, information about fetal hemodynamics and oxygenation status should be available during labor to have insight in the condition of the fetus. However, these values cannot be measured directly. Since FHR is derived from these values, this is a practical tool to estimate fetal wellbeing.

Various maternal, placental and fetal parameters influence FHR, such as maternal cardiac output and saturation, oxygen diffusion capacity in the placenta, fetal cerebral blood flow, fetal oxygen consumption, baro- and chemoreceptor responses and vagal- and sympathetic nerve responses. Recently, a mathematical simulation model is developed to give insight into the complex relationship between these parameters [124, 125].

When FHR is reassuring, this reflects a normally oxygenated fetus. However, in clinical practice, FHR patterns are often not unequivocal. In only 16% of vaginal births, FHR is completely normal [25]. When FHR shows less baseline variability, decelerations or bradycardia, this may be a sign of fetal hypoxia [4, 25, 68, 80]. In case of suspected fetal distress, intrauterine resuscitation can be applied in order to improve fetal oxygen levels and prevent acidosis. In literature, several intrauterine resuscitation techniques are described, although poor sustainable evidence is available to prove the beneficial effect of these techniques [112]. One of these techniques is maternal hyperoxygenation in order to increase oxygen transport to the fetus. Several clinical trials have shown that maternal hyperoxygenation, by administering 100% oxygen, increases maternal arterial pO_2 and leads to an increase in fetal oxygen status by diffusion in the placenta [4, 32, 46, 63, 99, 100, 112, 128]. Few studies investigated the effect of maternal hyperoxygenation on FHR. In these studies, a decrease in late decelerations on the cardiotocogram during maternal hyperoxygenation is noticed [4, 63, 80]. Despite the lack of a randomized controlled trial to investigate the effect of maternal hyperoxygenation during fetal distress on fetal outcome [27], in some hospitals the administration of oxygen to the mother in case of nonreassuring FHR patterns is common practice [13, 74].

In this study, we used a mathematical, computerized model to investigate the influence of maternal hyperoxygenation on fetal pO_2 and alterations in variable decelerations on the CTG. We hypothesized that maternal hyperoxygenation will cause an increase in fetal pO_2 and a concurrent decrease in deceleration depth and duration on the CTG.

6.2 Methods

6.2.1 Model design

A mathematical model was developed by our group and implemented in Matlab 2008a (Math-Works Inc USA). This feto-maternal oxygenation model is validated for simulation of decelerations in the CTG caused by reflex mechanisms [124, 125]. The model consists of several modules.

First, the cardiovascular system of mother and fetus are modelled. Cardiac function, blood flow, volume and pressure are variables included in this system.

Second, an oxygen distribution model is used to calculate oxygen concentrations in several compartments in the feto-maternal circulation. Oxygen distribution between the mother and fetus is dependent on arterial oxygen level in the mother, oxygen diffusion capacity in the placenta, fetal oxygen consumption, and feto-placental blood flows and volumes. Maternal arteries supply new oxygen into the intervillous space of the placenta. Diffusion of oxygen from the maternal to the fetal part of the placenta is mainly dependent on the oxygen pressure difference in the intervillous space and umbilical microcirculation and the diffusion capacity of the placental membrane. Oxygen diffuses into the fetal circulation and mixes with venous blood before entering the fetal arterial circulation. This blood is forwarded to cerebral and peripheral circulation where oxygen is consumed by metabolic uptake, and to the umbilical circulation, where new oxygen uptake takes place.

Third, cardiovascular regulation is provided by the fetal baro- and chemoreceptor that monitor fetal blood pressure and oxygen pressure, respectively. Stimulation of these receptors leads to changes in cardiovascular parameters, including FHR. In addition, cerebral autoregulation may increase cerebral flow during hypoxemia.

Finally, contractions are simulated by a contraction generator. Uterine pressure baseline level, contraction duration, peak strength and interval can be changed by the user. Intrauterine pressure changes may lead to alterations in fetal and maternal blood oxygenation, blood pressure and flow.

6.2.2 Simulation

We applied uniform uterine contractions within each simulation to simulate “uniform” variable decelerations originating from umbilical cord compression to exclude influence of random variation. We varied contraction strength for each simulation. Parameter settings for the model in different simulations can be found in Table 6.1.

For each simulation, the first two umbilical cord compressions are applied during maternal

Table 6.1: Parameter settings for each simulation.

Simulation	Peak strength [mmHg]	Duration [s]	Interval [s]	Figure
1	60	60	90	6.1a, 6.2
2	70	60	90	6.1b, 6.2
3	80	60	90	6.1c, 6.2

normoxia level (pO_2 98 mmHg) [63, 128]. After the second umbilical cord compression, 100% oxygen administration to the mother via a non-rebreathing mask is simulated by an exponential increase to a maternal pO_2 steady state of 475 mmHg, as reported by Vasicka et al. [128] Three simulations with different contraction strength (60 to 80 mmHg, increasing with steps of 10 mmHg, contraction interval 90 seconds) are used to investigate the effect of contraction amplitude on FHR and oxygenation.

6.2.3 Outcome

The primary outcome measure is the difference in duration and depth of decelerations during maternal normoxia and hyperoxia, as a reaction to contractions with different strength and interval.

Second, we compared fetal pO_2 before and after maternal hyperoxygenation. We compared pO_2 the intervillous space, umbilical vein and artery and the fetal cerebral- and microcirculation. All results are compared to results from clinical trials if available.

6.3 Results

Parameter settings for each simulation can be found in Table 6.1. Depending on the contraction strength, deceleration depth during normoxia was between -32 and -62 bpm, while deceleration duration varied between 109 and 140 seconds (Figure 6.1, Table 6.2). During maternal hyperoxygenation deceleration depth decreased for all cases and varied between -9 and -50 bpm, while deceleration duration varied between 22 to 60 seconds (Figure 6.1, Table 6.2).

The model showed a gradual increase in pO_2 in the intervillous space of 24-56 mmHg during hyperoxygenation, an increase in the umbilical vein from 24-55 mmHg and in the fetal cerebral and microcirculation from 2 and 2-3 mmHg respectively. The proportional increase is related with contraction strength (simulation 1-3, Figure 6.2). Table 6.3 shows the results from our simulation and the results from clinical trials.

With the increase of contraction strength, a decrease in rise of pO_2 is noticed in all compartments, except the umbilical vein and intervillous space where oxygen is accumulated in case of cord occlusion. Also, the stronger the contraction, the less the difference in pO_2 and decel-

Table 6.2: Differences in variable decelerations for normoxia and hyperoxia. Differences in FHR deceleration depth and duration of variable decelerations during maternal normoxia and hyperoxia, during simulations of three types of contractions (see Table 6.1).

Simulation		Normoxia	Hyperoxia	Difference
1	Deceleration depth [bpm]	-32	-9	23
	Duration [s]	109	22	-87
1	Deceleration depth [bpm]	-56	-32	24
	Duration [s]	140	50-	-90
1	Deceleration depth [bpm]	-62	-50	12
	Duration [s]	138	60	-78

Table 6.3: Fetal pO_2 during normoxia and hyperoxia. Fetal pO_2 values (mmHg) in different compartments during maternal hyperoxygenation obtained from literature and from the simulation model.

	Khazin et al. [63]		Vasicka et al. [128]		Gare et al. [32]		Prystowsky [99]		Model	
	21%	100%	21%	100%	21%	100%	21%	100%	21%	100%
Fetal microcirculation	19.38	25.18			14.7	18.1			14.7	17.2
Intervillous space			33.1	46.7			37.5	69	44.1	54.4
Umbilical vein			20.7	30.7	21.6	27.8	18.0	31.7	31.4	41.3
Umbilical artery			10.2	15.5	12.1	13.7	8	13.1	17.3	20.0

eration duration and depth is noticed (Figure 6.2, Table 6.2). In short, the effect of maternal hyperoxygenation decreased with an increase in contraction strength.

6.4 Discussion

This study showed that the effect of maternal hyperoxygenation on FHR and pO_2 as described by Althabe [4] and Vasicka et al. [128], can be reproduced with a mathematical model. Simulation results show that maternal hyperoxygenation causes an increase in maternal and fetal pO_2 which leads to a decrease in depth and duration of decelerations on the CTG.

Oxygen diffusion over the placental membrane is mainly dependent on the difference between maternal and fetal pO_2 . Several studies show the ability to increase maternal pO_2 by breathing 100% oxygen, although the maximum value in maternal blood to achieve varies from 280 to 606 mmHg [9, 32, 63, 128]. We based maternal pO_2 increase on Vasicka et al. [128], who described from minute to minute the maternal pO_2 in response to 100% oxygen administration via a non-rebreathing mask .

Recent clinical studies showed a beneficial effect of maternal hyperoxygenation on fetal oxygenation status. Vasicka et al. [128], Khazin et al. [63], Prystowsky [99], and Gare et al. [32] show an increase of pO_2 in the maternal artery, intervillous space, umbilical vein and artery dur-

ing maternal hyperoxygenation with 100% oxygen, compared to breathing room air (Table 6.2). Haydon et al. [46] tested the effect of maternal hyperoxygenation on fetal SpO_2 while breathing 40 and 100% oxygen. Fetal SpO_2 increased from 43.5%, to 48.4% and 50%, respectively. The lower the initial fetal SpO_2 , the greater the increase during maternal hyperoxygenation [32, 46]. In contrast to the admission of 100% oxygen, one study shows no increase in fetal oxygenation status of breathing 40% oxygen [21]. However, in Haydon's study, SpO_2 does significantly increase also while breathing 40% oxygen. The discrepancy with former studies may be due to the inclusion of patients with non-reassuring FHR in Haydon's study, what may reflect a lower initial oxygen status [46].

In line with results from literature, our simulation model shows a gradual increase in pO_2 in all fetal compartments during maternal hyperoxygenation with 100% oxygen. Table 6.3 shows our results compared to results obtained from clinical trials mentioned in literature. Values in fetal microcirculation and intervillous space are similar to values obtained from our model. However, pO_2 values in the umbilical cord estimated by our model are slightly higher when compared to values obtained from clinical experiments [80]. As there is no complete clinical dataset with all parameter values that affect feto-placental oxygenation, internal model parameters are obtained from different human and animal studies. These parameters define the specific oxygen pressures in the feto-placental circulation.

In literature little evidence is available on the effect of maternal hyperoxygenation during FHR decelerations. Althabe et al. [4] demonstrate an increase in pO_2 in capillary fetal blood from 22 to 33 mmHg after 10 minutes. This leads to an improvement of late decelerations. Khazin et al. [63] confirm this improvement of late decelerations during maternal hyperoxygenation. Our simulation model show a decrease in deceleration depth and duration during maternal hyperoxygenation as described in literature. Absolute values of both FHR and pO_2 dependent on contraction strength.

During labor, cord compressions caused by uterine contractions are a main cause of variable decelerations on the cardiotocogram. Cord compression causes a temporary accumulation of blood in the umbilical cord, leading to a rapid increase in fetal arterial blood pressure. The baroreceptor responds to this increase in blood pressure by increasing its fire rate. Due to an interruption in oxygen supply, a decrease in fetal arterial pO_2 appears, evoking a chemoreceptor response. Both activation of the baro- and chemoreceptor initiate a dominant vagal response leading to a drop in FHR [7]. We simulated uniform variable decelerations in the model to prevent FHR variations from variable cord occlusions, as they may interfere with changes in FHR due to the intervention. However, variable decelerations are characterized by their variation in shape, duration and onset, due to changes in compression grade and duration from contraction to contraction. Late decelerations, originating from uterine flow reduction during contraction are uniform and would be suitable for simulation of interventions. However, we chose not to test the effect of the intervention on late decelerations, because we believe in clinical practice variable decelerations are much more frequent and allow awaiting the effect of the intervention,

while in late decelerations immediate termination of labor is justified.

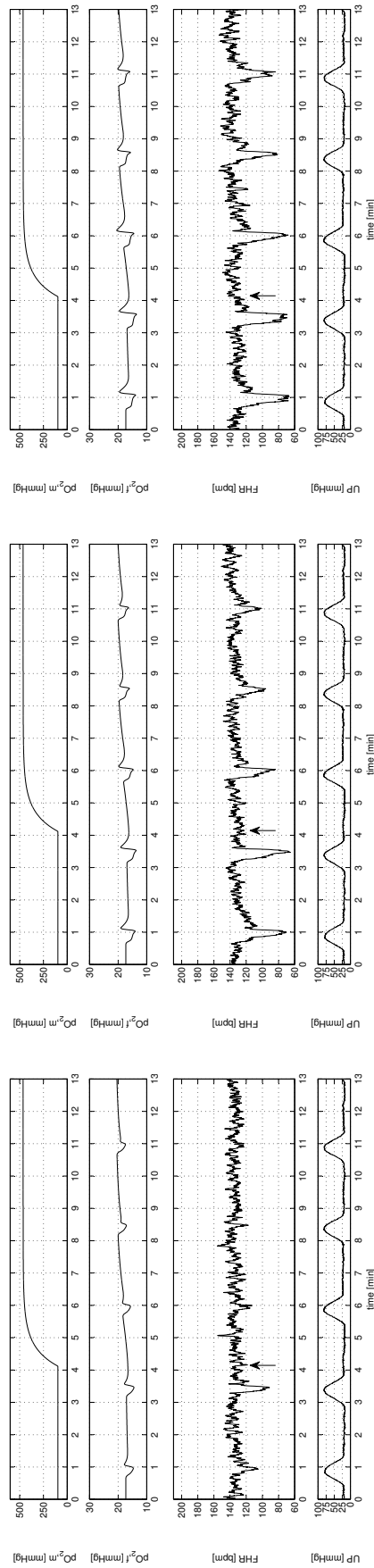
We simulated cord compressions caused by contractions of different strength and interval. Remarkably, the positive effect of hyperoxygenation on FHR and pO_2 decreased with increasing contraction strength. This can be explained by complete occlusion of the umbilical cord during strong contractions, which prevents the delivery of the additional oxygen towards the fetus. In case of incomplete occlusion of the placental vessels, the additional amount of oxygen in the umbilical vein can partly arrive at the fetus. This raises the question whether lowering intrauterine pressure, for example by temporary cessation of pushing during the second stage of labor, may also be an effective intervention in case of fetal distress.

The discussion on the possible harmful effect of administration of high concentrations of oxygen is on-going [119]. In animal experiments, vasoconstriction of the placental vessels is noticed, although in human studies harmful effects are not evident [32, 63, 87]. Also, the formation of free radicals damaging cell membranes in asphyxiated fetus is described [9]. Thorp et al. [119] show a negative effect on pH in the prophylactic use of oxygen for more than 10 minutes, they do not have a clear answer on the mechanism leading to deterioration in cord blood gas values. The study has no answer on the possible beneficial effect of oxygen administration in case of fetal distress. Furthermore, the optimal duration of oxygen administration in case of fetal distress has still to be distinguished.

A pitfall in simulation of physiological processes is the use of fixed estimated values in a mathematical model. The model represents a general term fetus of 3 kg and is therefore not patient-specific. Individual variation depends on individual differences for example in placental flow, fetal cardiac function and oxygen demand. Variation in model parameters is not implemented in the model yet. Also, heart rate variability as a result of different physiological processes is not integrated in the model. The simulation model is suitable as a qualitative tool that can be used to enhance insight in fetomaternal oxygenation status and for educational purposes.

Decelerations in FHR are suspect for fetal acidosis [4, 68]. When deceleration depth and duration decrease, improvement of fetal oxygenation status is likely, since the depth and duration of decelerations are related to metabolic acidemia in the fetus [42]. Little evidence is available on improvement of fetal pH during maternal hyperoxygenation [4, 63]. Our simulation model does not provide pH levels. The model neither takes into account the production of catecholamines influencing fetal hemodynamics. Therefore, influence of contraction interval and the absolute duration of labor do not influence FHR and fetal oxygenation status in this simulation.

In conclusion, this fetomaternal model is able to simulate the effect of maternal hyperoxygenation on FHR and pO_2 . Our model contributes to the insight into the complex relationship between parameters influencing fetal oxygenation status and FHR. The simulation indicates a positive effect of maternal hyperoxygenation on FHR and fetal pO_2 , suggesting a better fetal outcome. However, randomised controlled trials are needed to confirm the beneficial effect of hyperoxygenation on clinical outcome.



a. 60 mmHg

b. 70 mmHg

c. 80 mmHg

Figure 6.1: Maternal and fetal arterial pO_2 and fetal heart rate in relation to uterine contractions of 60, 70 and 80 mmHg. After the second contraction 100% oxygen is applied to the mother (indicated by the arrow in the figure).

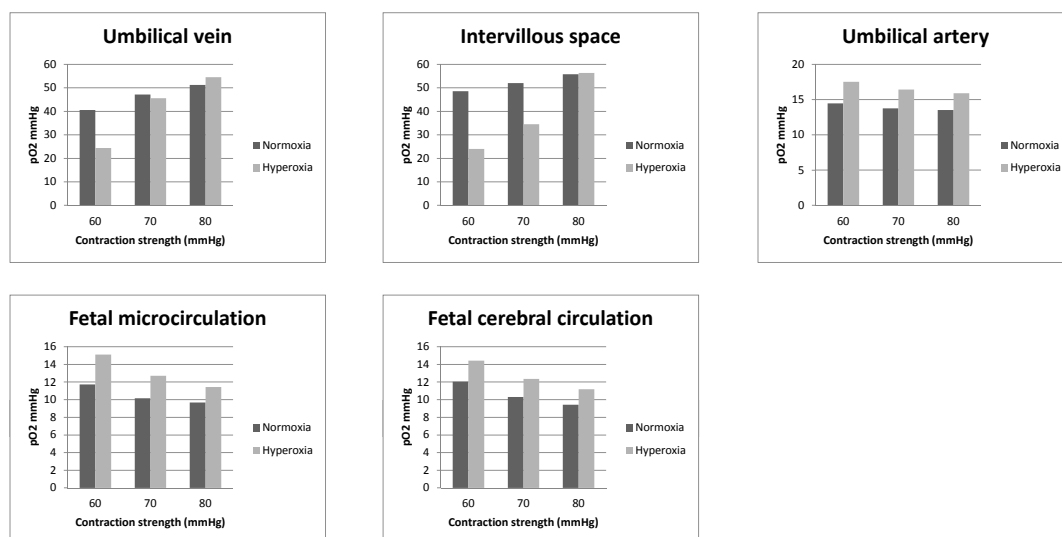


Figure 6.2: Effect of hyperoxygenation on pO_2 in different compartments during contractions of 60, 70 and 80 mmHg.

Chapter 7

General discussion

7.1 Introduction

Fetal wellbeing during labor and delivery is commonly monitored through the cardiotocogram (CTG), the combined registration of uterine contractions and fetal heart rate (FHR). From the CTG, the fetal oxygen state is estimated as the main indicator of the fetal condition, but this estimate is difficult to make, due to the complex relation between oxygen state and CTG. Mathematical models can be used to assist in interpretation of the CTG, since they enable quantitative modeling of the flow of events through which uterine contractions affect fetal oxygenation and FHR. This thesis aims to contribute to a better understanding of the physiologic processes leading to fetal heart rate (FHR) decelerations in labor by means of mathematical modeling. In order to contribute to a better obstetric care and improved feto-maternal outcome, the engineering approach consists of a chain of analyzing, modeling and evaluation. This chapter will discuss the major findings and outline future perspectives.

7.2 Main contributions

In **Chapter 2**, a mathematical model is developed to simulate FHR as function of uterine contractions that lead to caput compression. The model is tested for steady state (normoxia) and caput compression leading to early decelerations via direct vagal nerve stimulus from local hypoxia. A user evaluation with six gynaecologist-perinatologists indicates that cardiotocograms (CTGs) with real and computer-generated early heart rate decelerations get similar ratings for realism. In addition, the raters cannot identify the origin of the real and computer-generated tracings.

In **Chapter 3** the model is extended with autonomous nervous system feedback from an adult cardiovascular regulation model [122] that was rescaled to the fetal physiologic working points for blood pressure and oxygenation. In addition, cerebral autoregulation was included. With the model, late decelerations were investigated, i.e. decelerations originating from uteroplacental insufficiency, inducing fetal hypoxemia. Indeed, model simulations with uterine flow reductions during labor contractions cause a delayed fetal hypoxemia that, via the chemoreceptor, leads to flow redistribution. This is also known as the “brain-sparing mechanism”. The amount of redistribution is dependent on the buffer capacity of the placenta. These simulations show the primary FHR response to severe hypoxemia, which is bradycardia. Jensen et al. [55] show that this primary response dominates in their 60 s occlusions. However, in their 90 s occlusions a secondary increase in FHR is observed. This finding is in line with observations in clinical practice, that prolonged hypoxemia induces tachycardia. The mechanism believed responsible for this secondary FHR response, namely fetal catecholamines produced by the adrenal gland, are not incorporated in the model.

In **Chapter 4** the model is slightly adapted by explicitly modeling the umbilical arterial circulation, which was previously lumped into the fetal arterial compartment. This now allows the

simulation of variable decelerations originating from compression of the umbilical veins and/or arteries. During simulation of the uterine flow reductions (Chapter 3), it was noticed that fetal blood pressure could be maintained. From sheep experiments it is known that the fetal baroreceptor reflex is less effective than the adult baroreceptor reflex [18]. Since fetal blood pressure is directly affected by umbilical cord compression, the baroreceptor gain was reduced. Indeed, during umbilical cord compression simulations, fetal blood pressure increases with 40%, which is in line with reported animal data. Fetal heart rate response is proportional to changes in oxygenation and blood pressure, irrespective of contraction amplitude and duration. As expected, no overshoot is present in our simulations, independent of the severity of the compression, as the catecholamines which are believed to be responsible for this reaction, is not included in the model.

Although the preliminary CTG evaluation presented in Chapter 2 indicates that the clinical experts did not rate real tracings differently than computer-generated tracings, this evaluation was only held with six experts and one scenario. Therefore a larger study was carried out. The results are described in **Chapter 5**. The majority of a total of 102 clinicians identified real CTGs with late decelerations correctly. However, only half of them classified computer-generated tracings with late decelerations as computer-generated, the other half classified these tracings as real. Nevertheless, there seem to be only small differences in their judgement on suitability for use of real and computer-generated tracings in simulation training. Main concerns include the absence of irregularities (e.g. due to recording) and the regularity of the variability signal. FHR beat-to-beat variability was not included in the model, but added in a post-processing step to allow CTG evaluation by clinicians, as CTGs without this variability are of no physiological meaning. A similar user evaluation was held to investigate the simulated CTGs from early and variable decelerations. However, due to organizational issues, the dataset was too small to draw conclusions with sufficient statistical accuracy. The results of this study show that for variable decelerations (27 clinicians) real and computer-generated tracings cannot be distinguished. The majority of the tracings is found suitable for simulation training. For early decelerations, only 15 clinicians participated in a workshop where the CTGs were evaluated. The results indicate that these clinicians were able to distinguish computer-generated from real tracings (identical tracings as in the preliminary study in Chapter 2). This was also expressed in their judgement on suitability of these tracings for use in simulation training. During the subsequent group discussion, the clinicians agreed that they found all computer-generated and real tracings suitable for use in simulation training, as they are clear and do not show physiological inconsistencies. According to these clinicians, the fact that the tracings might be recognized as computer-generated is not a major issue for use in simulation training.

The model thus seems to be of added value for both simulation training purposes and insight into the physiologic processes during reflex FHR decelerations induced by uterine contractions. Moreover, the model can be used to investigate clinical hypotheses. As an example, the model was used to test the hypothesis that maternal hyperoxygenation leads to an increased fetal pO_2 and thus to less severe FHR decelerations. **Chapter 6** shows that maternal hyperoxygenation

in the model leads to increased fetal oxygenation and a decrease in the duration and depth of variable FHR decelerations from umbilical cord compression. This can be explained by the increase in maternal pO_2 , that via diffusion increases fetal pO_2 . Since the fetal chemoreceptor plays a major role in the physiologic cascade of umbilical cord compression, a decrease in chemoreceptor activation will also reduce the extent of FHR response. However, severe and prolonged compression may still lead to severe decelerations, as the oxygen buffer provided by maternal hyperoxygenation may not be sufficient for these severe hypoxic episodes.

7.3 Future perspectives

7.3.1 Simulation model

From the above, it is clear that the simulation model provides opportunities for improving physiological insight and enhancement of simulation training. Still, there are several areas for improvement. Major improvements include model extension with catecholamine regulation due to severe hypoxemia to model the secondary cardiovascular responses [57, 84]. It is expected that this will allow the occurrence of FHR overshoot following severe variable decelerations [129] and tachycardia developed during longterm hypoxemia [57].

Furthermore, a true modeling of beat-to-beat variability, may contribute to insight into the relation between the autonomous nerve system, acidotic state and FHR variability [84, 126]. Currently, variability is added in a postprocessing step, with a frequency spectrum corresponding to that found in real signals. Ideally, beat-to-beat variability is included in the closed loop and modeled as function of fetal physiologic state, determined a.o. by fetal sleep patterns, maturation, movement and pH [84, 126]. Coupling of FHR variability to pH would also provide additional information to clinicians, as pH is often used to confirm or exclude fetal acidosis when the CTG is non-reassuring. As indicated by the comments from the user evaluation in Chapter 5, variability plays a major role in the interpretation of CTGs. A more fundamental modeling approach will probably also contribute to the realism of simulated CTGs.

In the model, the maternal cardiovascular system is currently not under reflex control. Moreover, besides a homeostatic cardiovascular function, maternal breathing is assumed to be sufficient to provide a continuous normoxic blood flow to the placenta. However, several obstetric emergencies are known to negatively affect maternal cardiovascular function and oxygenation [37]. Thus in order to simulate obstetric scenarios that cause maternal cardiovascular and oxygenation changes, at least neurological feedback from the baro- and chemoreceptor needs to be included, as this can seriously influence the blood flow and oxygenation level of the blood towards the intervillous space and thus to the fetus. With this extension, a larger range of clinical scenarios and possible intervention strategies, such as oxygen administration to the mother, could be investigated. Oxygen administration during labor is not common in the Netherlands. Some Dutch hospitals provide oxygen when the fetus is believed to be hypoxic, but this is rare

in our country. It would be of interest to compare the simulation results with CTGs with and without maternal hyperoxygenation. Simulation results then not only contribute to the debate of clinical interventions, but the simulation model validity may also profit from such clinical studies.

7.3.2 Application

The model is implemented in Matlab (MathWorks Inc. USA), which is not widely available in the clinic. Hence to facilitate the educational use of the model in a clinical environment, an implementation in a web-based environment or e.g. as an App would contribute to its availability for clinicians “in the field”. Currently, the model is being incorporated in a “serious game” (Birthplay), in which common as well as rare clinical situations during deliveries are simulated and practiced. At present, within our research group, the game and the physiological model are subject of research within a randomized trial [20]. The simulation model can provide realistic CTG tracings in each scenario. In addition, the model could be coupled to a full-body delivery simulator to provide patient data such as the CTG and maternal hemodynamics. To provide all clinically measurable fetal parameters, the model requires fetal scalp blood parameters and APGAR score. During labor, a fetal scalp blood sample is often used to assess fetal wellbeing via pH and acid-base status. In the postnatal stage, the APGAR score is used one and five minutes after birth to assess fetal wellbeing by means of heart rate, breathing, skin color, reflex irritability and muscle tone.

Currently, the model is not yet suitable for clinical decision support and patient-specific prediction, as it represents a generalized term fetus with input data from different sources, including fetal estimates which are based on human adults and fetal sheep. A first important step towards patient-specific modelling includes a thorough sensitivity analysis to discriminate between parameters that can be generalized for all term pregnancies and parameters that need to be determined patient-specifically due to high sensitivity or important parameter interactions [49, 50]. Once these parameters are identified, each parameter has to be estimated based on personal data. This is difficult for most parameters due to the limited availability of intrapartum measurement techniques. Hence before the model can be used in clinical decision support, it is of the utmost importance that these parameters can be accurately measured for each patient, or that estimations of patient-specific parameters can be validated. Besides availability of relevant clinical data, the short time span of labor presents a serious challenge for identifying model parameter values, and subsequent simulation of candidate intervention scenarios to achieve better fetomaternal care. Even if the techniques are available, limitations in time and organization complicate the clinical use of the model in labor. However, time and organization limitations play a smaller role in the care of imminent preterm labor patients, as these patients are often for several days or even weeks at the hospital. Nevertheless, this requires that technical issues as described above are taken care of.

And last, but not least, the implementation of any technology in a clinical environment requires careful collaboration between clinicians and engineers in the complete process of data collection, patient-specific modeling and simulation, model output interpretation and treatment. The patient will only benefit when both professionals combine their expertises: accurate knowledge of medical care, analytical evaluation of processes (either medical or technical), the ability to discriminate between general principles and individual variations, the development of new techniques and technologies, and empathy with each individual patient.

7.4 Conclusion

In this thesis, a mathematical model was developed to successfully simulate the physiologic effects of uterine contraction pressure on fetal blood pressure, oxygenation and heart rate for three different scenarios. Model output was evaluated via literature data and expert opinion. The clinicians judge the model-generated CTGs as suitable for educational use. Furthermore, the model was used to test the hypothesis that fetal heart rate will improve following oxygen administration to the mother during variable fetal heart rate decelerations. The model can contribute to a better understanding of fetal cardiovascular physiology in labor, which should finally result in improved patient care.

Bibliography

- [1] A.E. Abbas, S. Lester, and H. Connolly. Pregnancy and the cardiovascular system. *Int J Cardiol*, 98:179–189, 2005.
- [2] I. Ahmer-Walin, S. Arulkumaran, H. Hagberg, K. Maršál, and G.H.A. Visser. Fetal electrocardiogram: St waveform analysis in intrapartum surveillance. *Br J Obstet Gynecol*, 114:1191–1193, 2007.
- [3] C.J. Aldrich, D. D’Antona, J.A.D. Spencer, D.T. Delpy, E.O.R. Reynolds, and J.S. Wyatt. Fetal heart rate changes and cerebral oxygenation measured by near-infrared spectroscopy during the first stage of labour. *Europ J Obstet Gynecol Reprod Biol*, 64:189–195, 1996.
- [4] O. Althabe Jr., R.L. Schwarcz, S.V. Pose, L. Escarcena, and R. Caldeyro-Barcia. Effects on heart rate and fetal pO₂ of oxygen administration to the mother. *Am J Obstet Gynecol*, 98:858–870, 1967.
- [5] T. Arts, P. Bovendeerd, T. Delhaas, and F. Prinzen. Modeling the relation between cardiac pump function and myofiber mechanics. *J Biomechanics*, 36:731–736, 2003.
- [6] T. Arts, T. Delhaas, P. Bovendeerd, X. Verbeek, and F.W. Prinzen. Adaptation to mechanical load determines shape and properties of heart and circulation: the CircAdapt model. *Am J Physiol Heart Circ Physiol*, 288:H1943–1954, 2005.
- [7] R.H. Ball and J.T. Parer. The physiologic mechanisms of variable decelerations. *Am J Obstet Gynecol*, 166:1683–1689, 1992.
- [8] J. Barcroft. *The development of vascular reflexes. In: researches on pre-natal life*. Blackwell Scientific Publications, Oxford, 1946.

- [9] J. Bartnicki and E. Saling. The influence of maternal oxygen administration on the fetus. *Int J Gynecol Obstet*, 45:87–95, 1994.
- [10] L.F. Bastos, M.F. Lobo, W.L. van Meurs, and D. Ayres-de Campos. An intrauterine pressure generator for educational simulation of labour and delivery. *Med Eng Phys*, 32:740–745, 2010.
- [11] L. Bennet, J.A. Westgate, Y.C. Liu, G. Wassink, and A.J. Gunn. Fetal acidosis and hypotension during repeated umbilical cord occlusions are associated with enhanced chemoreflex responses in near-term fetal sheep. *J Appl Physiol*, 99:1477–1482, 2005.
- [12] P.H.M. Bovendeerd, P. Borsje, T. Arts, and F.N. van de Vosse. Dependence of intramyocardial pressure and coronary flow on ventricular loading and contractility: a model study. *Ann Biomed Eng*, 34:1833–1845, 2006.
- [13] University Hospitals Bristol. Intrauterine resuscitation guideline, november 2008. <http://www.oaa-anaes.ac.uk>.
- [14] R. Caldeyro-Barcia, C. Méndez-Bauer, J.J. Poseiro, L.A. Escarena, S.V. Pose, J. Bienenarz, I. Arnt, L. Gulin, and O. Althabe. *The heart and circulation in the newborn and infant*. In: *Control of the human fetal heart rate during labor*, pages 7–36. Grune & Stratton, New York, 1966.
- [15] W.L. Capper, J.G. Cowper, and L.J. Myers. A transferfunction-based mathematical model of the fetal-placental circulation. *Ultrasound Med Biol*, 28:1421–1431, 2002.
- [16] I. Cetin, S. Boito, and T. Radaelli. Evaluation of fetal growth and fetal well-being. *Semin Ultrasound CT MRI*, 29:136–146, 2008.
- [17] W.R. Cohen, J. Piasecki, and B. Jacksono. Plasma catecholamines during hypoxemia in fetal lamb. *Am J Physiol Regul Integr Comp Physiol*, 12:R520–R525, 1982.
- [18] G.S. Dawes, B.M. Johnston, and D.W. Walker. Relationship of arterial pressure and heart rate in fetal, new-born and adult sheep. *J Physiol*, 309:405–417, 1980.
- [19] J. de Haan, A.J. Gunn, and P.D. Gluckman. Fetal heart rate changes do not reflect cardiovascular deterioration during brief repeated umbilical cord occlusions in near-term fetal lambs. *Am J Obstet Gynecol*, 176:8–17, 1997.
- [20] L.D. de Wit-Zuurendonk and S.G. Oei. Serious gaming in women’s health. *BJOG*, 118:17–21, 2011.
- [21] G.A. Dildy, S.L. Clark, and C.A. Loucks. Intrapartum fetal pulse oximetry: the effects of maternal hyperoxia on fetal arteriolar oxygen saturation. *Am J Obstet Gynecol*, 171:1120–1124, 1994.

- [22] T. Draycott, J.F. Crofts, J.P. Ash, L.V. Wilson, E. Yard, T. Sibanda, and A. Whitelaw. Improving neonatal outcome through practical shoulder dystocia training. *Obstet Gynecol*, 112:14–20, 2008.
- [23] T. Draycott, T. Sibanda, L. Owen, V. Akande, C. Winter, and A. Whitelaw. Does training in obstetric emergencies improve neonatal outcome? *BJOG*, 113:177–182, 2006.
- [24] L.J. Edwards, G. Simonetta, J.A. Owens, Robinson J.S., and I.C. McMillen. Restriction of placental and fetal growth in sheep alters fetal blood pressure responses to angiotensin II and captopril. *J Physiol*, 515:897–904, 1999.
- [25] C. Elliott, P.A. Warrick, E. Graham, and E.F. Hamilton. Graded classification of fetal heart rate tracings: association with neonatal metabolic acidosis and neurologic morbidity. *Am J Obstet Gynecol*, 202:258.e1–258.e8, 2010.
- [26] J.H.L. Evers, J. de Haan, A.J. Jongsma, A.J. Crevels, T.H.M. Arts, and C.B. Martin Jr. The preejection period of the fetal cardiac cycle. II. umbilical cord occlusions. *Europ J Obstet Gynecol Reprod Biol*, 11:401–418, 1981.
- [27] B. Fawole and G.J. Hofmeyr. Maternal oxygen administration for fetal distress. *Cochrane Database Syst Rev*, 4:CD000136, 2003.
- [28] K. Flo, T. Wilsgaard, Å. Vårtun, and G. Acharya. A longitudinal study of the relationship between maternal cardiac output measured by impedance cardiography and uterine artery blood flow in the second half of pregnancy. *BJOG*, 117:837–844, 2010.
- [29] National Institute for Clinical Excellence. *Clinical guideline 55. Intrapartum care: care of healthy women and their babies during childbirth*. NICE, London, 2007.
- [30] R.K. Freeman, T.J. Garite, and M.P. Nageotte. *Fetal heart rate monitoring*. Lippincott Williams & Wilkins, Philadelphia, 2000.
- [31] Y.C. Fung. *Biomechanics: Circulation*. Springer-Verlag, New York, 1997.
- [32] D.J. Gare, J. Shime, W.M. Paul, and M. Hoskins. Oxygen administration during labor. *Am J Obstet Gynecol*, 105:954–961, 1969.
- [33] T. Geva, M.B. Mauer, L. Striker, B. Kirshon, and J.M. Pivarnik. Effects of physiologic load of pregnancy on left ventricular contractility and remodeling. *Am Heart J*, 133:53–59, 1997.
- [34] D.A. Giussani, J.A.D. Spencer, and M.A. Hanson. Fetal cardiovascular reflex responses to hypoaemia. *Fetal Matern Med Rev*, 6:17–37, 1994.
- [35] D.A. Giussani, N. Unno, S.L. Jenkins, R.A. Wentworth, J.B. Derks, J.H. Collins, and P. Nathanielsz. Dynamics of cardiovascular responses to repeated partial umbilical cord compression in late-gestation sheep fetus. *Am J Physiol Heart Circ Physiol*, 273:H2351–2360, 1997.

- [36] J.W. Goldkrand, D.H. Moore, S.U. Lentz, S.P. Clements, D.U. Turner, and J.L. Bryant. Volumetric flow in the umbilical artery: normative data. *J Matern Foetal Med*, 9:224–228, 2000.
- [37] K. Grady, C. Howel, and C. Cox. *The MOET course manual. Managing obstetric emergencies and trauma*. RCOG Press, London, 2007.
- [38] E.M. Graham, K.A. Ruis, A.L. Hartman, F.J. Northington, and H.E. Fox. A systematic review of the role of intrapartum hypoxia-ischemia in the causation of neonatal encephalopathy. *Am J Obstet Gynecol*, 199:587–595, 2008.
- [39] F. Greiss. *Glob Libr Women's Med*. DOI 10.3843/GLOWM.10197, 2008.
- [40] A. Guettouche, J.C. Challier, Y. Ito, C. Papapanayotou, Y. Cherruault, and A. Azancot-Benisty. Mathematical modeling of the human fetal arterial blood circulation. *Int J Biomed Comput*, 31:127–129, 1992.
- [41] A.C. Guyton and J.E. Hall. *Textbook of medical physiology*. Saunders company, Philadelphia, 2000.
- [42] E. Hamilton, P. Warrick, and D. O'Keeffe. Variable decelerations: do size and shape matter? *J Matern Fetal Neonatal Med*, 25:648–653, 2012.
- [43] M.A. Hanson. Do we now understand the control of the fetal circulation? *Eur J Obstet Gynecol Reprod Biol*, 75:55–61, 1997.
- [44] J.L. Harris, T.R. Krueger, and J.T. Parer. Mechanisms of late decelerations of the fetal heart rate during hypoxia. *Am J Obstet Gynecol*, 144:491–496, 1982.
- [45] T.H.M. Hasaart and J. de Haan. Depression of uterine blood flow during total umbilical cord occlusion in fetal sheep. *Europ J Obstet Gynecol Reprod Biol*, 19:125–131, 1985.
- [46] M.L. Haydon, D.M. Gorenberg, M.P. Nageotte, M. Ghamsary, P.J. Rumney, C. Patillo, and T.J. Garite. The effect of maternal oxygen administration on fetal pulse oximetry during labor in fetuses with nonreassuring fetal heart rate patterns. *Am J Obstet Gynecol*, 195:735–738, 2006.
- [47] M.A. Hofman. Evolution of brain size in neonatal and adult placental mammals: a theoretical approach. *J Theor Biol*, 105:317–332, 1983.
- [48] A. Holdcroft and T.A. Thomas. *Principles and practice of obstetric anaesthesia and analgesia*. Wiley-Blackwell, Oxford, 2000.
- [49] W. Huberts, C. de Jonge, W.P.M. van der Linden, M.A. Inda, K. Passera, J.H.M. Tordoir, F.N. van de Vosse, and E.H.M. Bosboom. A sensitivity analysis of a personalized pulse wave propagation model for arteriovenous fistula surgery. Part B: Identification of possible generic model parameters. *Med Eng Phys*, <http://dx.doi.org/10.1016/j.medengphy.2012.08.012>, 2012.

- [50] W. Huberts, C. de Jonge, W.P.M. van der Linden, M.A. Inda, J.H.M. Tordoir, F.N. van de Vosse, and E.H.M. Bosboom. A sensitivity analysis of a personalized pulse wave propagation model for arteriovenous fistula surgery. Part A: Identification of most influential model parameters. *Med Eng Phys*, <http://dx.doi.org/10.1016/j.medengphy.2012.08.013>, 2012.
- [51] F. Huikeshoven, T.G. Coleman, and H.W. Jongsma. Mathematical model of the fetal cardiovascular system: the uncontrolled case. *Am J Physiol*, 239:R317–R325, 1980.
- [52] F. Huikeshoven, I.D. Hope, G.G. Power, R.D. Gilbert, and L.D. Longo. Mathematical model of fetal circulation and oxygen delivery. *Am J Physiol*, 249:R192–R202, 1985.
- [53] J. Itskovitz, B.W. Goetzman, and A.M. Rudolph. The mechanism of late deceleration of the heart rate and its relationship to oxygenation in normoxic and chronically hypoxemic fetal lambs. *Am J Obstet Gynecol*, 142:66–71, 1982.
- [54] J. Itskovitz, E.F. LaGamma, and A.M. Rudolph. The effect of reducing umbilical blood flow on fetal oxygenation. *Am J Obstet Gynecol*, 145:813–818, 1983.
- [55] J. Itskovitz, E.F. LaGamma, and A.M. Rudolph. Heart rate and blood pressure responses to umbilical cord compression in fetal lambs with special reference to the mechanism of variable deceleration. *Am J Obstet Gynecol*, 147:451–457, 1983.
- [56] J. Itskovitz, E.F. LaGamma, and A.M. Rudolph. Effects of cord compression on fetal blood flow distribution and O₂ delivery. *Am J Physiol Heart Circ Physiol*, 252:H100–H109, 1987.
- [57] A. Jensen, Y. Garnier, and R. Berger. Dynamics of fetal circulatory responses to hypoxia and asphyxia. *Reprod Biol*, 84:155–172, 1999.
- [58] A. Jensen, W. Künzel, and Kastendieck E. Repetitive reduction of uterine blood flow and its influence on fetal transcutaneous pO₂ and cardiovascular variables. *J Dev Physiol*, 7:75–87, 1985.
- [59] P. Johnson, D.J. Maxwell, M.J. Tynan, and L.D. Allan. Intracardiac pressures in the human fetus. *Heart*, 84:59–63, 2000.
- [60] J.J. Joyce, P.I. Dickson, N. Qi, J.E. Noble, J.U. Raj, and B.G. Baylen. Normal right and left ventricular mass development during early infancy. *Am J Cardiol*, 93:797–801, 2004.
- [61] J. Kakogawa, K. Sumimoto, T. Kawamura, S. Minoura, and N. Kanayama. Noninvasive monitoring of placental oxygenation by near-infrared spectroscopy. *Semin Thromb Hemost*, 31:297–301, 2005.

- [62] R. Katz, J.S. Karliner, and R. Resnik. Effects of a natural volume overload state (pregnancy) on left ventricular performance in normal human subjects. *Circulation*, 58:434–441, 1978.
- [63] A.F. Khazin, E.H. Hon, and F.W. Hehre. Effects of maternal hyperoxia on the fetus. I. oxygen tension. *Am J Obstet Gynecol*, 109:628–637, 1971.
- [64] T. Kiserud. Foetal circulation. *Semin Foetal Neonatal Med*, 10:493–503, 2005.
- [65] J.C. Konje, K. Abrams, S.C. Bell, R.D. de Chazal, and D.J. Taylor. The application of color power angiography to the longitudinal quantification of blood flow volume in the fetal middle cerebral arteries, ascending aorta, descending aorta, and renal arteries during gestation. *Am J Obstet Gynecol*, 182:393–400, 2000.
- [66] J.C. Konje, E.S. Howarth, P. Kaufmann, and D.J. Taylor. Longitudinal quantification of uterine artery blood volume flow changes during gestation in pregnancies complicated by intrauterine growth restriction. *Br J Obstet Gynecol*, 110:301–305, 2003.
- [67] A. Kozák-Bárány, E. Jokinen, P. Kero, J. Tuominen, T. Rönnemaa, and I. Välimäki. Impaired left ventricular diastolic function in newborn infants of mothers with pregestational or gestational diabetes with good glycemic control. *Early Hum Dev*, 77:13–22, 2004.
- [68] F.W. Kubli, E.H. Hon, A.F. Khazin, and H. Takemura. Observations on heart rate and pH in the human fetus during labor. *Am J Obstet Gynecol*, 104:1190–1206, 1969.
- [69] J.D. Larma, A.M. Silva, C.J. Holcroft, R.E. Thompson, P.K. Donohue, and E.M. Graham. Intrapartum electronic fetal heart rate monitoring and the identification of metabolic acidosis and hypoxic-ischemic encephalopathy. *Am J Obstet Gynecol*, 197:301.e1–301.e8, 2007.
- [70] C.Y. Lee, P.C. Di Loreto, and J.M. O’Lane. A study of fetal heart rate acceleration patterns. *Obstet Gynecol*, 48:19–26, 1976.
- [71] H. Li, S. Gudmundsson, and P. Olofsson. Uterine artery blood flow velocity waveforms during uterine contractions. *Ultrasound Obstet Gynecol*, 22:578–585, 2003.
- [72] H. Li, S. Gudmundsson, and P. Olofsson. Acute centralization of blood flow in compromised human fetuses evoked by uterine contractions. *Early Hum Dev*, 82:747–752, 2006.
- [73] G. Link, K.E. Clark, and U. Lang. Umbilical blood flow during pregnancy: evidence for decreasing placental perfusion. *Am J Obstet Gynecol*, 196:489e1–489e7, 2007.
- [74] R. Liston, D. Sawchuck, D. Young, Society of Obstetrics & Gynaecologists of Canada, and British Columbia Perinatal Health Program. Fetal health surveillance: antepartum and intrapartum consensus guideline. *J Obstet Gynaecol Can*, 29:S3–S56, 2007.

- [75] J.A. Low, B.G. Lindsay, and E.J. Derrick. Threshold of metabolic acidosis associated with newborn complications. *Am J Obstet Gynecol*, 177:1391–1394, 1997.
- [76] G.A. Macones, G.D. Hankins, C.Y. Spong, J. Hauth, and T. Moore. The 2008 National Institute of Child Health and Human Development workshop report on electronic fetal monitoring: update on definitions, interpretation and research guidelines. *J Obstet Gynecol Neonatal Nurs*, 37:510–515, 2008.
- [77] C.B. Martin Jr. Normal fetal physiology and behavior, and adaptive responses with hypoxemia. *Semin Perinatol*, 32:239–242, 2008.
- [78] C.B. Martin Jr., J. de Haan, B. van der Wildt, H.W. Jongsma, A. Dieleman, and T.H.M. Arts. Mechanism of late decelerations in the fetal heart rate. a study with autonomic blocking agents in the fetal lamb. *Europ J Obstet Gynec Reprod Biol*, 9:361–373, 1979.
- [79] W.C. McGaghie, Draycott T.J., W.F. Dunn, C.M. Lopez, and D. Stefanidis. Evaluating the impact of simulation on translational patient outcomes. *Simul Healthc*, 6:S42–S47, 2011.
- [80] C. Méndez-Bauer, I.C. Arnt, L. Gulin, L. Escarcena, and R. Caldeyro-Barcia. Relationship between blood pH and heart rate in the human fetus during labor. *Am J Obstet Gynecol*, 97:530–545, 1967.
- [81] J. Metcalfe, H. Bartels, and W. Moll. Gas exchange in the pregnant uterus. *Physiol Rev*, 47:782–838, 1967.
- [82] T. van Mieghem, P. DeKoninck, P. Steenhaut, and J. Deprest. Methods for prenatal assessment of fetal cardiac function. *Prenat Diagn*, 29:1193–1203, 2009.
- [83] A.D. Mohangoo, S.E. Buitendijk, C.W.P.M. Hukkelhoven, A.C.J. Ravelli, G.C. Rijninks-van Driel, P. Tamminga, and J.G. Nijhuis. Hoge perinatale sterfte in Nederland vergeleken met andere landen: de Peristat-II-studie. *Ned Tijdschr Geneeskd*, 152:2718–2727, 2008.
- [84] M. Murray. *Antepartal and intrapartal fetal monitoring*. Springer Publishing Company, New York, 2007.
- [85] Stichting Perinatale Audit Nederland. *A terme sterfte in 2010. Perinatale audit: eerste verkenningen*. Utrecht, 2011.
- [86] Nederlandse Vereniging voor Obstetrie en Gynaecologie. *Richtlijn foetale bewaking*. NVOG, Utrecht, 2003.
- [87] G. Nyberg and B. Westin. The influence of oxygen tension and some drugs on human placental vessels. *Acta Physiol Scand*, 39:216–227, 1957.

- [88] S. O'Brien, M. Doyle, P. Rolfe, Y. Wickramasinghe, R. Houston, and A. Warwick. Near infrared spectroscopy: a new technique for intrapartum fetal surveillance. *Conf Proc IEEE Eng Med Biol Soc*, 14:2493–2494, 1992.
- [89] M. Okane, S. Shigemitsu, J. Inaba, M. Koresawa, T. Kubo, and H. Iwasaki. Non-invasive continuous fetal transcutaneous pO₂ and pCO₂ monitoring during labor. *J Perinat Med*, 17:399–410, 1989.
- [90] A.C.C. van Oppen, I. van der Tweel, G.P.J. Alsbach, R.M. Heethaar, and H.W. Bruinse. A longitudinal study of maternal hemodynamics during normal pregnancy. *Obstet Gynecol*, 88:40–46, 1996.
- [91] J.T. Parer. Obstetrics and gynecology - epitomes of progress: two mechanisms of late decelerations: reflex and myocardial hypoxia. *West J Med*, 134:530–531, 1981.
- [92] J.T. Parer. Evaluation of the fetus during labor. *Curr Probl Pediatr*, 12:3–25, 1982.
- [93] J.T. Parer. *Handbook of fetal heart rate monitoring*. W.B. Saunders Co. Philadelphia, 2009.
- [94] J.T. Parer, T.R. Krueger, and J.L. Harris. Fetal oxygen consumption and mechanisms of heart rate response during artificially produced late decelerations of fetal heart rate in sheep. *Am J Obstet Gynecol*, 136:478–482, 1980.
- [95] L.L.H. Peeters, R.E. Sheldon, M.D. Jones Jr., A.L. Makowski, and G. Meschia. Blood flow to fetal organs as a function of arterial oxygen content. *Am J Obstet Gynecol*, 135:637–646, 1979.
- [96] G. Pennati, M. Bellotti, and R. Fumero. Mathematical modelling of the human fetal cardiovascular system based on doppler ultrasound data. *Med Eng Phys*, 19:327–335, 1997.
- [97] EURO-PERISTAT project in collaboration with SCPE, EUROCAT and EURONEONET. *European perinatal health report. Better statistics for better health for pregnant women and their babies in 2004*. 2008.
- [98] H. Prystowsky. Fetal blood studies, VII. The oxygen pressure gradient between the maternal and fetal bloods of the human in normal and abnormal pregnancy. *Bull Johns Hopkins Hosp*, 101:48–56, 1957.
- [99] H. Prystowsky. Fetal blood studies. XI. The effect of prophylactic oxygen on the oxygen pressure gradient between the maternal and fetal bloods of the human in normal and abnormal pregnancy. *Am J Obstet Gynecol*, 78:483–488, 1959.
- [100] E.J. Quilligan, A. Vasicka, R. Aznar, P.J. Lipsitz, T. Moore, and B.M. Bloor. Partial pressure of oxygen in the intervillous space and the umbilical vessels. *Am J Obstet Gynecol*, 79:1048–1052, 1960.

- [101] S.R.M. Reynolds. Bradycardia in the lamb fetus in response to circulatory distress. *Am J Physiol*, 176:169–174, 1954.
- [102] B.S. Richardson, L. Carmichael, J. Homan, L. Johnston, and R. Gagnon. Fetal cerebral, circulatory, and metabolic responses during heart rate decelerations with umbilical cord compression. *Am J Obstet Gynecol*, 175:929–936, 1996.
- [103] B. Robinson. A review of NICHD standardized nomenclature for cardiotocography: the importance of speaking a common language when describing electronic fetal monitoring. *Rev Obstet Gynecol*, 1:56–60, 2008.
- [104] S. Rodbard and K. Kuramoto. Transmural pressure and vascular resistance in soft-walled vessels. *Am J Heart*, 66:786–791, 1963.
- [105] A.A. Rosenberg, M.D. Jones Jr., R.J. Traystman, M.A. Simmons, and R.A. Molteni. Response of cerebral blood flow to changes in pCO₂ in fetal, newborn and adult sheep. *Am J Physiol*, 242:H862–H866, 1982.
- [106] S. Rubler, P.M. Damani, and E.R. Pinto. Cardiac size and performance during pregnancy estimated with echocardiography. *Am J Cardiology*, 40:534–540, 1997.
- [107] A.M. Rudolph. *Congenital diseases of the heart*. Wiley-Blackwell, Oxford, 2009.
- [108] P.M. Sá Couto, W.L. van Meurs, J.F. Bernardes, J.P. Marques de Sà, and J.A. Goodwin. Mathematical model for educational simulation of the oxygen delivery to the fetus. *Control Eng Prac*, 10:59–66, 2002.
- [109] K.G. Schmidt, N.H. Silverman, and J.I.E. Hoffman. Determination of ventricular volumes in human fetal hearts by two-dimensional echocardiography. *Am J Cardiol*, 76:1313–1316, 1995.
- [110] W. Schmidt and A. Kurjak. *Color Doppler sonography in gynecology and obstetrics*. Thieme Medical Publishers, Stuttgart, 2005.
- [111] J.W. Severinghaus. Simple, accurate equations for blood O₂ dissociation computations. *J Appl Physiol*, 46:599–602, 1979.
- [112] K.R. Simpson. Intrauterine resuscitation during labor: review of current methods and supportive evidence. *J Midwifery Womens Health*, 52:229–237, 2007.
- [113] S. Sjöstedt, G. Rooth, and F. Caligara. The oxygen tension of the blood in the umbilical cord and the intervillous space. *Arch Dis Child*, 35:529–533, 1960.
- [114] C. Skillman, M.A. Plessinger, J.R. Woods, and K.E. Clark. Effect of graded reductions in uteroplacental blood flow on the fetal lamb. *Am J Physiol Heart Circ Physiol*, 249:H1098–H1105, 1985.

- [115] A.D. Stevens and E.R. Lumbers. Effects of reduced uterine blood flow on fetal cardiovascular, renal, and lung function. *Am J Physiol Regul Integr Comp Physiol*, 259:R1004–R1011, 1990.
- [116] P.C. Struijk. *Assessment of hemodynamic parameters in the fetal and uteroplacental circulation using Doppler ultrasound*. PhD thesis, Erasmus University Rotterdam, The Netherlands, 2006.
- [117] H. Suga, K. Sagawa, and A.A. Shoukas. Load independence of the instantaneous pressure-volume ratio of the canine left ventricle and effects of epinephrine and heart rate on the ratio. *Circ Res*, 32:314–322, 1973.
- [118] G.S. Sykes, P.M. Molloy, J.C. Wollner, P.J. Burton, B. Wolton, P. Rolfe, P. Johnson, and A.C. Turnbull. Continuous, noninvasive measurement of fetal oxygen and carbon dioxide levels in labor by use of mass spectrometry. *Am J Obstet Gynecol*, 150:847–858, 1984.
- [119] J.A. Thorp, T. Trobough, R. Evans, J. Hedrick, and J.D. Yeast. The effect of maternal oxygen administration during the second stage of labor on umbilical cord blood gas values: A randomized controlled prospective trial. *Am J Obstet Gynecol*, 172:465:474, 1995.
- [120] T. Todros, C. Guiot, and P.G. Piantà. Modelling the fetoplacental circulation: II. A continuous approach to explain normal and abnormal flow velocity waveforms in the umbilical arteries. *Ultrasound Med Biol*, 18:545–551, 1992.
- [121] M.E. Towell. The relationship between arterial and tissue pO₂ in the fetal lamb. *J Perinat Med*, 16:139–149, 1992.
- [122] M. Ursino and E. Magosso. Acute cardiovascular response to isocapnic hypoxia. I. A mathematical model. *Am J Physiol Heart Circ Physiol*, 279:H149–H165, 2000.
- [123] M.B. van der Hout-van der Jagt, G.J.L.M. Jongen, P.H.M. Bovendeerd, and S.G. Oei. Insight into variable fetal heart rate decelerations from a mathematical model. *Early Human Dev*, <http://dx.doi.org/10.1016/j.earlhumdev.2012.12.001>, 2012.
- [124] M.B. van der Hout-van der Jagt, S.G. Oei, and P.H.M. Bovendeerd. A mathematical model for simulation of early decelerations in the cardiotocogram during labor. *Med Eng Phys*, 34:579–589, 2012.
- [125] M.B. van der Hout-van der Jagt, S.G. Oei, and P.H.M. Bovendeerd. Simulation of reflex late decelerations in labor with a mathematical model. *Early Human Dev*, 89:7–19, 2013.
- [126] C.H. van Laar, J.O.E.H. and Peters, S. Houterman, P.F. Wijn, A. Kwee, and S.G. Oei. Normalized spectral power of fetal heart rate variability is associated with scalp blood pH. *Early Human Dev*, 87:259–263, 2011.

- [127] W.L. van Meurs. *Modeling and simulation in biomedical engineering. Applications in cardiorespiratory physiology*. McGraw-Hill, New York, 2011.
- [128] A. Vasicka, E.J. Quilligan, R. Aznar, P.J. Lipsitz, and B.M. Bloor. Oxygen tension in maternal and fetal blood, amniotic fluid, and cerebrospinal fluid of the mother and the baby. *Am J Obstet Gynecol*, 79:1041–1047, 1960.
- [129] J.A. Westgate, L. Bennet, H.H. de Haan, and A.J. Gunn. Fetal heart rate overshoot during repeated umbilical cord occlusion in sheep. *Obstet Gynecol*, 97:454–459, 2001.
- [130] J.A. Westgate, B. Wibbens, L. Bennet, G. Wassink, J.T. Parer, and A.J. Gunn. The intrapartum deceleration in center stage: a physiologic approach to the interpretation of fetal heart rate changes in labor. *Am J Obstet Gynecol*, 197:236.e1–236.e11, 2007.
- [131] J.S. Wyatt, M. Cope, C.E Richardson, A.D. Edwards, S. Wray, and E.O.R. Reynolds. Quantitation of cerebral blood volume in human infants by near-infrared spectroscopy. *J Appl Physiol*, 68:1086–1091, 1990.
- [132] A.C. Yao, M. Moinian, and J. Lind. Distribution of blood between infant and placenta after birth. *Lancet*, 294:871–873, 1969.

Nederlandse samenvatting

De meest gebruikte methode voor foetale bewaking tijdens de bevalling is de registratie van het foetaal hartritme (FHR) in combinatie met de baarmoedercontracties, beter bekend als het cardiotocogram (CTG). Het CTG wordt gebruikt om een schatting van de foetale oxygenatiestatus te maken, omdat de beschikbare hoeveelheid zuurstof in sterke mate het foetaal welzijn bepaalt. Echter, het is niet eenvoudig om hiervan een schatting te maken op basis van het CTG, omdat de relatie tussen beide complex is. Mathematische modellen kunnen hierbij helpen, aangezien de invloed van weeën op foetale oxygenatie en FHR kwantitatief in kaart kan worden gebracht. In dit proefschrift wordt de ontwikkeling van een model beschreven dat de fysiologische cascade voor verschillende klinische scenario's kan reproduceren.

Allereerst is een model ontwikkeld dat de relatie beschrijft tussen uteruscontracties, hemodynamica van moeder en kind, zuurstof distributie in de foeto-maternale circulatie, en foetale cardiovasculaire reflexregulatie voor veranderingen in bloed- en zuurstofdrukken. Het model is deels gebaseerd op eerder gepubliceerde modellen voor hartfunctie, regulatie op basis van zuurstofconcentratie bij de volwassene (chemoreceptorreflex) en zuurstof distributie in de foetale circulatie. Deze modellen zijn aan elkaar gekoppeld en waarnodig geschaald naar foeto-maternale afmetingen. Het model is gecompleteerd met een beschrijving van de weeën en een foeto-maternale circulatie. De modelrespons is getest met een eerste scenario, waarbij de hersendoorbloeding afneemt bij weeën tijdens de eerste fase van de indaling van het hoofd in het geboortekanaal. In een pilotstudie is de kwaliteit van de gesimuleerde signalen getest met behulp van klinische experts. De experts waren niet in staat om onderscheid te maken tussen echte en gesimuleerde signalen, wat suggereert dat het model gebruikt kan worden voor educatieve doeleinden.

In de tweede plaats is het model uitgebreid met een baroreceptorreflex die op basis van veranderingen in bloeddruk eigenschappen in hart en vaten aanpast. Hierdoor kon een tweede kli-

nisch scenario gesimuleerd worden, waarbij zowel de chemo- als de baroreceptorreflexpaden leiden tot een deceleratie (vertraging) in het foetaal hartritme in reactie op verminderde doorbloeding in de baarmoedercirculatie tijdens contracties. Resultaten laten zien dat de partiële zuurstofdrukken in de foetus in verhouding met de sterkte en de duur van de wee verminderen. Daarnaast zijn FHR-deceleraties voor verschillende scenarios van uteroplacentaire insufficiëntie gesimuleerd. De resultaten voor een vermindering in uteroplacentaire bloedflow en voor verminderde placentaire zuurstofdiffusiecapaciteit laten zien dat de hoogte van de basislijn van het FHR vermindert en dat de diepte van de deceleraties afneemt. Een vermindering in uteroplacentair bloedvolume leidt slechts tot afname van de deceleratiediepte. Het model laat daarnaast zien dat voor blokkade van specifieke zenuwen de resultaten in overeenstemming zijn met experimentele data uit schaapexperimenten, wat suggereert dat de sympatovagale balans in het model correct is.

Ten derde is het model gebruikt voor een derde deceleratietype, namelijk variabele deceleraties veroorzaakt door navelstrengcompressie. Verschillende compressiesterktes zijn onderzocht. Een toename in contractieamplitude en -duur leidt tot een toename in de mate van navelstrengcompressie, en daarmee de mate van veranderingen in bloeddruk, bloedstroomredistributie en FHR respons. Er is een duidelijke relatie tussen de mate van zuurstofreductie, bloeddrukstijging en het resulterende FHR. De mate van navelstrengcompressie en dus van FHR-deceleratie is zowel afhankelijk van de duur en amplitude van de contractie als de gevoeligheid van de navelstrengweerstand voor de druk in de baarmoeder als gevolg van de wee.

Als vierde is aan gynaecologen, verloskundigen en arts-assistenten gynaecologie gevraagd om een set CTG's te beoordelen, waarbij een deel van de CTG's uit het model afkomstig is en een deel uit de database van de kliniek. Dit is gedaan voor drie klinische scenarios. Echte CTG's hadden een grotere kans hebben om correct herkend te worden dan CTG's uit het model. De geschiktheid van zowel echte als computer-gegenereerde CTG's werd echter min of meer gelijk geacht. Door de beperkte hoeveelheid data voor variabele en vroege deceleraties blijkt de statistische data-analyse alleen mogelijk te zijn voor de CTG's met late deceleraties. Via aanvullende opmerkingen van de respondenten bleek dat FHR variabiliteit en de (afwezigheid van) irregulariteiten de belangrijkste indicator zijn voor het herkennen van de oorsprong van het CTG. De betrokken klinici zijn het er tenslotte over eens dat, zolang een bepaald CTG eenduidig is en geen fysiologische onjuistheden bevat, het geschikt is voor trainingsdoeleinden. Dit bleek voor alle gesimuleerde CTG's het geval.

Als vijfde is het model gebruikt om de klinische hypothese te testen dat het toedienen van zuurstof aan de moeder het FHR zal verbeteren in aanwezigheid van variabele deceleraties. Het model is gebruikt om de foetale zuurstof- en FHR-respons te simuleren bij het toedienen van 100% zuurstof aan de moeder. Modeluitkomsten suggereren dat het FHR profiteert van zuurstoftoediening aan de moeder, aangezien zowel de duur als diepte van de deceleraties verminderen. Daarnaast verbetert de foetale oxygenatie. De positieve invloed van maternale hyperoxygenatie op de foetus vermindert echter gedurende ernstige variabele deceleraties.

Concluderend, er is een model ontwikkeld om de fysiologische cascade van uteruscontractie tot deceleratie in het foetale hartritme in kaart te brengen. Modeluitkomsten voor verschillende klinische scenarios zijn in overeenstemming met bevindingen uit experimentele data. Het model kan in een educatieve setting gebruikt worden voor de simulatie van kortetermijn responsie van het foetale cardiovasculaire systeem op uteruscontracties voor het vergroten van inzicht in de complexe fysiologie. Bovendien kan het model geïntegreerd worden in een "full-body" bevallingssimulator voor het optimaliseren van simulatietrainingen voor verloskundige teams.

Dankwoord

Graag wil ik een aantal mensen met name bedanken voor hun betrokkenheid, feedback, tijd en inzet bij mijn promotieonderzoek.

Prof.dr. Oei, beste Guid, dank je wel voor de kans die je me hebt gegeven om aan te sluiten bij het perinatologisch onderzoek! Het is ontzettend inspirerend om te zien hoe jij voor vrijwel elke technologische gadget een toepassing kunt verzinnen voor de obstetrie en/of de obstetrische simulatie. Bedankt ook voor alle projecten waar je me bij betrokken hebt en voor alle activiteiten tijdens en buiten congressen!

Dr.ir. Bovendeerd, beste Peter, dank je wel voor je begeleiding bij het onderzoek, voor alle tijd en energie die je wekelijks hebt gestoken in het verbeteren van mijn gevoel voor detail, voor het luisteren naar eindeloze verloskundige scenario's, het meedenken in schema's (al dan niet "organisch"), het bouwen van CaVasCo (of was het cisco?), je geduld bij het reviewen van alle abstracts en artikelen, en natuurlijk alle gezellige off-topic momenten tussendoor. Dit alles heb ik meer dan gewaardeerd!

Prof.dr.ir. Frans van de Vosse, bedankt voor alle hulp op de achtergrond en het warme welkom in de cardiovascular biomechanics group met alle leuke uitjes van dien, ondanks dat ik officieel bij electro hoorde. Prof.dr.ir. Jan Bergmans, ook al was ik vaak op afstand bij MMC of BMT, de betrokkenheid vanuit SPS en de uitnodigingen voor het jaarlijkse fietsuitje heb ik altijd heel erg gewaardeerd, en niet te vergeten het "drie-en-een-halve-maand-overbruggingscontract", hartelijk dank.

Graag wil ik prof.dr.ir. Backx, dr.ir. Van Meurs, prof.dr. Nijhuis en prof.dr. Vandenbussche bedanken voor het beoordelen van mijn proefschrift en hun bereidheid om zitting te nemen in mijn promotiecommissie.

Een onderzoek doen waarbij meerdere faculteiten betrokken zijn op de TU/e is een hele uitdaging. Dank aan alle secretaresses en conciërges die meer dan regelmatig pasjes en accounts

gedeblokkeerd hebben, formulieren opnieuw opgestuurd, telefoontjes gepleegd, fietsenstallingen hebben geopend en nog duizend dingen meer. Ineke, Karlijn, Samantha, Toon, Anja, Diana, Alice, Mila en Loes, dankzij jullie is het elke keer weer goedgekomen! Bedankt ook voor alle kletsmomentjes en niet te vergeten, de legendarische koekjes bij de SMPE/e!

Graag wil ik Guid, Frans en Herman bedanken voor de mogelijkheid om mijn promotieonderzoek te koppelen aan een QME-opleiding. Het heeft me de kans gegeven om de theoretische kennis van het onderzoek op een praktische manier te linken aan de kliniek en de “echte” simulatietrainingen. Rob, Niels en Pieter, jullie bedankt voor het uitdelen van de enquêtes en voor de tijd bij Medsim, waar ik een hoop geleerd heb over o.m. trainingen, organisatie en techniek. Thanks to all of you from *the* Center of Medical Simulation for the opportunity to spend one month in Boston in your very inspiring company. Roxane, thank you for all your help and friendship!

Graag wil ik ook Judith van Laar, Peter Andriessen, Barbara Vermeulen en Lenny Meijer bedanken voor hun betrokkenheid bij diverse deelaspecten. Dank voor jullie kritische blik, fysiologische kennis en praktische hulp.

Ik heb ook heel veel gehad aan de reflectie, feedback en onmisbare gezelligheid van en met kamer-, SMPE/e- en/of lunchgenootjes van de afgelopen jaren: Wouter Huberts, Maarten Merkx, Saskia Aarnink, Esther Martens, Germaine Jongen en Saskia van Loon van de TU/e; Job Gutteling, Ward Jennekens en Rik Vullings uit MMC. Bedankt voor alle leuke inhoudelijke en niet-inhoudelijke (lunch)praat! Wouter en Maarten, jullie speciaal bedankt voor alle gezelligheid in NLaag, dat was toch een mooie tijd! Deze rol wordt inmiddels goed waargenomen door de FUNmeeting-genootjes, Annemarie, Laura en Marion, jullie ook met name bedankt voor jullie kritische, fysiologische vragen en verdere feedback op mijn werk.

Zonder Germaine Jongen en Lauren Bullens had dit proefschrift wat hoofdstukken gemist. Germaine, het is superleuk om met je samen te werken, niet alleen omdat je zo nauwkeurig bent en een scherp oog hebt voor details, maar ook omdat het heel inspirerend en gezellig is met je samen te werken, met name op de MMC-dinsdagen. Ik denk aan the BG's, oneindige catecholamineconcentraties en niet te vergeten, de chocolademelkmomentjes in MMC. Dank je wel voor al je hulp! Lauren, met jou is het ook fantastisch samenwerken! Dank je voor al je hartelijkheid, je bereidheid om het model in een klinische setting te testen, Matlab te leren, en natuurlijk je hulp bij alle regedingetjes in MMC! Dank jullie wel voor jullie vriendschap.

Papa, Mama, Maarten & Camilla, Carlien & Egbert +Ben, Gert & Sara, Susanne & Erwin, Gabriëlle, Daniëlle, Pieter, Irene, Astrid, Thomas en Eliane, Pa, Ma, Gerda & David +Eloïse +Nathan, Adriaan & Sarah en Marinda & Jaap, bedankt dat jullie mijn leuke familie vormen en regelmatig mijn uitweidingen hebben willen aanhoren.

Maar zonder mijn maatje was het allemaal zeker niet gelukt, dank je lieve Han dat je al zo lang betrokken bent bij alles wat ik doe, (verrassend?) haarfijn weet wanneer en hoe ik dingen handiger aan kan pakken en af en toe ook inhoudelijk de gouden tip hebt! Nu m'n thesis af is kunnen we echt samen aan het volgende project klussen, gelukkig heb je nog wat verbouwing voor me overgelaten. There's treasury everywhere, zullen we maar zeggen.

Curriculum Vitae

Beatrijs van der Hout-van der Jagt was born on May 12th, 1981, in The Hague (The Netherlands). She obtained her Gymnasium diplom in 1999 and moved to Ghent, Belgium, to study Midwifery. In 2002 she graduated and went to Eindhoven to study Biomedical Engineering. After obtaining her BSc in 2005, she continued with the master program Medical Engineering. She did her internship and graduation project at the obstetrics and gynaecology department in Máxima Medical Center in Veldhoven, under supervision of prof.dr. Guid Oei. The graduation project was the base for the feto-maternal cardiovascular model, as described in this thesis. She obtained her MSc in 2007 and continued the research of her master thesis in a PhD project. From 2007 to 2010, this was combined with a post master program Qualified Medical Engineering at the School of Medical Physics & Engineering, Eindhoven, focused at medical simulation training for obstetrics. In 2009 and 2010 she worked parttime as a simulation specialist in Medical Simulation and Education Center Medsim in Eindhoven. Beatrijs works as a medical engineer at the department of obstetrics and gynaecology in Máxima Medical Center in Veldhoven and is married to Jan van der Hout.

Scientific output

Peer-reviewed journal articles

M.B. van der Hout-van der Jagt, S.G. Oei, and P.H.M. Bovendeerd. A mathematical model for simulation of early decelerations in the cardiotocogram during labor. *Med Eng Phys*, 34:579589, 2012.

M.B. van der Hout-van der Jagt, S.G. Oei, and P.H.M. Bovendeerd. Simulation of reflex late decelerations in labor with a mathematical model. *Early Human Dev*, 89:719, 2013.

M.B. van der Hout-van der Jagt, G.J.L.M. Jongen, P.H.M. Bovendeerd, and S.G. Oei. Insight into variable fetal heart rate decelerations from a mathematical model. *Early Human Dev*, <http://dx.doi.org/10.1016/j.earlhumdev.2012.12.001>, 2012.

Journal articles under peer-review

L.Bullens, M.B. van der Hout-van der Jagt, P.J. van Runnard Heimeel, and S.G. Oei. Intrauterine resuscitation by maternal hyperoxygenation evaluated in a simulation model. Submitted to *Early Human Dev*.

Conference abstracts

M.B. van der Hout-van der Jagt, P.H.M. Bovendeerd, F.N. van de Vosse, S.G. Oei. Development of a simulation model of the fetomaternal circulation. Oral presentation, SESAM 2008 14th Annual Meeting of the Society in Europe for Simulation Applied to Medicine. Hatfield (UK).

June 19-21, 2008.

M.B. van der Hout-van der Jagt, A.E.R. Mérien, P.H.M. Bovendeerd, F.N. van de Vosse, S.G. Oei. Development of a simulation model of the feto-maternal circulation. Poster presentation, FNPS 2008 - 35th meeting of the Fetal and Neonatal Physiological Society. Maastricht (NL), June 22-25, 2008.

M.B. van der Hout-van der Jagt, P.H.M. Bovendeerd, F.N. van de Vosse, S.G. Oei. Wiskundig simulatiemodel van de foeto-maternale circulatie. Oral presentation, DSSH 2008 - Najaarsvergadering van de Dutch Society of Simulation in Healthcare. Utrecht (NL), September 25, 2008.

M.B. van der Hout-van der Jagt, P.H.M. Bovendeerd, F.N. van de Vosse, S.G. Oei. Mathematical model for obstetric team trainings. Poster presentation, IMSH 2009 - 9th International Meeting of the Society of Simulation in Healthcare. Orlando (FL, USA), January 11-14, 2009.

M.B. van der Hout-van der Jagt, P.H.M. Bovendeerd, F.N. van de Vosse, S.G. Oei. Mathematical model for simulation of early decelerations in labor. Poster presentation, SESAM 2009 15th Annual Meeting of the Society in Europe for Simulation Applied to Medicine. Mainz (DE). June 11-13, 2009.

M.B. van der Hout-van der Jagt, P.H.M. Bovendeerd, F.N. van de Vosse, S.G. Oei. Mathematical model for simulation of early decelerations in labor. Oral presentation, IMSH 2010 - 10th International Meeting of the Society of Simulation in Healthcare. Phoenix (AZ, USA), January 24-27, 2010.

M.B. van der Hout-van der Jagt, S.G. Oei. Setting up obstetric training in a simulation centre. Workshop, ECOSIM 2010 - 1st European Conference on Simulation in Womens Health. London (UK), February 25-26, 2010.

M.B. van der Hout-van der Jagt, P.H.M. Bovendeerd, S.G. Oei. The design of a simulation model of the cardiotocogram (CTG). Oral presentation, DSSH 2010 - Voorjaarssymposium van de Dutch Society of Simulation in Healthcare. Utrecht (NL), March 31, 2010.

M.B. van der Hout-van der Jagt, P.H.M. Bovendeerd, S.G. Oei. Simulation of late decelerations in labor with a mathematical model. Poster presentation, IMSH 2011 - 11th International Meeting of the Society of Simulation in Healthcare. New Orleans (LA, USA), January 23-26, 2011.

M.B. van der Hout-van der Jagt, A.F. Fransen, S.G. Oei. What about your gaming skills?! & How effective is your training?!, Workshop ECOSIM 2011 - 2nd European Conference on Simulation in Womens Health. London (UK), November 17-18, 2011.

M.B. van der Hout-van der Jagt, P.H.M. Bovendeerd, S.G. Oei. Contribution of reflex pathways

to late decelerations in uteroplacental insufficiency with a mathematical model. Poster presentation, IMSH 2012 - 12th International Meeting of the Society of Simulation in Healthcare. San Diego (CA, USA), January 29-February 1, 2012.

M.B. van der Hout-van der Jagt, A.F. Fransen, L.D. de Wit-Zuurendonk, S.G. Oei. Serious gaming in obstetrics. Workshop, IMSH 2012 - 12th International Meeting of the Society of Simulation in Healthcare. San Diego (CA, USA), January 29-February 1, 2012.

M.B. van der Hout-van der Jagt, L.D. de Wit-Zuurendonk. Birthplay - Serious game voor stuitbevallling. Workshop, DSSH 2012 - Voorjaarssymposium van de Dutch Society of Simulation in Healthcare. Utrecht (NL), March 28, 2012.

M.B. van der Hout-van der Jagt, G.J.L.M. Jongen, L. Bullens, A.F. Fransen, S.G. Oei. Physiologic Models in Simulation: An OB Case Study. Workshop, IMSH 2013 - 13th International Meeting of the Society of Simulation in Healthcare. Orlando (FL, USA), January 27-30, 2013.

Awards

MMC Award (Best Poster 2009)

Emerging and Innovative Methods and Technology Abstract Winner (IMSH 2010)

Young Talent Award (DSSH 2010)

Herman Beijerinck Award (Best Clinical Project 2006-2010)